ABSTRACT

WILLIAMS, JOHN ROBERT, JR. A Study of the Electromagnetic Decay of the Low-Lying Excited States in ^{29}Al and ^{61}Ni. (Under the direction of DAVID R. TILLEY and CHRISTOPHER R. GOULD.)

This dissertation is the result of a continuing research program in low energy gamma ray spectroscopy for light and medium mass nuclei using the charged particle acceleration facilities at Triangle Universities Nuclear Laboratory, Durham, N. C.

A Compton linear polarimeter has been designed and constructed with five identical, 1.5 by 2.0 inch sodium iodide (NaI) crystals. This instrument and the experimental techniques developed for its application have been incorporated with the already well established procedures for nuclear lifetime and gamma ray angular correlation measurements, the result being an expanded research capability.

The NaI polarimeter has been used in a study of the low-lying excited states in ^{29}Al using the ^{26}Mg$(\alpha,p\gamma)^{29}$Al reaction with $E_\alpha = 11.26$ MeV. When considered together with the results of lifetime and angular correlation studies from other works, these measurements confirm the $3/2^+$ spin-parity assignment for the level at 2.88 MeV. A definite $J^\pi = 3/2^+$ assignment is made for the 2.23 MeV level, and a $7/2^+$ assignment is favored for the level at 1.76 MeV. These results, along with the experimental M1E2 transition strengths, are compared with the theoretical predictions of the shell model and the Nilsson model.

A second Compton polarimeter, purchased commercially and consisting of two 30 c.c., germanium (GeLi) crystals, has been employed in a comprehensive study of the seventeen levels in ^{61}Ni below 2200 keV.

This study has also included lifetime measurements using the Doppler shift attenuation method and gamma ray angular correlation measurements based on Method II of Litherland and Ferguson. The excited states in ^{61}Ni were populated using the $^{58}Fe(\alpha,n\gamma)^{61}Ni$ reaction with $E_\alpha = 8.0$ MeV . The results of these measurements confirm most of the spin-parity assignments made previously from stripping and pickup reaction studies and studies of the β^+-decay of the ground state of ^{61}Cu . Additional J^π assignments of $7/2^-$, $5/2^-$, $3/2^-$ and $7/2^+$ have been made for the levels at 1016, 1611, 1730, and 2020 keV, respectively. The experimental results are compared to recent theoretical calculations made using the shell model and the core coupling model. The experimental M1E2 transition strengths have been found to be in agreement with those measured for other $1f_{7/2}$ shell nuclei.

A STUDY OF THE ELECTROMAGNETIC DECAY OF THE LOW-LYING EXCITED STATES IN ^{29}Al AND ^{61}Ni

by

JOHN ROBERT WILLIAMS, JR.

A thesis submitted to the Graduate Faculty of
North Carolina State University at Raleigh
in partial fulfillment of the
requirements for the Degree of
Doctor of Philosophy

DEPARTMENT OF PHYSICS

RALEIGH

1 9 7 4

APPROVED BY:

Co-Chairman of Advisory Committee	Co-Chairman of Advisory Committee

Corrections:

Page	Paragraph	Line	Error	Correction
[Biography - in 5th publication]			Low Low Lying	Low-Lying
[Table of Contents - Section 2.1]			2.1.1 2.1.1	2.1.1 2.1.2
9	1	13	and after,	and, after
10	2	8	well-established	well established
14	2	12	multipoles.	multipoles. Also, $e = (-1)^{I-J+K/2}$.
16	[in Eq. 2.20]		$\delta_{L'}^{<\pi>}$	$\delta_{L'}^{<\pi'>}$
17	1	7	page 15.	page 15.)
17	2	3	E1, E2, E3	E1, M2, E3
34	1	19	correspooded	corresponded
71	3	13	quadrapole .	quadrupole
94	1	11	with 0.2 keV	within 0.2 keV
151	2	5	make	makes
155	[Table 4.1]		$76\pm$ $8\pm$ $16\pm$	76 ± 5 8 ± 3 16 ± 3
157	[Table 4.1]		$1/2\cdots$ 2 5/2	$1/2\cdots$ a 5/2
163	[Reference 31]		Pucl.	Nucl.

BIOGRAPHY

Name: John Robert Williams, Jr.

Personal: Born November 17, 1946, Albany, Georgia

Education: B. S. in Physics, North Georgia College, 1968

Positions: Teaching Assistant, N.C.S.U., 1968 to 1969

NDEA Fellowship, N.C.S.U., 1969 to 1972

Research Assistant, N.C.S.U., 1972 to present

Membership: Sigma Pi Sigma, American Physical Society

Publications: The Application of Polarized Deuterons in (d,pγ) Angular Correlation Measurements, C. R. Gould, R. O. Nelson, J. R. Williams, D. R. Tilley, J. D. Hutton, N. R. Roberson, T. B. Clegg, and C. E. Busch, Phy. Rev. Lett. 30, 298 (1973)

Linear Polarization Measurements in ^{29}Al, J. R. Williams, C. R. Gould, R. O. Nelson, and D. R. Tilley, (In preparation)

The ^{6}Li(p,^{3}He)^{4}He Reaction from 3 to 8 MeV, C. R. Gould, R. O. Nelson, J. R. Williams, and J. R. Boyce, (To be published in Nuclear Science and Engineering)

Angular Correlation Studies and Lifetime Measurements in ^{61}Ni, J. R. Williams, C. R. Gould, R. O. Nelson, D. R. Tilley, D. G. Rickel, and N. R. Roberson, (In preparation)

Linear Polarization and Lifetime Studies of the Low Low Lying Levels in ^{50}V, N. R. Roberson, D. G. Rickel, D. R. Tilley, R. O. Nelson, and J. R. Williams, (In preparation)

Abstracts: The Application of Polarized Deuterons in (d,pγ) Angular Correlation Measurements, C. R. Gould, R. O. Nelson, J. R. Williams, D. R. Tilley, J. D. Hutton, N. R. Roberson, T. B. Clegg, and C. E. Busch, Bull. Am. Phys. Soc. 11, 18 (1973)

Linear Polarization Measurements in ^{29}Al, J. R. Williams, C. R. Gould, R. O. Nelson, and D. R. Tilley, Southeastern Section of the Am. Phys. Soc. 30, November (1973)

The ^{6}Li(p,^{3}He)^{4}He Reaction from 3 to 8 MeV, C. R. Gould, R. O. Nelson, J. R. Williams, and J. R. Boyce, Bull. Am. Phys. Soc. 11, 19, 15 (1974)

Angular Correlation Studies and Lifetime Measurements in ^{61}Ni, J. R. Williams, C. R. Gould, R. O. Nelson, D. R. Tilley, D. G. Rickel, and N. R. Roberson, Bull. Am. Phys. Soc. 11 19, 430 (1974)

Linear Polarization Studies of Gamma-Ray Transitions in ^{50}V Using a Two Crystal Compton Polarimeter, N. R. Roberson, D. G. Rickel, D. R. Tilley, R. O. Nelson, and J. R. Williams, Bull. Am. Phys. Soc. 11 19, 546 (1974).

Mean Lifetimes and Gamma-Ray Angular Distributions for ^{50}V, D. G. Rickel, N. R. Roberson, R. O. Nelson, D. R. Tilley, and J. R. Williams, Bull. Am. Phys. Soc. 11 19, 546 (1974)

Lifetimes of Levels in ^{55}Co, R. O. Nelson, J. R. Williams, D. R. Tilley, D. G. Rickel, and N. R. Roberson, Bull, Am. Phys. Soc. 11 19, 429 (1974)

ACKNOWLEDGMENTS

I am grateful to many people for the situation in which I find myself at the present time. Foremost among these persons are my graduate advisors, Professors D. R. Tilley and C. R. Gould, who, in addition to making this dissertation possible, have contributed so much to my training during the last three years.

I also wish to extend my appreciation to Professor N. R. Roberson for his many helpful discussions during my stay here at T.U.N.L. I have also profited from similar discussions with Drs. R. O. Nelson and D. G. Rickel who rendered invaluable assistance during the experiments which have led to this thesis. Additionally, I wish to thank Professor Reiner Bass of Frankfurt University, Frankfurt, West Germany for his assistance in the successful development of the NaI polarimeter.

During the first years of my graduate education, I enjoyed the counseling and indulgence of Professors G. E. Mitchell and D. R. Tilley. Their patience and understanding have continued since that time, and for it I am very grateful.

I have found the facilities here at T.U.N.L. to be of the highest quality, and for this I must thank Professors H. W. Newson and E. G. Bilpuch. Also I wish to thank the following T.U.N.L. personal for their help with the construction and maintenance of the equipment provided for my use: S. E. Edwards, R. L. Rummel, M. T. Smith, A. W. Lovette, R. G. Hogan, and E. P. Harris. The figures in this dissertation were expertly prepared by Mrs. Joseph Bailey.

I also wish to thank my parents for their continued support over the years, and, at North Georgia College, I shall always remember Professors E. G. Pigg and D. E. Kinkaid for their encouragement during my undergraduate study.

And finally, I wish to express my sincerest appreciation to my wife, Bonnie, whose patience and understanding during the last six years have done so much toward making this work possible.

TABLE OF CONTENTS

TABLE OF CONTENTS (Continued)

1. INTRODUCTION

1.1 General Discussion of Gamma Ray Spectroscopy

With the development of the charged particle accelerator and the computer, experimental nuclear physics has become a sophisticated science which encompasses the entire periodic table. At the present time, and in addition to the higher incident beam energies which are always sought, the introduction of polarized beams and heavy ion acceleration facilities promises to add to the power of the already established procedures which have been developed over the years in a continuing effort to understand the nucleus. The study of the gamma decay of excited nuclear states is but one of many standard approaches, and it is with this procedure that the present work is concerned.

Gamma ray spectroscopic measurements are particularly well suited for testing the validity of the wave functions generated with some given nuclear model. As a first step, the model should predict the energies of the excited states in the nucleus to which it is applied. However, calculation of the excitation energies is relatively insensitive to the details of the wave functions so that more stringent tests are required. These test are provided by comparison with experiment of the theoretically calculated electromagnetic matrix elements for the multipole operators which describe the electromagnetic interaction between excited states in the nucleus. In contrast to other experimental procedures involving reaction mechanism studies, the form taken by these multipole operators is well understood from electromagnetic field theory. Therefore, uncertainties in the theoretical calculations result from discrepancies in the wave functions predicted by the model [61].

The diagram in Figure 1.1 corresponds to a typical procedure for producing a nucleus in an excited state. A target nucleus in its ground state with spin, $\bar{A}$, is bombarded by particles with orbital angular momentum, $\bar{\ell}_1$, and spin, $\bar{s}_1$. A compound nuclear state with spin, $\bar{B}$, may or may not then be formed depending on the reaction mechanism. In general, higher bombarding energies favor direct reactions while lower bombarding energies favor compound nuclear reactions. Whichever the case, the combination of the target nucleus and the incident particle is in an excited state much above the threshold for decay by particle emission. Therefore, a secondary particle is emitted with orbital and spin angular momentum, $\bar{\ell}_2$ and $\bar{s}_2$, and this process leads to the population of an excited state with total spin

$$\bar{J} = \bar{A} + \bar{\ell}_1 + \bar{s}_1 - \bar{\ell}_2 - \bar{s}_2 \qquad 1.11$$

in the residual nucleus.

The reactions described above occur symmetrically about a unique spatial axis whose orientation is described by the direction of the incident beam. The projections of $\bar{J}$ onto this symmetry axis range in increments of one from $-|\bar{J}|$ to $|\bar{J}|$. For anyone of these magnetic substate quantum numbers

$$m_J = m_A + m_{\ell_1} + m_{s_1} + m_{\ell_2} + m_{s_2} \qquad 1.12$$

where each component refers to the projection onto the symmetry axis of the appropriate angular momentum vector from Equation 1.11.

Figure 1.1 A diagram which corresponds to a standard method for populating a state in a residual nucleus

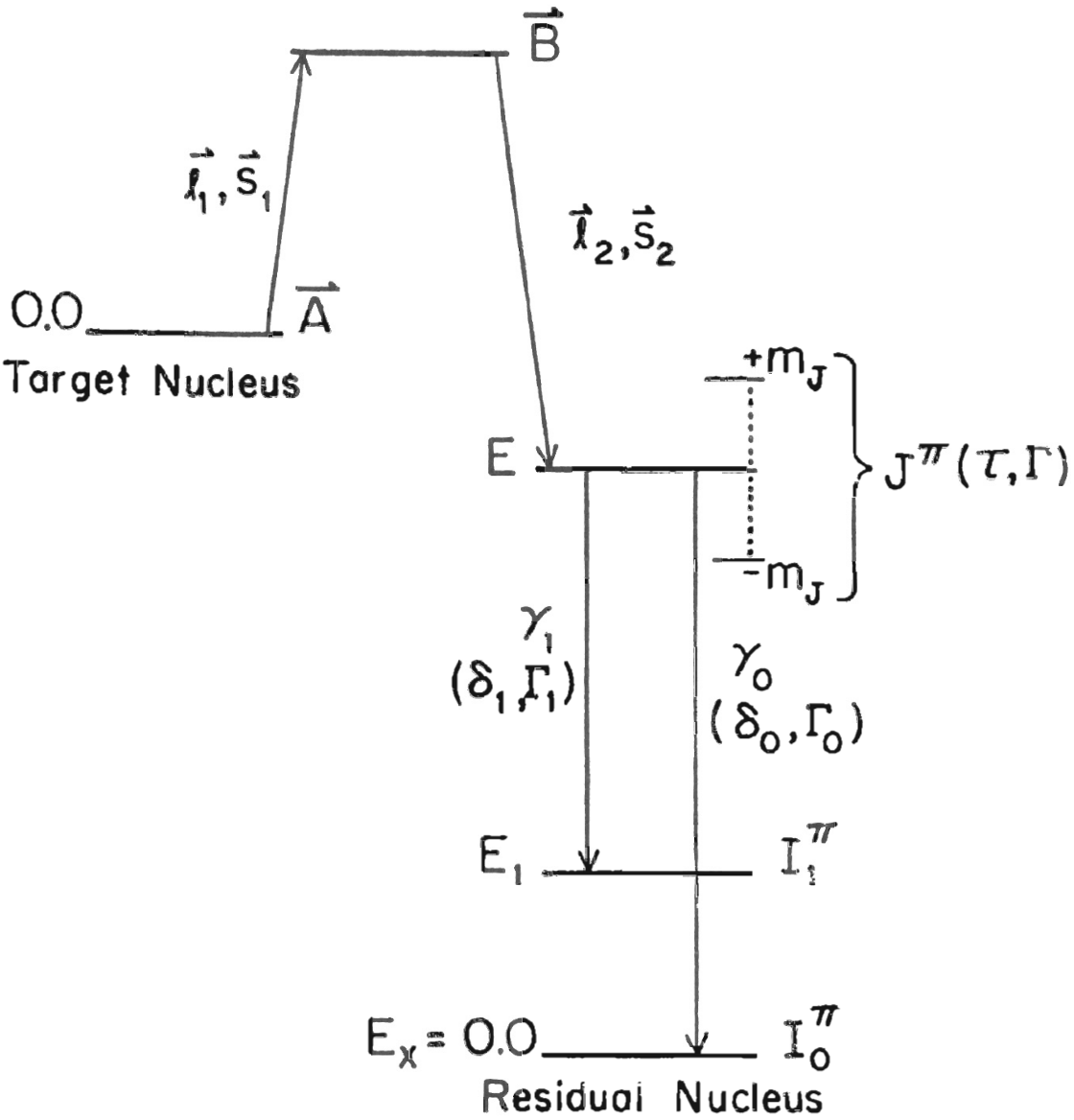
B
$\vec{l}_1, \vec{s}_1$
$\vec{l}_2, \vec{s}_2$
0.0
A
Target Nucleus
$+m_J$
E
$J^\pi(\tau,\Gamma)$
$-m_J$
γ_1
(δ_1,Γ_1)
γ_0
(δ_0,Γ_0)
E_1
I_1^π
$E_x = 0.0$
I_0^π
Residual Nucleus

The state $\bar{J}$ is characterized by a definite parity, π, an excitation energy, E, and a lifetime, τ. The total radiative width of the level is

$$\Gamma_T = \hbar/\tau \qquad 1.13$$

where $\hbar$ is Planck's constant divided by 2π. After the time, τ, the state decays by gamma ray emission to a state of lower excitation energy. Decay to more than one lower state is possible, and the fractional decay to each of these states is given by a branching ratio. For a given branch, the order of the multipoles involved in the decay can range between $|J - I_1|$ and $J + I_1$ again in increments of one and where $\bar{I}_1$ is the spin of the final state. Usually however, only the two multipoles of lowest order are assumed to contribute to the decay so that, subject to the requirements of parity conservation given in Section 2.1,

$$L = |J - I_1| \qquad 1.14$$

and

$$L' = L + 1 \ . \qquad 1.15$$

The contribution of each multipole is given by the multipole mixing ratio, δ, which is defined as the ratio of the reduced matrix elements for the two multipoles, i.e.,

$$\delta = \frac{\langle J \| L' \| I_1 \rangle}{\langle J \| L \| I_1 \rangle} \qquad 1.16$$

where L and L' represent the multipole operators involved, and $|J>$ and $|I_1>$ are wave functions describing the initial and final states, respectively [51].

As shown by Equation 1.16, the experimental determination of δ provides only the magnitude and relative sign of a ratio of two matrix elements. However, the magnitudes of the individual matrix elements are proportional to the partial radiative widths for the decay of an excited state, and these partial widths are determined as follows [61]. First, the total radiative width from Equation 1.13 is separated into contributions from each branch.

$$\begin{aligned} \Gamma_T &= \Gamma_1 + \Gamma_0 \\ &= \Gamma_1(1 + \Gamma_0/\Gamma_1) \\ &= \Gamma_1(1 + BR) \end{aligned} \qquad 1.17$$

where BR is the appropriate branching ratio. Next, the width, Γ_1, is written as a sum of contributions from the two multipoles, L and L'.

$$\begin{aligned} \Gamma_1 &= \Gamma_1^L + \Gamma_1^{L'} \\ &= \Gamma_1^L(1 + \Gamma_1^{L'}/\Gamma_1^L) \\ &= \Gamma_1^L(1 + \delta^2) \end{aligned} \qquad 1.18$$

where

$$\delta^2 = \Gamma_1^{L'}/\Gamma_1^{L} \ . \qquad 1.19$$

Equations 1.13, 1.17, and 1.18 then give

$$\Gamma_T = \hbar/\tau = \Gamma_1^{L}(1 + \delta^2)(1 + BR)$$

or

$$\Gamma_1^{L} = \frac{\hbar}{\tau(1 + \delta^2)(1 + BR)} \ . \qquad 1.20$$

Equation 1.20 expresses Γ_1^{L} , the partial radiative width for a multipole of order, L , in terms of three of the quantities which characterize the decay of an excited state: the branching ratio, the electromagnetic mixing ratio, and the mean lifetime. Once these three quantities are measured experimentally, the value of Γ_1^{L} is determined and compared to a value calculated using an appropriate nuclear model. This comparison provides the final test for the wave functions predicted by the model.

The research program from which this work has resulted consists basically of three different measurements which, when taken together, determine the quantities on the right side of Equation 1.20. These three measurements are briefly outlined here; however, they are discussed with references and in more detail in other parts of this presentation.

First, the lifetime of an excited state is determined using one of several techniques which have been developed over the past years [48, 61]. The lifetime measurements made in the present work were performed using the Doppler shift attenuation method. This procedure

consists of measuring an attenuated Doppler shift in the energy of a gamma ray produced by the decay of an excited state in a nucleus which is recoiling with a finite velocity through some backing material. This energy shift can also be calculated as a function of the lifetime of the excited state using stopping power theories which describe the way in which the recoiling nucleus slows down in the backing material. Then, the measured and calculated values of the energy shift are compared, and the lifetime is extracted.

The spin of an excited state along with the branching ratios and multipole mixing ratios for the associated gamma radiation are determined from angular correlation measurements made when the nuclei of interest are "oriented". Two types of nuclear orientation can be distinguished, alignment and polarization. In the case of alignment, an axis of rotational symmetry (normally the beam axis) is established, but the sense of this axis is not determined. In the case of polarization, an axis is established which provides a single perferred direction in space. If the spin of the nuclear state is J and its component along the axis is m_J and if the relative population of the substate, m_J, is $P(m_J)$, then the condition for alignment is $P(m_J) = P(-m_J)$ and that for polarization is $P(m_J) \neq P(-m_J)$. If the $P(m_J)$ are all equal, the nuclei are not oriented.

All further discussion in this presentation will be concerned only with alignment orientation which can be insured by standard experimental techniques. Under these conditions, the variation in the intensity of the detected gamma radiation can be expressed as an expansion in even ordered Legendre polynomials

$$W(\theta) = \sum_{K} A_K P_K (\cos \theta) \qquad 1.21$$

where θ is measured with respect to the beam axis and where the coefficients, A_2, A_4, etc. take on explicit mathematical form and depend on the spins of the initial and final states, the multipole mixing ratio of the gamma radiation, and the population parameters for the magnetic substates of the initial level. Usually, the population parameters can be restricted to some physically reasonable set of values, and the spin of the final state is known. Then, the spin of the initial state and the mixing ratio of the gamma radiation are determined by systematically varying their values until a set of expansion coefficients is determined which gives the best fit to the experimental data. The term, A_0, in Equation 1.21 is merely a normalization constant, and after, the correlations for all branches of an excited state have been determined, these constants are used to determine the branching ratios.

Gamma ray angular correlation techniques provide a powerful method for measuring spins and multipole mixing ratios. Occasionally, however, ambiguous conclusions result from this method when several initial spins along with their corresponding mixing ratios are found to fit the experimental data equally well. In these cases, linear polarization measurements on the gamma radiation can sometimes determine the correct spin and mixing ratio (see Chapters 2 and 3). The linear polarization of a gamma ray is produced by the same alignment process used for the correlation measurements, and its value depends upon the same variables as do the expansion coefficients in Equation 1.21 [21, 55]. The linear polarization can be calculated explicitly for each

theoretical correlation, and these values can then be compared to the measured polarization which is determined using some polarization sensitive procedure such as the Compton scattering process. Very often the results uniquely determine a spin and its corresponding mixing ratio.

1.2 Objectives of the Present Work

When plans were initially made for the work which has resulted in this dissertation, priority was given to the development of a gamma ray polarimeter along with the experimental procedures through which the instrument could be used for linear polarization measurements. This development process and its successful completion are discussed in detail in Chapter 2. These new techniques were then combined with the already well-established procedures for lifetime and angular correlation measurements, and the result was an expanded experimental capability which was then applied to two nuclei, ^{29}Al and ^{61}Ni.

Linear polarization measurements made on ^{29}Al are discussed in Chapter 3. These measurements, when combined with the results of lifetime and angular correlation studies made by other groups, permit the calculation of partial widths for the low lying states in ^{29}Al. These widths are then compared to those calculated using the Nilsson model.

The final chapter deals with lifetime, angular correlation, and linear polarization measurements made on ^{61}Ni. The experimental procedures for the lifetime and angular correlation measurements are discussed, and the results of all three studies are compared to the

shell model calculations of Glaudemans et al. and the core coupling model calculations of Hoffmann-Pinther et al.

2. LINEAR POLARIZATION PHENOMENA

2.1 Theory

2.1.1 Angular correlations. The presentation of the material contained in this section closely follows that of Taras [55] in which gamma ray angular distribution and linear polarization formulas are presented in terms of the phase-defined reduced matrix elements of Rose and Brink [51]. The phase consistent approach used by Rose and Brink to define and manipulate the reduced matrix elements of the multipole interaction operators has done much toward removing the confusion concerning the sign of the multipole mixing ratio, δ, which has existed for a number of years as a result of the different approaches taken by various authors [44,18,10].

This entire discussion is restricted to the study of the gamma decay of an excited state which is produced and aligned by the bombardment of target nuclei by a suitable beam of incident particles (see Figure 1.1). The beam is assumed to be unpolarized, and the spins of the target nuclei must be randomly oriented. Under these conditions and for an excited state with total spin, J, there is equal population of the positive and negative magnetic substates. That is,

$$P(m) = P(-m) \qquad 2.11$$

where $P(m)$ is a parameter which gives the relative population of a substate with projection, m, onto the symmetry axis defined by the direction of the incident beam. The population parameter describing a

particular substate is usually defined as the sum of the parameters which describe the population of the posititve and negative projections of the substate. These new population parameters are normalized so that

$$\sum_{m\geq 0} P'(m) = 1 \ . \qquad 2.12$$

The orbital angular momentum vector for a particle in the incident beam is given by

$$\bar{\ell}_1 = \bar{r} \times \bar{p}_1 \qquad 2.13$$

where $\bar{r}$ and $\bar{p}_1$ define the position and linear momentum of the incident particle with respect to the target nucleus. Since $\bar{\ell}_1$ is perpendicular to both $\bar{r}$ and $\bar{p}_1$, there can be no projection of $\bar{\ell}_1$ onto the symmetry axis. Therefore, $m_{\ell_1} = 0$, and Equation 1.12 gives

$$m = m_A + m_{s_1} + m_{\ell_2} + m_{s_2} \ . \qquad 2.14$$

If the outgoing particles are detected along the beam axis at either 0° or 180°, then $m_{\ell_2} = 0$, and

$$m = m_A + m_{s_1} + m_{s_2} \ . \qquad 2.15$$

Equation 2.15 states that the magnetic quantum number of the highest substate populated is equal to the sum of the intrinsic spins of the target nucleus, the incident particle, and the outgoing particle. Under the proper experimental conditions and for an excited state with spin, J, this value of m may be less than J, thus assuring aligned orientation of the residual nucleus.

The technique whereby gamma radiation is studied in coincidence with particles detected along the beam axis is commonly referred to as Method II of Litherland and Ferguson [44], and it is a widely used procedure for the production of aligned states. However, the detection of the secondary particle is not always necessary. Under the proper experimental conditions the outgoing particles may be described as s-waves ($\ell = 0$) or p-waves ($\ell = 1$) in which case m_{ℓ_2} in Equation 2.14 is a small number. Very often, the alignment produced in this manner is all that is needed for the gamma ray studies.

The total probability per unit time per unit solid angle that a state $|J>$ will decay to a state $|I>$ through the emission of a gamma ray in the direction $\bar{k}$ is given by [55]

$$P(\bar{k}) = \frac{k}{2\pi\hbar} \sum_{\substack{KLL' \\ \pi\pi'}} \rho_{KQ}(-1)^{e} Z_1(LJL'J,IK) P_K(\cos\theta) \times$$

$$\{1 + (-1)^{L+L'+\pi+\pi'-k}\}$$

$$\times \frac{<J\|T_L^{<\pi>}\|I><J\|T_{L'}^{<\pi'>}\|I>}{(2L+1)^{\frac{1}{2}}(2L'+1)^{\frac{1}{2}}} \qquad 2.16$$

where the emitting level is allowed to have mixed parities and where the following definitions apply:

(1) If L represents all the magnetic multipoles involved in the gamma emission, L' represents all the electric multipoles. If L represents electric multipoles, L' then represents magnetic multipoles.

(2) π is 0 for electric radiation and 1 for magnetic radiation. The same is true for π'.

(3) $\bar{k}$ is the wave vector for the emitted radiation. Its magnitude, k, should not be confused with, K, the order of the ordinary Legendre polynomial, $P_K(\cos\theta)$

(4) $\langle J\|T_L^{\langle\pi\rangle}\|I\rangle$ is a reduced matrix element for an electric or magnetic multipole operator depending on which one is represented by L and π.

(5) $Z_1(LJL'J,IK)$ is a general coefficient composed of a Clebsch-Gordon coefficient and a Racah coefficient. The numerical values of these Z_1 coefficients are tabulated in reference [55].

(6) ρ_{k_0} is a statistical tensor describing the orientation of the emitting level and may be expressed as follows in terms of the population parameters, $P(m)$:

$$\rho_{KO} = \sum_{m\geq 0} (-1)^{J-m} P(m) (JJm-m|\,KO) \qquad 2.17$$

where $\rho_{00} = (2J+1)^{-\frac{1}{2}}$. The ρ_{KO} are non-zero only when k is even since the Clebsch-Gordon coefficients in Equation 2.17 are identically zero for odd K.

In Equation 2.16, $P(\bar{k})$ is the sum of two emission probabilities. That is,

$$P(\bar{k}) = P^{q=+1}(\bar{k}) + P^{q=-1}(\bar{k}) \qquad 2.18$$

where $q = \pm 1$ refers to a gamma ray which is circularly polarized parallel $(+1)$ and anti-parallel (-1) to the direction defined by the wave vector, $\vec{k}$ [11]. The gamma ray energy dependence implied by the wave number, k, is important only when a comparison is made between absolute emission probabilities for gamma rays of different energies. Since interest here lies only in obtaining the angular distribution equation for a single gamma ray, the factor, $k/2\pi\hbar$, shall not be carried further.

The multipole mixing ratios defined by Rose and Brink are

$$\delta_L^{\langle\pi\rangle} = \frac{\langle J\|T_L^{\langle\pi\rangle}\|I\rangle (2L+1)^{\frac{1}{2}}}{\langle J\|T_{\underline{L}}^{\langle\pi\rangle}\|I\rangle (2\underline{L}+1)^{\frac{1}{2}}} \qquad 2.19$$

where $\underline{L}$ and $\underline{\pi}$ represent the lowest order multipolarity occurring in the transition $J \rightarrow I$. Using this definition, Equation 2.16 becomes

$$\omega(\theta) = \sum_{\substack{LL'\pi\pi' \\ K(\text{even})}} (-1)^e \rho_{K0} Z_1(LJL'J,IK) P_K(\cos\theta) \times$$

$$\{1 + (-1)^{L+L'+\pi+\pi'-K}\} \delta_L^{\langle\pi\rangle} \delta_{L'}^{\langle\pi\rangle}/2 \qquad 2.20$$

Equation 2.20 is applicable when neither the circular nor linear polarization of the emitted gamma ray is observed. The emitting level is assumed to have a definite spin, J, and an axis of symmetry with respect to which θ is measured; however, the state, J, need not have a definite parity.

For the gamma decay of a initial state, $|J\rangle$, to a final state, $|I\rangle$, there exists a definite relationship between the parities of

the two states and the multipole orders involved in the gamma ray emission [32]

$$(\pi_J \cdot \pi_I) = (-1)^L \quad \text{for electric radiation, } E(L) \qquad 2.21$$

and

$$(\pi_J \cdot \pi_I) = (-1)^{L+1} \quad \text{for magnetic radiation, } M(L) . \qquad 2.22$$

(Note, the quantities π_J and π_I should not be confused with π and π' which are defined on page 15.

If the levels I and J have the same parities, then $\pi_J \cdot \pi_I$ is positive and only M1 , E2 , M3 , E4 ... radiations are allowed by Equations 2.21 and 2.22. Likewise, only E1, E2 , E3 , M4 ... radiations are allowed when J and I have opposite parities. These results imply that, for any two allowed multipole radiations, $L + L'$ is always odd as is $\pi + \pi'$ (see definitions of π and π' on page 15). Therefore, since K is even,

$$(-1)^{L+L'+\pi+\pi'-K} = 1 ,$$

and Equation 2.20 may be written as

$$\omega(\theta) = \sum_{\substack{LL'\pi\pi' \\ K\ (\text{even})}} (-1)^e \rho_{KO} Z_1(LJL'J,IK) \delta_L^{<\pi>} \delta_{L'}^{<\pi'>} P_K(\cos\theta). \qquad 2.23$$

At this point it is worthwhile to summarize the conditions under which Equation 2.23 is applicable.

(1) Neither the circular nor linear polarization of the gamma radiation is observed, i.e., only the intensity is determined as a function of the angle, θ.

(2) The states J and I must have definite parity.

(3) The sum over (L,π) and (L',π') is over all multipoles consistent with the conservation of parity and angular momentum. Recall that

$$|J - I| \leq L,L' \leq J + I \; ; \quad L,L' \neq 0 \; .$$

(4) The sum is over even K only (see page 15 and the discussion of the statistical tensors, ρ_{K0}).

Equation 2.23 may be simplified further by assuming that, of all allowed multipoles, only the two of lowest order contribute to the transition. In this case,

$$\underline{L} = L \quad \text{and} \quad L' = L + 1$$

and

$$\omega(\theta) = \sum_K (-1)^{I-J+K/2} \rho_{K0} [Z_1(LJLJ,IK) - 2\delta Z_1(LJL'J,IK) + \delta^2 Z_1(L'JL'J,IK)] P_K(\cos\theta) \; . \qquad 2.24$$

Equation 2.24 describes the gamma ray angular distribution assuming a point detection geometry when, in reality, the gamma ray

detector subtends a finite solid angle centered about the direction, θ . Corrections for this finite geometry effect can be calculated and included for each order of the different terms in the expansion for $\omega(\theta)$ [40,48]. Finally, Equation 2.24 takes the form

$$\omega(\epsilon) = \sum_K a_K Q_K P_K(\cos\theta) \qquad 2.25$$

where the Q_K's are the finite geometry corrections mentioned above, and

$$a_K = (-1)^{I-J+K/2}\rho_{KO}[Z_1(LJLJ,IK) - 2\delta Z_1(LJL'J,IK) + \delta^2 Z_1(L'JL'J,IK)] . \qquad 2.25a$$

For $K = 0$,

$$Z_1(LJL'J,IO) = \begin{cases} 0, & L = L' \\ (-1)^{I-J}(2J+1)^{1/2}, & L \neq L' \end{cases}$$

and

$$\rho_{OO} = (2J+1)^{-1/2}$$

so that

$$a_O = (1+\delta^2)^{1/2} .$$

The coefficients, a_K , are usually normalized through division by $(1 + \delta^2)$. That is,

$$A_K = \frac{a_K}{(1+\delta^2)}$$

so that

$$A_0 = 1$$

and

$$A_K = (-1)^{I-J+K/2}\rho_{KO}\{Z_1(LJLJ,IK) - 2\delta Z_1(LJL'J,IK) \quad (K > 0)$$
$$+ \delta^2 Z_1(L'JL'J,IK)\} . \qquad 2.25b$$

Normal procedure for gamma ray angular correlation studies involves fitting Equation 2.25 to a measured angular distribution. The spin, I, of the final state is usually known, and the ρ_{KO} may or may not be known, depending on the experimental situation. For instance, using Method II of Litherland and Ferguson, $(\alpha, n\gamma)$ reactions on even-even target nuclei (ground state spin = 0) can populate only $\pm 1/2$ magnetic substates for levels in the residual nuclei. In this case, the population parameter, $P(m)$, is known exactly, and the statistical tensors, ρ_{KO}, may be calculated using Equation 2.17. The spin, J, of the initial state and the multipole mixing ratio, δ, are then varied until one or more combinations are found which give equally acceptable χ^2 values, χ^2 being a measure of the goodness of the theoretical fit to the experimental data. For cases in which the population parameters are not known exactly, the $P(m)$ must be treated as unknown parameters and varied along with J and δ. However, for a substantial number of reactions characterized

as endoergic (i.e., those with negative Q-values), upper limits can be set for the population parameters by performing transmission probability calculations.

Before proceding with a discussion of the gamma ray linear polarization distribution, the explicit form taken by the A_K's in Equation 2.25b will be given for two special cases. The order of the terms involved in the expansion for $\omega(\theta)$ is limited to $K \leq \min(2L',2J)$ [47] so that

for dipole-quadrupole radiation (M1E2 or E1M2),

$$A_2 = \frac{-(-1)^{I-J}\rho_{20}[Z_1(1J1J,I2)-2\delta Z_1(1J2J,I2)+\delta^2 Z_1(2J2J,I2)]}{(1+\delta^2)} \qquad 2.26$$

and

$$A_4 = \frac{(-1)^{I-J}\rho_{40}\delta^2 Z_1(2J2J,I4)}{(1+\delta^2)} ;$$

for quadrupole-octupole radiation (M2E3 or E2M3)

$$A_2 = \frac{-(-1)^{I-J}\rho_{20}[Z_1(2J2J,I2)-2\delta Z_1(2J3J,I2)+\delta^2 Z_1(3J3J,I2)]}{(1+\delta^2)}$$

$$A_4 = \frac{(-1)^{I-J}\rho_{40}[Z_1(2J2J,I4)-2\delta Z_1(2J3J,I4)+\delta^2 Z_1(3J3J,I4)]}{(1+\delta^2)} , \qquad 2.27$$

and

$$A_6 = \frac{-(-1)^{I-J}\rho_{60}\delta^2 Z_1(3J3J,I6)}{(1+\delta^2)} .$$

The A_K coefficients expressed by Equations 2.26 and 2.27 depend upon the following parameters: J, the spin of the initial state (the spin, I, of the final state is usually known), δ, the multipole mixing ratio, and the statistical tensors ρ_{20}, ρ_{40}, and ρ_{60}. These parameters vary indpendently during any fitting procedure, and it is not difficult to understand how more than one combination might be found to fit the experimental data. In such ambiguous situations, gamma ray linear polarization measurements often provide the additional information needed to clarify the results, for, as shall be shown in Section 2.1, the linear polarization depends upon the same three parameters as do the A_K coefficients. Whenever angular correlation and linear polarization measurements are made simultaneously, they form a powerful method for determining spins, parities, and multipole mixing ratios.

2.1.2 Linear polarization. The linear polairzation intensity distribution for a gamma ray of multipolarity L,L' can be obtained from Equation 2.23 by replacing $P_K(\cos\theta)$ with the expression [21, 51]

$$P_K(\cos\theta) + (\pm)_{L'}K_K(LL')\cos 2\varphi P_K^{(2)}(\cos\theta) .$$

Therefore,

$$\omega(\theta,\varphi) = \sum_{\substack{LL'\pi\pi' \\ K\ (\text{even})}} (-1)^{e}\rho_{KO}Z_1(LJL'J,IK)\delta_L^{<\pi>}\delta_{L'}^{<\pi'>}$$

$$\{P_K(\cos\theta) + (\pm)_{L'}K_K(LL')\cos 2\varphi P_K^{(2)}(\cos\theta)\} \qquad 2.28$$

where φ is the angle between the reaction plane and the electric vector of the incident gamma radiation. The coefficient $K_K(LL')$ is defined as [21]

$$K_K(LL') = -[(K-2)!/(K=2)!]^{1/2}(LL'11/K2)/(LL'1-1/K0)\ ,$$

and $P_K^{(2)}(\cos\theta)$ is the associated Legendre polynomial. The plus or minus sign is taken according to whether the $2^{L'}$-pole radiation is electirc (+) or magnetic (-).

Again assuming that only the two lowest order multipoles contribute, Equation 2.28 becomes

$$\omega(\theta,\varphi) = \left[\begin{array}{l} \sum_K (-1)^{I-J+K/2}\rho_{KO}\{Z_1(LL,K)-2\delta Z_1(LL',K)+\delta^2 Z_1(L'L',K)\} \\ \qquad P_K(\cos\theta) + \\ \sum_K (-1)^{I-J+K/2}\rho_{KO}\cos 2\varphi\{(\pm)_L Z_1(LL,K)K_K(LL) - \\ \qquad (\pm)_{L'}2\delta Z_1(LL',K)K_K(LL') + (\pm)_{L'}\delta^2 Z_1 \\ \qquad (L'L',K)K_K(L'L')\}P_K^{(2)}(\cos\theta) \end{array}\right] \qquad 2.29$$

where

$$Z_1(LL',K) = Z_1(LJL'J,IK) \ .$$

As standard procedure, the intensity of the polarized radiation is measured at $\varphi = 0^\circ$ and $\varphi = 90^\circ$, and the linear polarization is defined as

$$P(\theta) = \frac{J_0(\varphi=0) - J_{90}(\varphi = 90^\circ)}{J_0(\varphi=0) + J_{90}(\varphi = 90^\circ)} \ . \qquad 2.30$$

The intensities J_0 and J_{90} are given by Equation 2.29 which, when combined with Equation 2.30, gives

$$P(\theta) = \frac{\sum_K (-1)^{I-J+K/2} \rho_{KO} \left[\begin{array}{l} (\pm)_L Z_1(LL,K) K_K(LL) - (\pm)_{L'} \\ 2\delta Z_1(LL',K) K_K(LL') \\ +(\pm)_{L'} \delta^2 Z_1(L'L',K) K_k(L'L') \end{array} \right] P_K^{(2)} (\cos\theta)}{\sum_K a_K P_K(\cos\theta)}$$

2.31

where the a_K are defined as in Equation 2.25b. Numerical values for the K_K's and $P_K^{(2)}$'s are given in references [21] and [55].

Careful inspection of Equation 2.31 reveals that

$$P[E(L)M(L')] = -P[M(L)E(L')] \ . \qquad 2.31a$$

That is, the sign of the linear polarization changes according to whether the higher multipolarity is electric or magnetic. Therefore, for cases involving a known mixing ratio, and assuming that the parity of the final level is known, the parity of the emitting level can be

obtained by determining the sign of the linear polarization. Under normal circumstances, polarization measurements are made at only one angle, $\theta = 90°$. At this angle, $P_2^{(2)}(0)$ is maximum, and a_2 is very often larger than a_4 and a_6. In such cases, the linear polarization is largest at right angles to the incident beam. However, for situations in which a_2 and a_4 are comparable, the linear polarization may be largest at some angle other than $90°$ [47]. In any event, after substituting the appropriate values for $K_K(LL')$, $P_K(\cos\theta)$, and $P_K^{(2)}(\cos\theta)$, the expression for the linear polarization at $\theta = 90°$ may be written explicitly for the following cases: (i) M1E2 radiation

$$P(90°) = \frac{\dfrac{-(-1)^{I-J}}{(1+\delta^2)}\left\{3\rho_{20}\left[\dfrac{\frac{1}{2}Z_1(11,2)+\frac{1}{3}\delta Z_1(12,2)}{+\frac{1}{2}\delta^2 Z(22,2)}\right]-5\rho_{40}\delta^2 Z_1(22,4)\right\}}{8}}{1+\dfrac{(-1)^{I-J}}{(1+\delta^2)}\left\{\dfrac{\rho_{20}}{2}\left[\dfrac{Z_1(11,2)-2\delta Z_1(12,2)}{+\delta^2 Z_1(22,2)}\right]+3\rho_{40}\delta^2 Z_1(22,4)\right\}}{8}} \qquad 2.32$$

where $P_i(\cos\theta) = 1$ and $P_0^{(2)}(\cos\theta) = 1$ for all θ.

(ii) For M2E3 radiation

$$P(90°) = \frac{\dfrac{(-1)^{I-J}}{(1+\delta)^2}\left\{-3\rho_{20}\left[-\frac{1}{2}Z_1(22,2)+\frac{1}{2}\delta Z_1(23,2)\right.\right.}{\left.\left.+\frac{1}{3}\delta^2 Z_1(33,2)\right]-\frac{5\rho_{40}}{8}\left[\frac{1}{2}Z_1(22,4)+\frac{1}{16}Z_1(23,4)+\frac{1}{3}\delta^2 Z_1(33,4)\right]+\frac{\rho_{60}\delta^2 Z_1(33,6)}{30}\right\}}{1+\dfrac{(-1)^{I-J}}{(1+\delta^2)}\left\{\dfrac{\rho_{20}}{2}\left[\dfrac{Z_1(22,2)-2\delta Z_1(23,2)}{+\delta^2 Z_1(33,2)}\right]+\dfrac{3\rho_{40}}{8}\left[\dfrac{Z_1(22,4)-2\delta Z_1(23,4)}{+\delta^2 Z_1(33,4)}\right]+\dfrac{5\rho_{60}\delta^2 Z_1(33,6)}{16}\right\}} \qquad 2.33$$

where again

$$Z_1(LL',K) = Z_1(LJL'J,IK) \ .$$

Whenever the linear polarization and the angular correlation measurements are made under the same experimental conditions, the statistical tensors appearing in Equations 2.26 and 2.32 are identical, and so are those in Equations 2.27 and 2.33. Thus, Equations 2.32 and 2.33 may be rewritten in terms of the expansion coefficients, a_K, determined by the correlation measurements. For the special case of pure E2 radiation, either Equations 2.26 and 2.32 (with $\delta = \infty$) or Equations 2.27, 2.31a, and 2.33 (with $\delta = 0$) give

$$P_{E2}(90^\circ) = \frac{\frac{3}{2} A_2 + \frac{5}{8} A_4}{1 - \frac{1}{2} A_2 + \frac{3}{8} A_4} \ . \qquad 2.34$$

Suppose now the angular correlation measurements have failed to distinguish between sets of different values, $[J_1,\delta_1,P_1(m)]$ and $[J_2,\delta_2,P_2(m)]$, for the initial spin, mixing ratio, and population parameters involved in the transition $J \rightarrow I$. The linear polarization at 90° could be calculated using these different results and compared to an experimentally determined value. Such a comparison quite often will eliminate one set of the parameters. Also, once the mixing ratio and the sign of the linear polarization have been determined, the parity of the emitting level can be obtained, assuming the parity of the final state is known.

The remainder of this chapter deals with the construction and calibration of a Compton polarimeter which has been used in polarization measurements.

2.2 The Compton Linear Polarimeter

2.2.1 Design and construction. Several physical processes have been found to be useful for the detection of gamma ray polarization [21]. When judged by their frequency of application, the most important of these processes is the Compton effect. As shall be shown below, the Compton cross section is larger for scattering at right angles to the electric vector of the incident radiation. Therefore, an asymmetry can be measured between the total numbers of counts detected in two planes which are respectively parallel and perpendicular to the direction of the incident electric vector. This asymmetry is directly proportional to the linear polarization of the initial radiation.

The particular polarimeter construction for this work is similar to that of Taras et al. [57], and a diagram of the instrument is shown in Figure 2.1. The detectors consist of five identical NaI crystals with the center crystal serving to Compton scatter the incident gamma radiation. The scattered photons are detected in the outside crystals in coincidence with recoil electrons detected in the center crystal. There is no difference between the intensities of the scattered photons detected by the two vertical crystals, and the use of two such detectors instead of one serves simply to double the coincidence counting rate for a given period of time. The same is true of the horizontal crystals. Further details on the physical dimensions of the polarimeter will be given later in this section.

Figure 2-1 A diagram of the five crystal, NaI polarimeter

AC is the direction of propagation of the incident radiation whose energy is E_0

AD is the direction of propagation of the scattered radiation whose energy is E'

θ is the Compton scattering angle

η is the angle between AB and the projection AD onto the plane perpendicular to AC

$$d\sigma = \frac{r_0^2}{2} d\Omega \left(\frac{E'}{E_0}\right)^2 \left(\frac{E_0}{E'} + \frac{E'}{E_0} - 2\sin^2\theta\cos^2\eta\right)$$

$$A = \frac{N_V - N_H}{N_V + N_H}$$

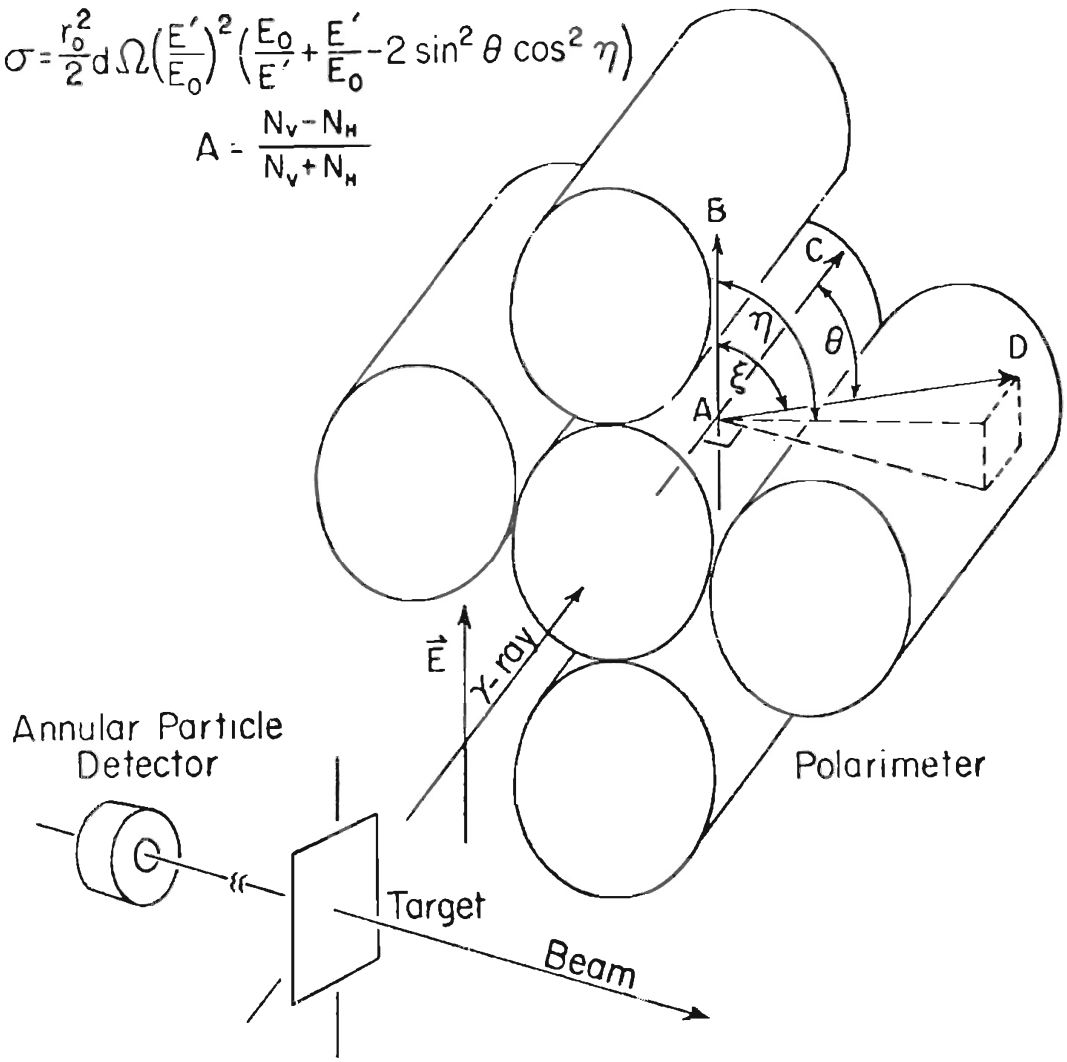

The sensitivity of the Compton effect to the polarization of the incident radiation can be obtained from the Klein-Nishina formula [20,39] which gives the differential cross section for the scattering process. The direction of polarization for the scattered photon is seldom of interest, so that the form of the Klein-Nishina formula most applicable is

$$d\sigma(\theta,\eta) = \frac{r_0^2}{2}\frac{E'^2}{E_0^2}\left[\frac{E_0}{E'} + \frac{E'}{E_0} - 2\sin^2\theta\cos^2\eta\right]d\Omega \qquad 2.35$$

where a summation has been made over all directions of polarization of the scattered gamma ray and where the following definitions apply (see Figure 2.1):

(1) $r_0 = e^2/m_0c^2$ = the classical radius of the electron.

(2) $d\Omega$ is the element of solid angle into which the photon is scattered.

(e) θ is the Compton scattering angle.

(4) η is the angle between the electric vector of the incident radiation and the plane containing the scattered photon (the ACD plane in Figure 2.1).

(5) ξ is the angle between the incident electric vector and the direction of propagation of the scattered photon ($\cos^2\xi = \sin^2\theta\cos^2\eta$).

(6) E_0 and E' are the energies of the incident and scattered photons, respectively. (Do not confuse E_0 and E' with $\bar{E}$, the electric vector of the incident radiation).

Now assume that the polarimeter of Figure 2.1 is composed of point sized detectors located infinitely far apart. The vertical crystals and the horizontal crystals lie in two mutually perpendicular planes, and the center crystal lies at some point along the line of intersection of these two planes. In their respective planes, the vertical and horizontal crystals may be positioned to detect radiation scattered at some angle, θ, from the center crystal. However, these photons will have resulted from the scattering of incident photons with either $\eta = 0°$ or $\eta = 90°$. Equation 2.35 shows that $d\sigma(\theta,\eta)$ is largest when $\eta = 90°$ and smallest for $\eta = 0°$. Therefore, the incident radiation is perferentially scattered at right angles to its electric vector so that, if the incident radiation is polarized, there will be a difference between the total numbers of scattered photons, N_V and N_H, detected by the vertical and horizontal crystals, respectively. N_V and N_H may be written as follows in terms of the scattering cross section and the incident gamma ray intensities, J_0 and J_{90}, defined in Equation 2.30.

$$N_V = J_{\varphi=0°} d\sigma(\theta,\eta=90°) + J_{\varphi=90°} d\sigma(\theta,\eta=0°)$$

and

$$N_H = J_{\varphi=0°} d\sigma(\theta,\eta=0°) + J_{\varphi=90°} d\sigma(\theta,\eta=90°) . \qquad 2.36$$

The angles φ and η are easily confused, and it is worthwhile to define them once again. φ is the angle between the reaction plane and the electric vector of the incident radiation. η is the angle between the electric vector of the incident radiation and the

scattering plane. The fractional asymmetry in the total number of counts detected by the vertical and horizontal crystals is defined as

$$A = \frac{N_V - N_H}{N_V + N_H} . \qquad 2.37$$

Equations 2.36 and 2.37 give

$$A = \frac{[d\sigma_{90}(\theta) - d\sigma_0(\theta)]}{[d\sigma_{90}(\theta) + d\sigma_0(\theta)]} \frac{(J_0 - J_{90})}{(J_0 + J_{90})} \qquad 2.38$$

or

$$A = S \cdot P \qquad 2.39$$

where

$$P = \frac{J_0 - J_{90}}{J_0 + J_{90}} \qquad 2.40$$

and

$$S = \frac{d\sigma_{90}(\theta) - d\sigma_0(\theta)}{d\sigma_{90}(\theta) + d\sigma_0(\theta)} . \qquad 2.41$$

P is just the linear polarization of the incident radiation as defined in Equation 2.30, and $S(\theta)$ is the polarization sensitivity. For this point scattering (p.s.) geometry and with $\theta = 90^\circ$, Equation 2.41 becomes

$$S_{p.s.} = \left[\frac{1}{E_0/E' + E'/E_0 - 1} \right]_{\theta = 90^\circ} \qquad 2.42$$

As a function of the incident gamma ray energy, E_0, $S_{p.s.}$ is the maximum value possible for the polarization sensitivity. With this geometry, the polarimeter attains its greatest sensitivity to the linear polarization of the incident radiation.

Obviously, the point scattering geometry described above represents an ideal case, and any physically reasonable polarimeter must be constructed with a finite scattering geometry. For such a polarimeter, the angles θ and η have finite ranges, and the polarization sensitivity is reduced by solid angle effects. Therefore, the new polarization sensitivity must be determined over some suitable range of incident photon energies. Once this is done, the linear polarization of any incident gamma ray may be found by measuring an experimental asymmetry, A, and then using Equation 2.39 with an appropriate value of $S(E)$. The calibration of the polarimeter used in this work is discussed in detail in the next section of this chapter.

The five detectors which comprise the polarimeter are identical 1.5 by 2.0 inch NaI crystals mounted as shown in Figure 2.1 inside a circular lucite holder. The outside crystals were shielded from the incident radiation by 5.0 cm of lead. The entire polarimeter was shielded from background radiation incident from the sides by 1.3 cm of lead, and the polarimeter could be rotated inside the lead shielding about a concentric axis through the center of the middle crystal. For reasons given earlier, all experimental measurements were made with the polarimeter positioned at 90° with respect to the beam axis. The distance between the target and the face of the center crystal was 15 cm.

Signals from the polarimeter were processed using the circuit shown in Figure 2.2. A main amplifier was used with each gamma ray detector to facilitate gain-matching between the five crystals. Acceptable events were those which produced a coincidence between the particle detector, the center crystal and either the horizontal or the vertical crystals, but not both. For each such event, five pieces of digital information were generated corresponding to the particle energy, the recoil electron energy from the center crystal, the scattered photon energy from a side crystal, the time difference for the particle-center crystal coincidence, and a routing signal which identified the scattering plane as vertical or horizontal. A DDP-224 computer was used to store this information event-by-event on magnetic tape for later use in off-line data analysis. This analysis consisted of reading back a magnetic tape subject to appropriate restrictions placed on the particle and time spectra. Also, upper and lower threshold levels could be set on the center and outside gamma ray detectors in order to limit the range of acceptable Compton scattering angles. The gamma ray pulse-height spectra generated in this manner correspooded to the sum of the energy signals from either the center and vertical or the center and horizontal detectors. These spectra were used to determine the experimental asymmetries, A, which were in turn used with Equation 2.39 to obtain the experimental linear polarizations.

2.2.2 Calibration. The polarimeter was first checked for instrumental asymmetries by measuring the experimental asymmetry for

Figure 2.2 A diagram of the electronic circuit used with the NaI polarimeter

AMP main amplifier

TFA timing filter amplifier

TSCA timing single channel analyzer

FAST DISC constant fraction discriminator

OR summing amplifier

TAC time-to-amplitude converter

AND overlap coincidence

GATE linear gated stretcher

SUM summing amplifier

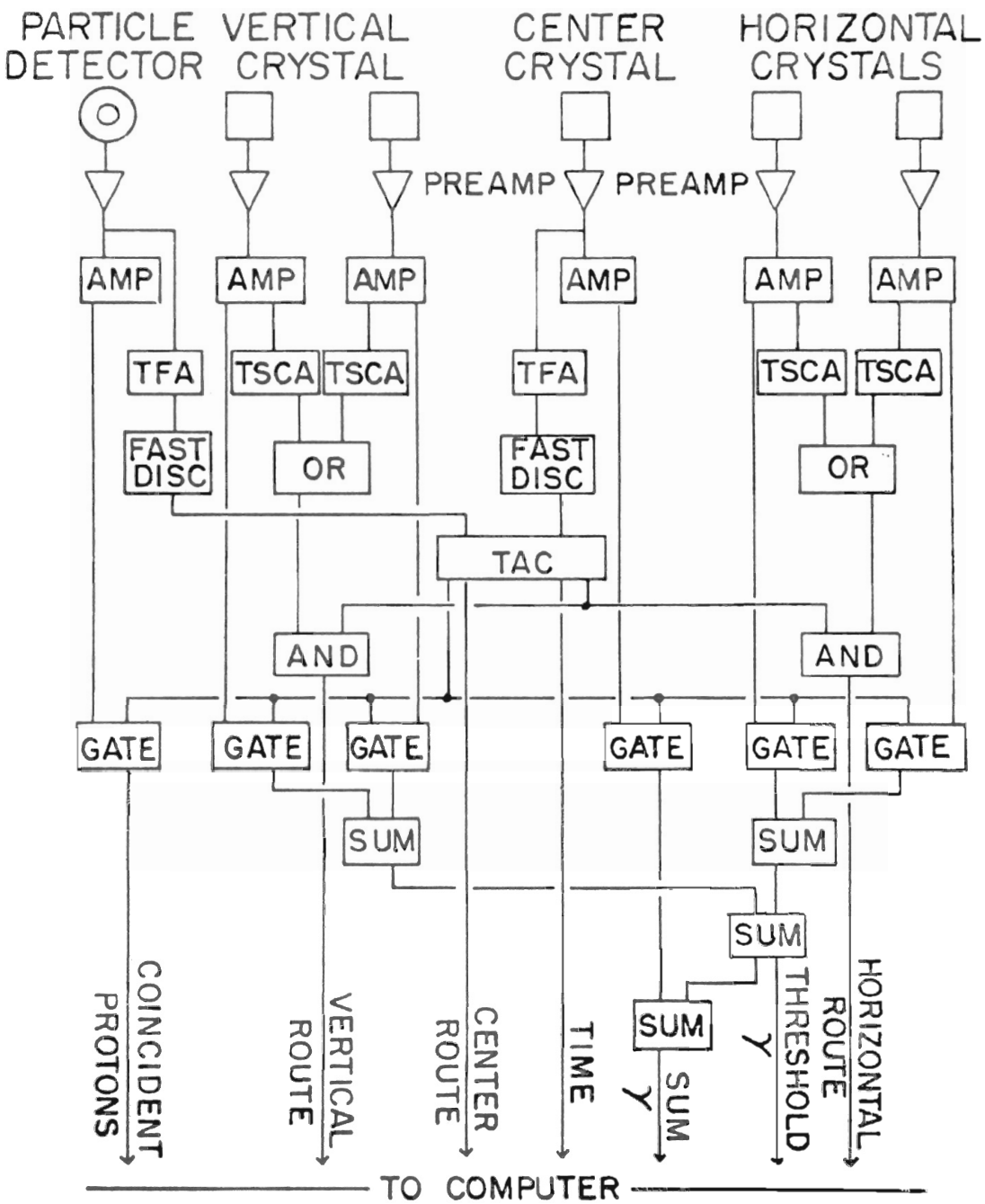
PARTICLE DETECTOR
VERTICAL CRYSTAL
CENTER CRYSTAL
HORIZONTAL CRYSTALS
PREAMP
PREAMP
AMP
AMP
AMP
AMP
AMP
AMP
TFA
TSCA
TSCA
TFA
TSCA
TSCA
FAST DISC
OR
FAST DISC
OR
TAC
AND
AND
GATE
GATE
GATE
GATE
GATE
GATE
SUM
SUM
SUM
SUM
COINCIDENT PROTONS
VERTICAL ROUTE
CENTER ROUTE
TIME
SUM γ
SUM γ THRESHOLD
HORIZONTAL ROUTE
TO COMPUTER

a radioactive ^{22}Na source with the polarimeter in several different positions. Four such positions were obtained by successively rotating the polarimeter through an angle of 90°. For each position the measured asymmetry was found to be zero within the statistical errors.

The polarization sensitivity was determined over an incident radiation energy range of 0.45 - 4.43 MeV using gamma rays of known linear polarization. All except one of these calibration gamma rays were produced by inelastic proton scattering to the first 2^{+} state in several different even-even target nuclei. For appropriate bombarding energies, these excited states are populated in the inelastic channel by the decay of an s-wave ($\ell = 0$) resonance. Thus, alignment of the residual nucleus is assured, and there is no need to detect the scattered protons along the beam axis. Each of these 2^{+} states decays by the emission of pure E2 radiation. Therefore, if the angular distribution of the emitted gamma ray is measured for the same experimental conditions used in the polarization measurement, Equation 2.34 may be used to calculate the linear polarization of the radiation.

The 1.33 MeV gamma ray from the β^{-}-decay of ^{60}Co was scattered through an angle of $70^{\circ} \pm 10^{\circ}$ in order to produce the remaining, low energy calibration point. The energy of the scattered radiation was 0.45 - 0.50 MeV, and its linear polarization was determined using the Klein-Nishina formula (Equation 2.35). Information on all the calibration gamma rays is summarized in Table 2.1.

Table 2 1 Calibration reactions for the NaI polarimeter

REACTION[a]	BOMBARDING ENERGY (MeV)	GAMMA RAY ENERGY (MeV)	POLARIZATION
$^{56}Fe(p,p'\gamma)$	3.01	0.847	$+0.56 \pm 0.03$
$^{48}Ti(p,p'\gamma)$	3.01	0.985	$+0.58 \pm 0.03$
$^{24}Mg(p,p'\gamma)$	3.01	1.368	$+0.78 \pm 0.03$
$^{28}Si(p,p'\gamma)$	3.01	1.78	$+0.80 \pm 0.03$
$^{12}C(p,p'\gamma)$	5.37	4.43	$+0.97 \pm 0.02$
$^{60}Co \xrightarrow{\beta^-} {}^{60}Ni$		0.45 - 0.50	$+0.39 \pm 0.03$

[a]All targets very thick

For each of these gamma rays, an experimental asymmetry was measured, and the corresponding polarization was then determined using Equation 2.39. The results of these measurements are shown as the data points in Figure 2.3.

The polarimeter was also calibrated with a computer code which averaged the expression for S given in Equation 2.41 over the finite geometry of the instrument [45,56]. The result of this calculation is shown as the lower curve in Figure 2.3 where the 200 KeV threshold was applied to each of the outside crystals. The best fit of this curve to the experimental data required no arbitrary normalization. The curve is shown as calculated. The remaining curve in Figure 2.3 is shown only for comparison purposes and is a plot of Equation 2.42 which gives the polarization sensitivity for the point scattering geometry with $\theta = 90^{\circ}$.

When threshold levels are placed on the five crystals of the polarimeter, the effect is to restrict the range of acceptable Compton scattering angles. This is equaivalent to changing the geometry of the polarimeter so that it more nearly resembles the situation for point scattering. For instance the application of either a lower level threshold to the center crystal or an upper level threshold to the outside crystals excludes small angle Compton scattering. This same result could be achieved by decreasing the length of the outside crystals. Under normal circumstances, the polarization sensitivity increases as a function of the threshold setting until, depending upon the geometry of the system, some combination of settings is found for which S is maximum [5]. The

Figure 2.3 The calibration curve for the NaI polarimeter showing the polarization sensitivity as a function of the energy of the incident radiation. For comparison purposes, the curve labeled "Point Scattering Geometry" was obtained by plotting the equation shown at the top of the figure.

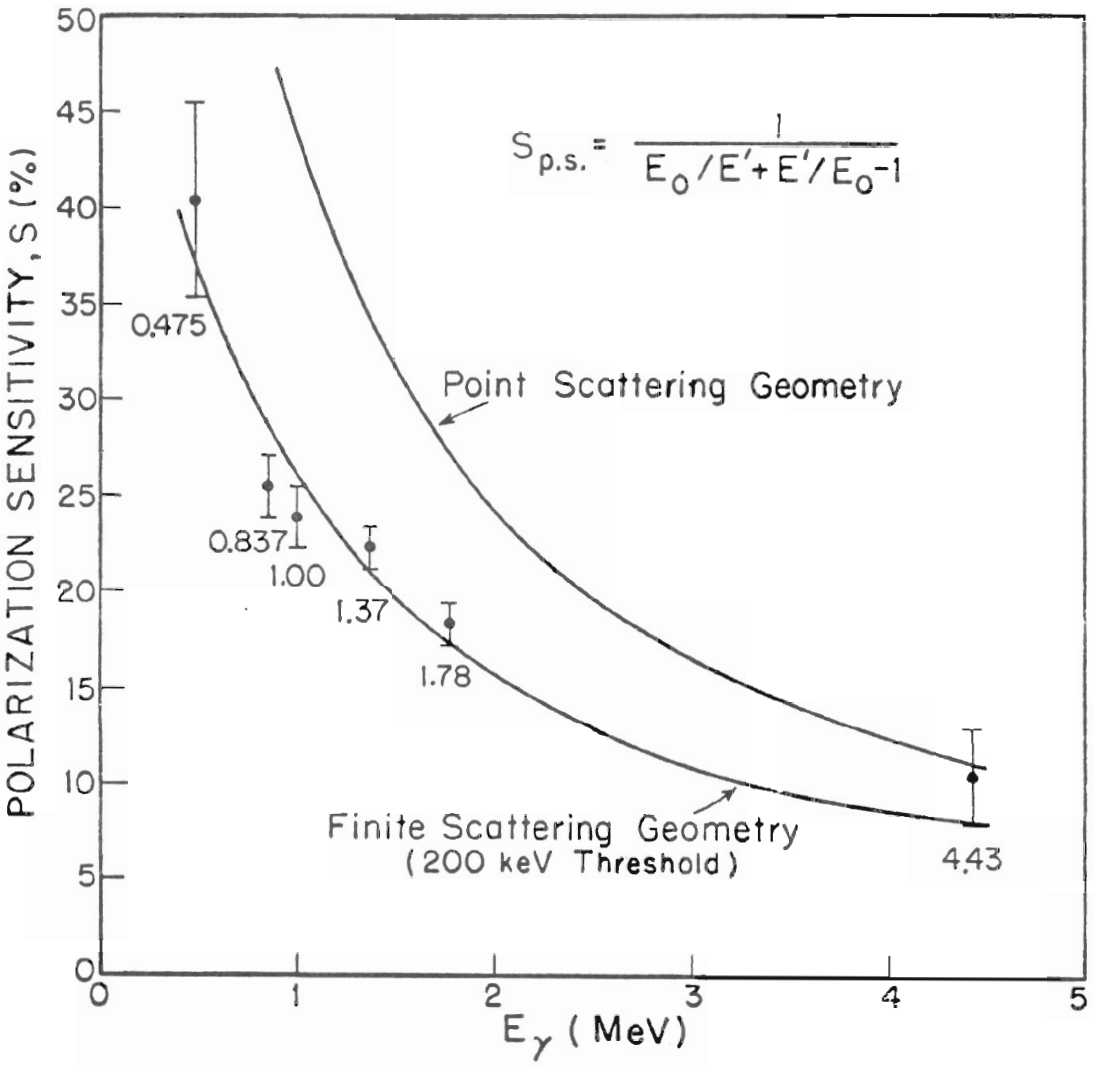
POLARIZATION SENSITIVITY, S (%)
$S_{p.s.} = \frac{1}{E_0/E' + E'/E_0 - 1}$
0.475
0.837
1.00
1.37
1.78
4.43
Point Scattering Geometry
Finite Scattering Geometry
(200 keV Threshold)
E_γ (MeV)

threshold levels chosen for a particular polarimeter must be weighed against counting rate considerations. However, once the settings are selected during the calibration procedure, they should be carefully maintained through all subsequent measurements.

After completion of the calibration process described above, the polarimeter was ready for incorporation into a general research program in gamma ray spectroscopy. The polarimeter was first used to resolve spin and mixing ratio ambiguities in ^{29}Al . The results of these measurements are the subject of Chapter 3.

3. LINEAR POLARIZATION MEASUREMENTS ON ^{29}Al

3.1 Review of the ^{29}Al Nucleus

The ^{29}Al nucleus lies in a region of the 2s-1d shell where there is considerable interest as to the applicability of the different nuclear models. Many particle shell model calculations have been made in the mass region A = 27 to 30 by de Voigt et al. [17] who used wave functions calculated with the Oak Ridge - Rochester shell model codes. These calculations were based upon a truncated $1d\frac{5}{2}$, $2s\frac{1}{2}$, $1d\frac{3}{2}$ configuration space with a maximum of four holes in the $1d\frac{5}{2}$ subshell. The modified surface delta interaction (MSDI) was used as the effective two-body interaction.

Nuclei in the mass region near A = 22 have been well described by the Nilsson strong-coupling model which assumes the single, odd nucleon to be coupled to a strongly deformed, prolate core. Theoretical calculations based on the low-lying rotational bands which result from such a description agree very well with experimental measurements.

However, the single particle Nilsson model has been much less successful when applied to nuclei of the 2s-1d shell with $A \geq 27$. Studies of ^{28}Si and ^{29}Si have suggested that these two nuclei may be described in terms of weak oblate core shapes, and, for this reason, the mass region near A = 28 - 29 is believed to constitute a region of transition from prolate to oblate deformation [28].

At the time the present work was undertaken, the available experimental information on the states in ^{29}Al below 3.6 MeV excitation energy was as summarized in Figure 3.1 and Table 3.1. The

Figure 3.1 Experimental information available for the states in ^{29}Al below 3.6 MeV at the time the present work was begun

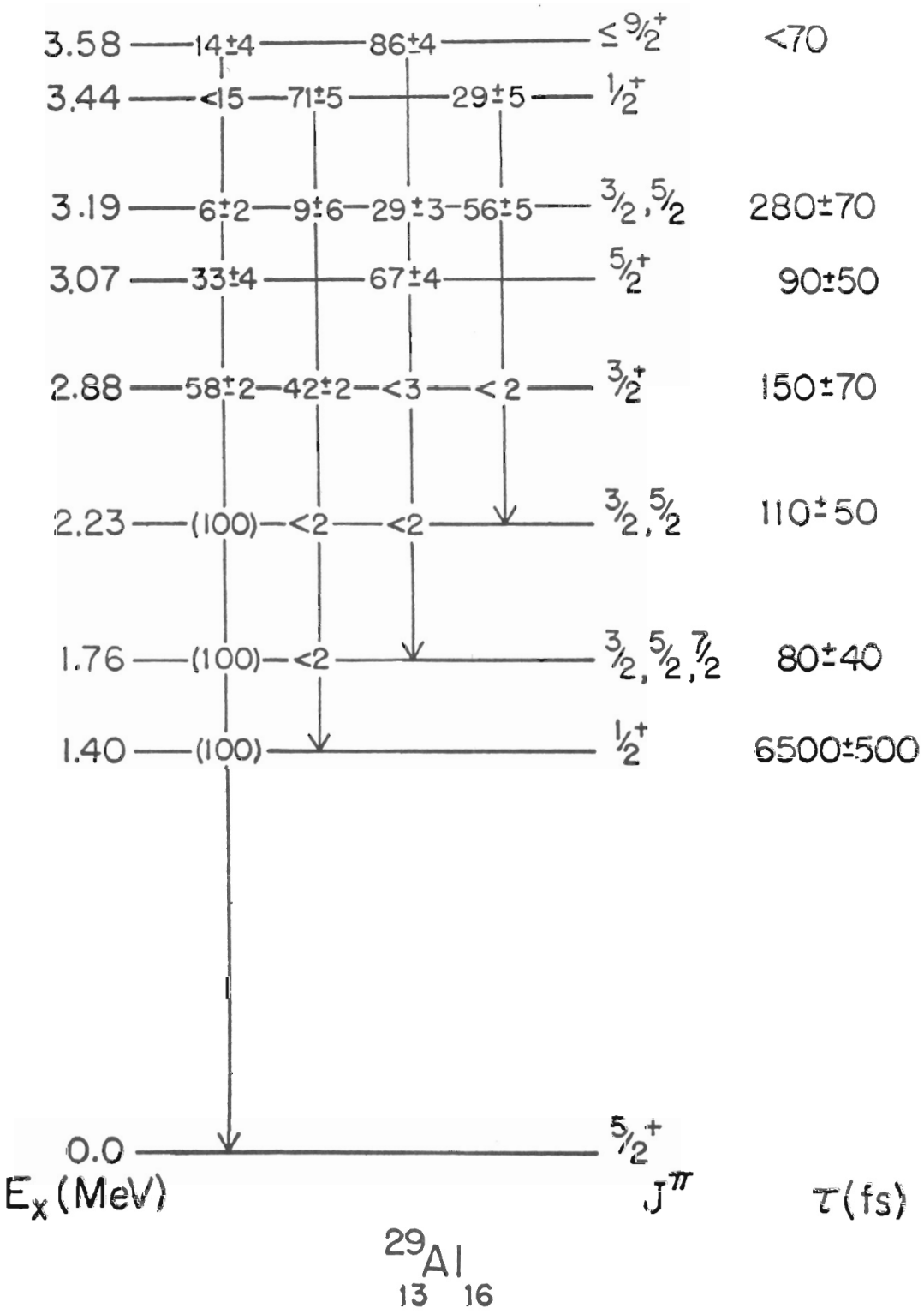
3.58
14±4
86±4
≤9/2+
<70
3.44
<15
71±5
29±5
1/2+
3.19
6±2
9±6
29±3
56±5
3/2, 5/2
280±70
3.07
33±4
67±4
5/2+
90±50
2.88
58±2
42±2
<3
<2
3/2+
150±70
2.23
(100)
<2
<2
3/2, 5/2
110±50
1.76
(100)
<2
3/2, 5/2, 7/2
80±40
1.40
(100)
1/2+
6500±500
0.0
5/2+
Ex (MeV)
Jπ
τ(fs)

$^{29}_{13}Al_{16}$

Table 3.1 Available experimental information for the low-lying states in ^{29}Al at the beginning of the present work

E_x	TRANSITION	J_i	J_f	δ
1.40	1.40 → 0	1/2	5/2	
1.76	1.76 → 0	3/2	5/2	$0.22 \begin{smallmatrix} + 0.10 \\ - 0.06 \end{smallmatrix}$
				$2.2 \begin{smallmatrix} + 0.4 \\ - 0.5 \end{smallmatrix}$
		5/2	5/2	$0.20 \begin{smallmatrix} + 0.06 \\ - 0.07 \end{smallmatrix}$
		7/2	5/2	-0.24 ± 0.03
2.23	2.23 → 0	3/2	5/2	0.33 ± 0.20[a]
				1.9 ± 0.7[a]
		5/2	5/2	0.16 ± 0.08
2.88	2.88 → 1.40	3/2	1/2	$0.0 \begin{smallmatrix} + 0.13 \\ - 0.08 \end{smallmatrix}$
				1.7 ± 0.5

[a] Mid-range values from reference [37]

spin and parity assignments for the ground state and the first excited state are from references [28,33] and [6 ,35], respectively. The J^{π} value assigned to the level at 2.88 MeV is from Jones et al. [35] while the positive parity of the eighth excited state (3.58 MeV) was determined by Jaffe et al. [33] who observed $\ell = 2$ particle transfer leading to the population of this level in the $^{27}Al(t,p)^{29}Al$ reaction. The lifetimes and branching ratios are, respectively, from Beck et al. [7] and Hirko et al. [28]. The spins and mixing ratio of Table 3.1 are taken from references [28] and [37].

Unlike the situation for many of the other mass 27 to 30 nuclei, there still existed many ambiguities concerning the spins, parities, and mixing ratios of the low-lying levels in ^{29}Al [17]. The failure of the angular correlation measurements to distinguish between the different spins of the various excited states can be attributed to the high ground state spin ($J = 5/2$) . In such cases, there is a characteristic insensitivity of the gamma ray angular distribution to the spin of the emitting level. These uncertainties in the experimental results have not enabled a choice as to which model best describes ^{29}Al .

The linear polarization measurements discussed in the present work were made in an attempt to clarify the ambiguities described above thus making more feasible the comparisons between experiment and theory.

3.2 Experimental Procedure

Excited states in ^{29}Al were studied with the reaction $^{26}Mg(\alpha,p\gamma)^{29}Al$. The targets were prepared by vacuum deposition of

99.7 percent isotopically pure ^{26}Mg onto 2-$\mu g/cm^2$ ^{12}C foils. These targets were bombarded with an 11.26 MeV alpha particle beam produced by the T.U.N.L. model FN tandem Van de Graaff accelerator. The signal handling arrangement was the same as that of Figure 2.2. As shown in Figure 3.2, the NaI polarimeter was positioned at right angles to the incident beam, and the outgoing protons were detected at 180° with an annular silicon detector. A two mil mylar foil positioned in front of the particle detector served to stop the backscattered alpha particles.

Particle-gamma-gamma coincidence data were accumulated over a 38 hour period and stored in buffered form on magnetic tape as described in Section 2.2. An energy versus channel number calibration was made for the analog-to-digital converter (ADC) used to process the energy signals (labeled "Threshold γ" in Figure 2.2) from the outside detectors of the polarimeter. This calibration curve allowed the off-line data analysis to be performed under threshold conditions identical to those used during the calibration process.

3.3 Analysis and Results

The data stored on magnetic tapes were analyzed in the following manner. First, the tapes were read back, and a pulse height versus channel number spectrum was produced which corresponded to the time difference between the detection of a particle in the annular detector and either the photoelectric absorption or the Compton scattering of an incident gamma ray by the center crystal of the polarimeter. Such time spectra contain a well-defined peak corresponding to coincidences between protons and gamma rays associated with the population and

Figure 3.2 Top view of the target chamber showing the relative positions of the NaI polarimeter and the solid state particle detector

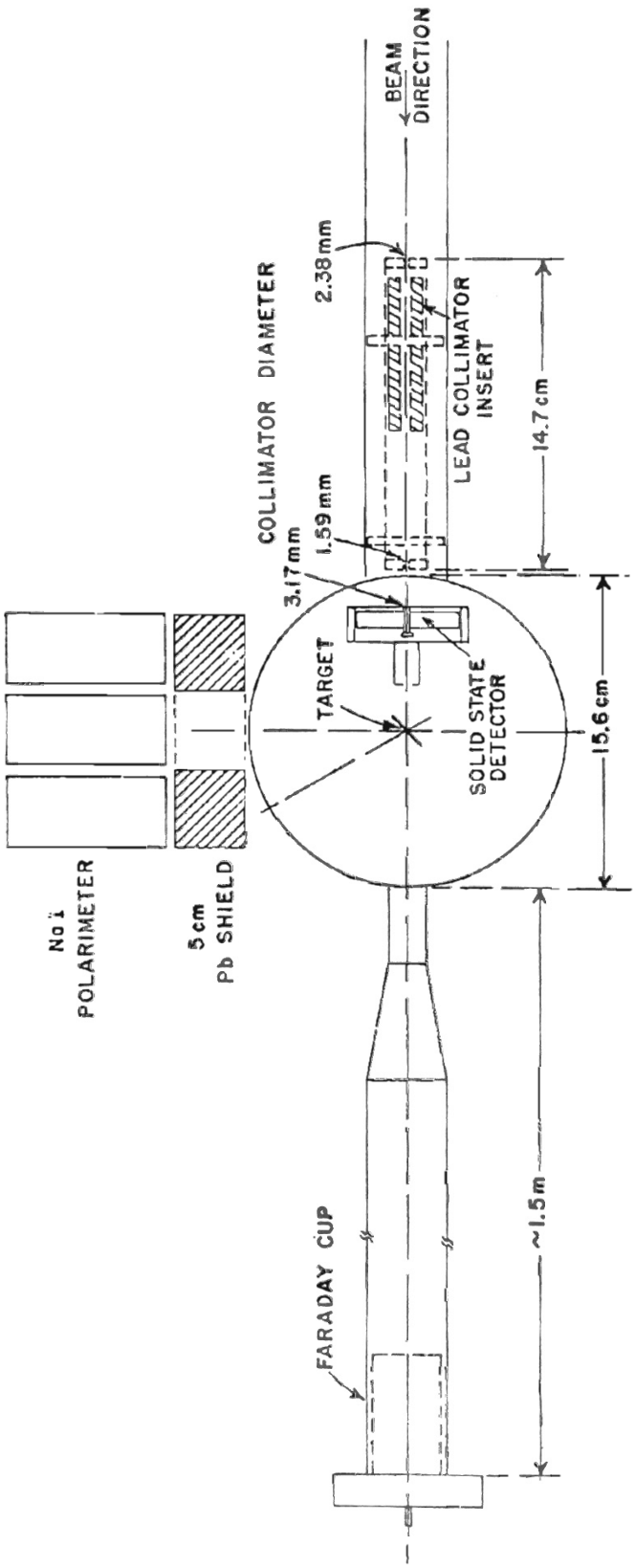

TOP VIEW OF CORRELATION CHAMBER

Figure 3.3 Coincident proton spectrum from the $^{26}Mg(\alpha,p\gamma)^{29}Al$ reaction. The peaks are numbered according to the level populated in the residual nucleus.

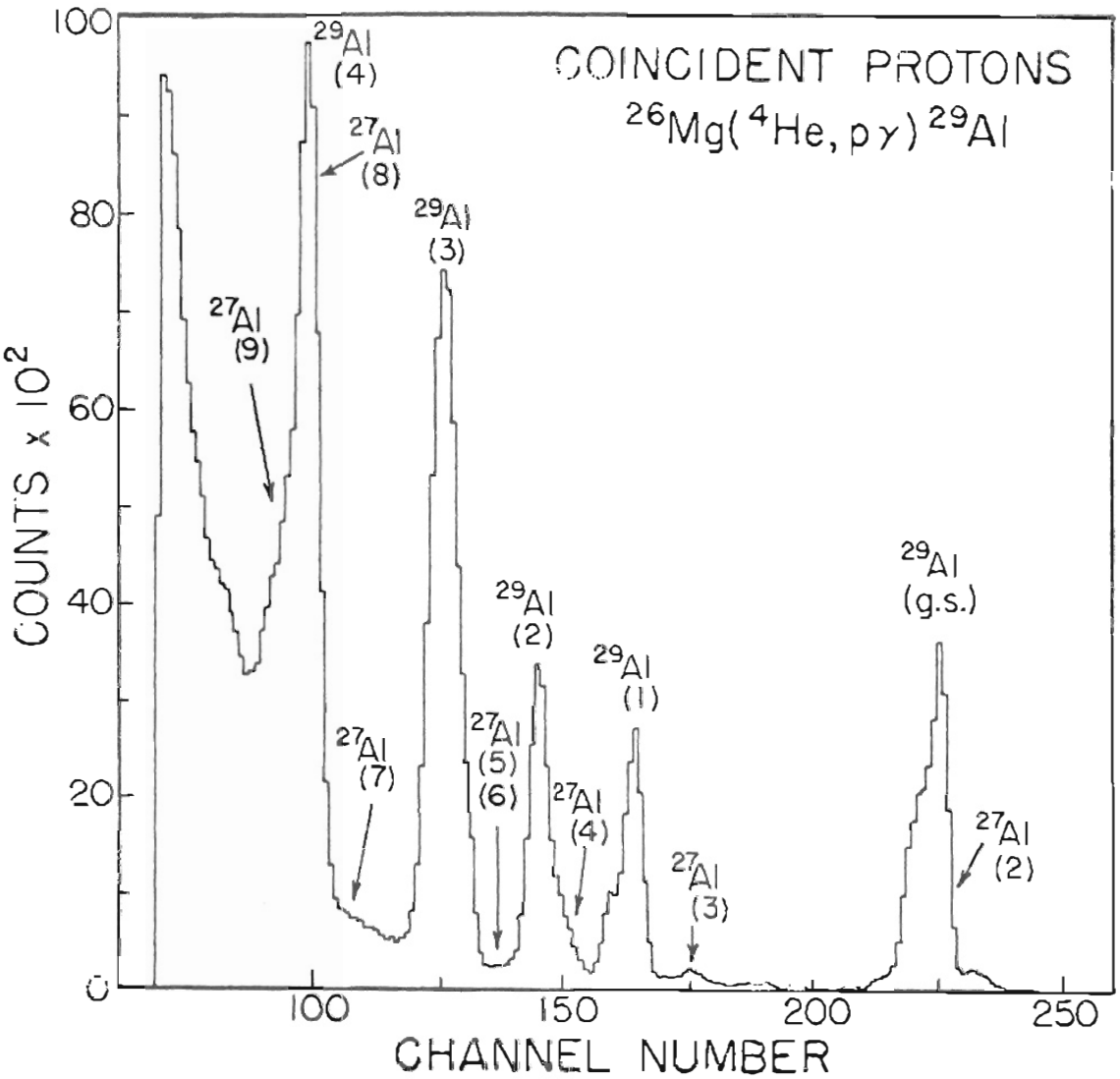
COINCIDENT PROTONS
$^{26}Mg(^{4}He, p\gamma)^{29}Al$
^{29}Al (4)
^{27}Al (8)
^{29}Al (3)
^{27}Al (9)
^{29}Al (2)
^{29}Al (1)
^{29}Al (g.s.)
^{27}Al (7)
^{27}Al (5) (6)
^{27}Al (4)
^{27}Al (3)
^{27}Al (2)
COUNTS x 10^2
CHANNEL NUMBER
0
20
40
60
80
100
100
150
200
250

Figure 3.4 Coincident gamma ray spectra from the ground state decay of the 2.23 MeV level in ^{29}Al . The photopeaks in the top two spectra were produced by summing the energy signals obtained from a Compton scattering event involving the center crystal of the polarimeter and one of either the horizontal or vertical sets of outside crystals.

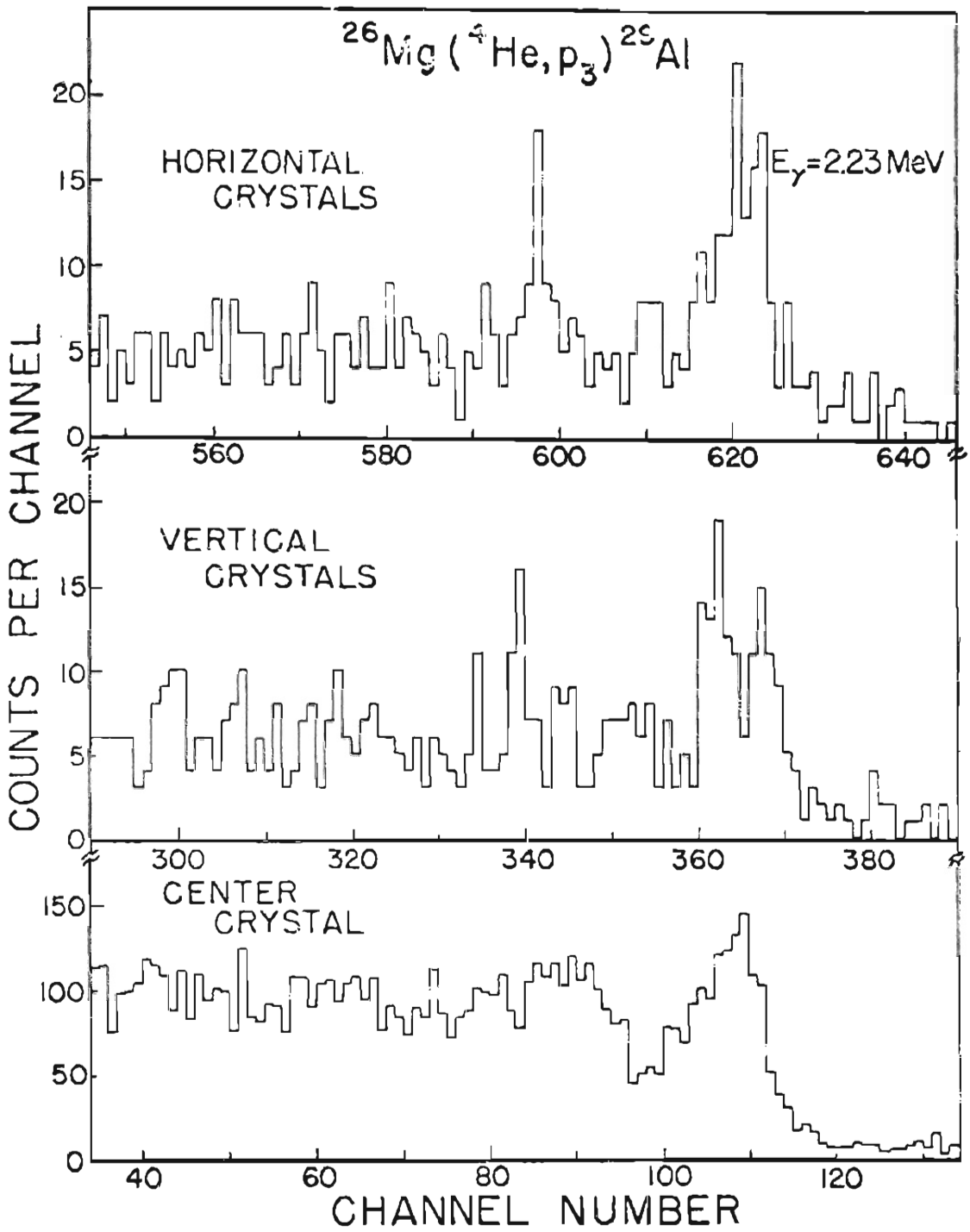
$^{26}Mg(^{4}He,p_3)^{29}Al$
HORIZONTAL CRYSTALS
E_γ=2.23 MeV
VERTICAL CRYSTALS
CENTER CRYSTAL
COUNTS PER CHANNEL
CHANNEL NUMBER

decay of a particular excited state, and this peak rests on a uniform background created by random coincidences between unrelated particles and gamma rays.

Next, a proton spectrum was generated which contained only those counts whose time parameter fell within an appropriate window set about the peak of the time spectrum. Proton counts resulting from chance coincidences were removed from this spectrum by subtracting any count having a time parameter within a second window set in the random background of the time spectrum. The widths of these "real" and "random" windows were equal. The proton spectrum produced in this manner is shown in Figure 3.3 where the various groups are labeled according to the level populated in the residual nucleus. As can be seen the first four excited states were populated reasonably well.

The gamma ray spectra shown in Figure 3.4 for the 100 percent ground state decay of the third excited state were produced subject to a particle window placed about the appropriate proton group in Figure 3.3. Also, and in addition to the time restrictions described above, these spectra met threshold requirements placed on the energy signals from the outside crystals of the polarimeter. The top and middle spectra represent, respectively, full energy events produced when scattered photons are detected in the horizontal or vertical crystals. The bottom spectrum represents gamma rays absorbed photoelectrically by the center crystal, and this spectrum is shown only for comparison purposes.

For the decay of each excited state, spectra corresponging to vertical and horizontal scattering were produced by simply choosing a particle window for the correct proton group. The numbers of photons scattered vertically, N_V , and horizontally, N_H , were then extracted and used in Equation 2.37 to calculate the experimental asymmetry, A . This assymmetry was in turn used with Equation 2.39 to obtain the experimental linear polarization. An appropriate value of S , the polarization sensitivity, was taken from the calibration curve shown in Figure 2.5.

The $^{26}Mg(\alpha, p\gamma)^{29}Al$ reaction, when used with a colinear detection geometry for the protons, populates only $\pm 1/2$ magnetic substrates for levels in the residual ^{29}Al nucleus (see Equation 2.15). Therefore, assuming the spin and parity of the final state are known, the linear polarization of a resulting gamma ray depends only upon the spin and parity of the initial state and the multipole mixing ratio of the emitted radiation. For each possible spin and parity, the linear polarization may be calculated as a function of the mixing ratio using the equation of Section 2.12. These calculated values may then be compared to the experimental results in an attempt to eliminate certain spin, parity, and mixing ratio assignments.

3.3.1 The 1.40 MeV level. The radiation emitted in the ground state decay of this level must be unpolarized since the state has a definite J^π assignment of $1/2^+$. The measurement for this transition resulted in a polarization of $P(90^\circ) = -0.49 \pm 0.34$. When checked using unpolarized randiation from a radioactive source,

Figure 3.5 Results of the linear polarization measurements for three excited states in ^{29}Al. The dashed curves represent theoretically calculated polarizations assuming each state to have positive parity. Inversion of these curves gives the results for negative parity, and the solid portion of each curve subtends a range of the mixing ratio allowed by the angular correlation measurements of references [28] and [37]. The range of the measured polarization is shown as a shaded area whereever there is overlap with the values of the polarization calculated using spins and mixing ratios consistent with the angular correlation results.

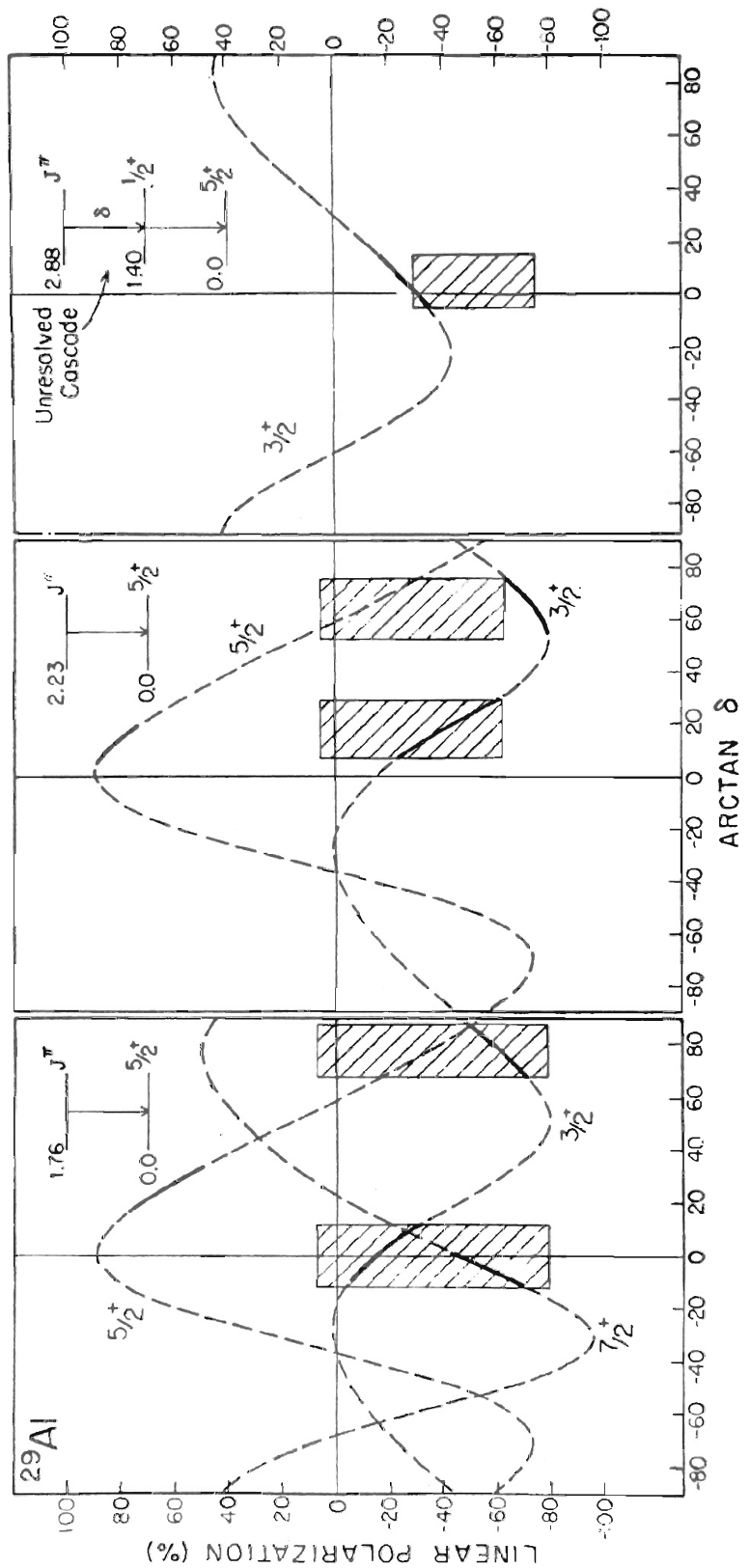
^{29}Al
LINEAR POLARIZATION (%)
ARCTAN δ
1.76
0.0
5/2+
5/2+
3/2+
7/2+
2.23
0.0
5/2+
5/2+
3/2+
Unresolved Cascade
2.88
1.40
0.0
1/2+
5/2+
δ
3/2+

the polarimeter was found to have zero instrumental asymmetry to within statistical errors, so that no ready explanation exists for the apparent discrepancy in the present measurement. However, this result is only slightly outside one standard deviation from zero, and since most of the results for the remaining three excited states do not depend critically upon the errors assigned to the measured polarizations, this descrepancy was not considered serious.

3.3.2 The 1.76 MeV level. Experimental results for the 1.76 → 0 MeV transition gave $P(90^\circ) = -0.35 \pm 0.43$. Assuming positive parity and using the spin limitations imposed on this level by the angular correlation measurements of Hirko et al. [28] and Kean et al. [37] theoretical values for $P(90^\circ)$ were calculated and plotted as a function of the mixing ratio, δ. These plots are shown on the left side of Figure 3.5 where the solid portions of each curve subtend the allowed ranges of the mixing ratio (see Table 3.1). The range of the measured polarization is shown as a shaded area wherever there is overlap with the values of the polarization calculated using spins and mixing ratios consistent with the angular correlation results. Inversion of the curves gives the calculated polarizations when the level is assumed to have negative parity (see Equation 2.31a).

As can be seen, the results of the polarization measurements allow only the following spin and parity assignments for the 1.76 MeV level: $7/2^+$, $5/2^-$, $3/2^+$ (including both ranges of δ), and $3/2^-$ (with the range of mixing ratios containing arctan $\delta = 0^\circ$).

The assignments, $3/2^-$ (with $65° \leq \arctan \delta \leq 85°$), $3/2^+$, and $7/2^-$ are all excluded.

Under the assumption of negative parity, E1M2 transition strengths were calculated for each possible spin using the equations of Section 1.1 and the appropriate lifetime, mixing ratio, and branching ratio from Figure 3.1 and Table 3.1. The M2 strengths in Weisskopf units (W.u.) assumed their smallest values when these calculations were performed using the largest and smallest allowed values for the lifetimes and mixing ratios, respectively. The following values were obtained for the M2 strengths: 58 W.u. ($3/2^-$, $\arctan \delta < 40°$), 1736 W.u. ($3/2^-$, $\arctan \delta > 50°$), 39 W.u. ($5/2^-$), and 99 W.u. ($7/2^-$). Each of these values is well above the upper limit of 3 W.u. set by Endt and van der Leun [19] in their tabulation of M2 strengths for nuclei with $A = 21 - 44$. For this reason then, the 1.76 MeV level was determined to have positive parity.

This result excluded two of the four J^π values allowed by the polarization measurement leaving either $7/2^+$ or $3/2^+$ as a possible assignment. For $J^\pi = 3/2^+$, notice that no distinction was made between the two different ranges of the mixing ratio. However, as shown in Figure 3.1, the level at 3.58 MeV decays to the 1.76 MeV level through an 86 percent branch, and there is evidence that the 3.58 MeV level has spin 9/2 [27]. Assuming this to be true, the $3/2^+$ assignment for the 1.76 MeV level is inconsistent since the radiation from the $3.58 \rightarrow 1.76$ MeV transition would be M3E4. Thus the spin-parity assignment for the 1.76 MeV level is most probably $7/2^+$.

3.3.3 The 2.23 MeV level. The results of the data analysis for this level are shown in the middle portion of Figure 3.5 where the range of the measured polarization is -0.29 ± 0.34 . The J^{π} values, $3/2^{+}$ (including both ranges of δ) and $5/2^{-}$, are allowed by the polarization measurement while the values, $3/2^{-}$ (also for both ranges of δ) and $5/2^{+}$, are ruled out. Once again, assuming the 2.23 MeV level to have negative parity, M2 transition strengths were calculated for each possible spin assignment. The following results were obtained: 9 W.u. ($3/2^{-}$, arctan $\delta < 40^{\circ}$) , 317 W.u. ($3/2^{-}$, arctan $\delta > 40^{\circ}$) , and 3.5 W.u. ($5/2^{-}$) . While the M2 strength for the $5/2^{-}$ assignment is only slightly larger than the 3 W.u. upper limit set by Endt and van der Leun, it must be remembered that this value was calculated using the most unfavorable assumptions concerning the lifetime and mixing ratio. Also, the upper limit itself is some six times larger than any measured M2 strength tabulated by Endt and van der Leun. Therefore, on the basis of these arguments, the 2.23 MeV level was assigned positive parity and, once this was done, the spin can be limited to 3/2 although there remain two possible ranges for the mixing ratio.

3.3.4 The 2.88 MeV level. The energy level diagram of Figure 3.1 shows that this level decays to the ground state through a 58 percent branch and to the 1.40 MeV , first excited state through a 42 percent branch. As stated in Section 3.2, data was taken for the polarization measurements over a 38 hour period. However, because of the reduced detection efficiency of the polarimeter, the

counting statistics accumulated during this time for the 2.88 → 0 MeV transition were not sufficient to permit a reliable measurement of the linear polarization. Therefore, a polarization measurement was made only on the radiation resulting from the 42 percent branch of the 2.88 MeV level to the first excited state. The polarimeter was not capable of resolving the 1.48 and 1.40 MeV gamma rays which resulted from the 2.88 → 1.40 → 0 MeV cascade so that the polarization was actually measured for the unresolved pair of gamma rays. The spin of the first excited state is 1/2 which required the 1.40 MeV radiation to have an isotropic angular distribution. This in turn required that the radiation be unpolarized so that equal numbers of the 1.40 MeV gamma rays were scattered into the vertical and horizontal crystals of the polarimeter. Therefore, as can be seen from Equation 2.37, the effect of the 1.40 MeV radiation was to reduce the size of any asymmetry measured for the polarized 1.48 MeV gamma ray resulting from the 2.88 → 1.40 MeV transition. This reduced asymmetry in turn gave a smaller value for the measured polarization.

The theoretical values for the linear polarization were calculated only for the 2.88 → 1.40 MeV transition and therefore could not be directly compared to the measured values. The calculated values were corrected to correspond to the measured polarizations in the following manner. Suppose first that both the 1.48 and the 1.40 MeV gamma rays had isotropic distributions. Then, since the two radiations are from a cascade, their intensities at 90° would be equal. Let this intensity be A_0. In reality

however, the 1.48 MeV gamma ray has some non-isotropic angular distribution so that, in general, its intensity at 90° will be

$$A_0[1 + a_2P_2(\cos 90^\circ)]$$

or

$$A_0(1 - a_2/2)$$

since

$$P_2(\cos 90^\circ) = - 1/2 .$$

Note that only terms of order less than or equal to two are needed to describe the distribution since the spin of the 2.88 MeV level is 3/2 . The linear polarization of the cascade may be written as

$$P_{Lab}(90^\circ) = \frac{[A_0/2+FA_0(1-a_2/2)]-[A_0/2+(1-F)A_0(1-a_2/2)]}{[A_0/2+FA_0(1-a_2/2)]+[A_0/2+(1-F)A_0(1-a_2/2)]}$$

or

$$P_{Lab}(90^\circ) = \frac{(1 - a_2/2)(2F - 1)}{(2 - a_2/2)} \qquad 3.1$$

where F represents the fraction of the 1.48 MeV gamma rays scattered vertically, and (1 - F) represents the fraction scattered horizontally. Now the calculated polarization concerns only the 2.88 → 1.40 MeV transition and is written as

$$P_{Calc.}(90^\circ) = \frac{FA_0(1-a_2/2)-(1-F)A_0(1-a_2/2)}{FA_0(1-a_2/2)+(1-F)A_0(1-a_2/2)}$$

or

$$P_{Calc.}(90^{\circ}) = \frac{(1-a_2/2)(2F-1)}{(1-a_2/2)} \cdot \qquad 3.2$$

Equations 3.1 and 3.2 show that the theoretical values for the polarization correspond to the measured values when the calculated values are multiplied by the fraction

$$\frac{2 - a_2}{4 - a_2} .$$

This correction can be easily made since, for a given value of the mixing ratio, the calculation of the linear polarization first requires the calculation of the expansion coefficient, a_2 .

The corrected curve for the calculated polarization is shown on the right side of Figure 3.5 where the measured polarization for the unresolved cascade is $P(90^{\circ}) = - 0.51 \pm 0.22$. As can be seen, the results confirm the previously known $3/2^+$ spin-parity assignment, and, of the two previously allowed ranges for the mixing ratio, the range of larger values is eliminated.

3.4 Summary

Figure 3.6 shows the experimental situation for the low lying levels of ^{29}Al as it is now believed to exist. The J^{π} assignments are from the results of the present work which is based upon previous measurements made in references [6,7,28,33, and 35 - 37].

Also shown in Figure 3.6 are the results of shell model calculations performed by de Voigt et al. [17]. There is reasonable agreement between the calculated and experimental excitation

Figure 3.6 Experimental results and theoretical calculations for the low-lying levels of ^{29}Al

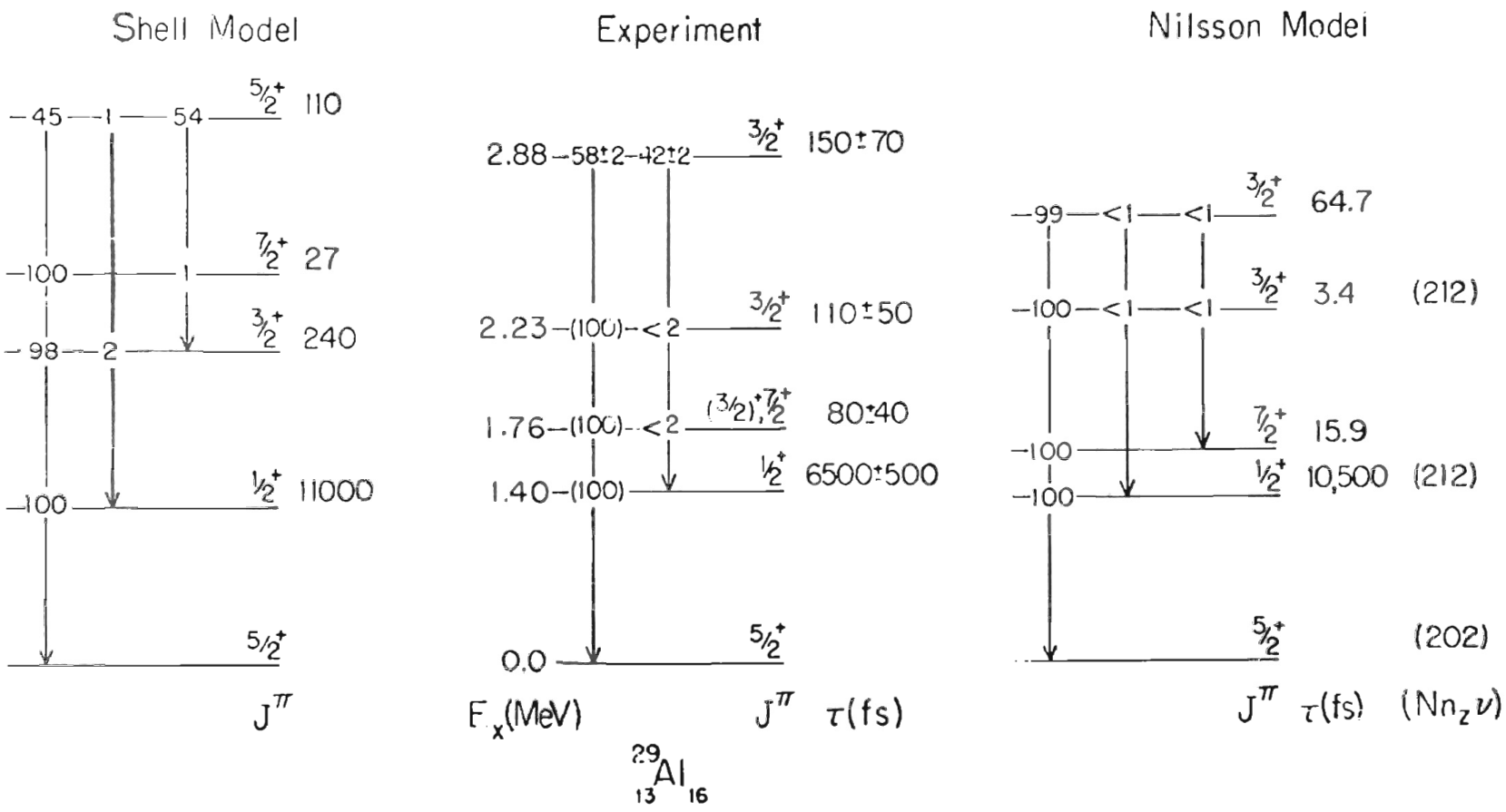
Shell Model
Experiment
Nilsson Model
-45 -1 -54 5/2+ 110
-100 -1 7/2+ 27
-98 -2 3/2+ 240
-100 1/2+ 11000
5/2+
Jπ
2.88 -58±2 -42±2 3/2+ 150±70
2.23 -(100) -<2 3/2+ 110±50
1.76 -(100) -<2 (3/2)+,7/2+ 80±40
1.40 -(100) 1/2+ 6500±500
0.0 5/2+
Ex(MeV) Jπ τ(fs)
29 13 Al 16
-99 -<1 -<1 3/2+ 64.7
-100 -<1 -<1 3/2+ 3.4 (212)
-100 7/2+ 15.9
-100 1/2+ 10,500 (212)
5/2+ (202)
Jπ τ(fs) (Nnzν)

energies. However, the theoretical and experimental spin sequences are inconsistent, and, as a result, there is also disagreement between the two sets of branching ratios. Shell model calculations for M1E2 transition strengths have been made only for the decay of the first excited state. Therefore, no comparison can be made with the experimental strengths measured for the higher excited states.

Both Jones et al. [36] and Hirko et al. [28] have presented Nilsson model interpretations of ^{29}Al assuming a prolate core deformation. Both works have proposed three low-lying rotational bands. A $K = 1/2$ band is based upon the $J^{\pi} = 1/2^{+}$ first excited state and includes the 2.88 MeV level as its $J = 3/2$ member. The level at 2.23 MeV is proposed as the bandhead of a $K = 3/2$ band while the level at 1.76 MeV is considered to be the second member of a $K = 5/2$ band based upon the $J^{\pi} = 5/2^{+}$ ground state. Clearly these interpretations are consistent with the experimental spin assignments of the present work.

Hilko et al. [27] have performed band mixing calculations for ^{29}Al based upon the band scheme described above. In addition to the three positive parity bands proposed by Kean and Hirko, two higher bands of positive parity and one of negative parity were mixed with the bandhead energies chosen to give the best agreement between the calculated and measured excitation energies for the low-lying levels. Their results are also shown in Figure 3.6 where the levels chosen as bandheads are labeled with their Nilsson quantum numbers $(Nn_z\Lambda)$. Again there appears to be reasonable agreement between experimental

and theoretical excitation energies; however, the calculations fail to account for the 42 percent branch of the 2.88 MeV level to the level at 1.40 MeV .

M1E2 transition strengths calculated by Hilko et al. are compared to the measured strengths in Table 3.2. There is excellent agreement for the E2 strengths, but the M1 strengths appear to be somewhat overestimated in the theoretical calculations. Hilko et al. attribute this result, in part, to a lack of knowledge concerning the form taken by the M1 operator in the deformed field of the nucleus.

At the present time, the experimental situation appears to favor the Nilsson model interpretation of ^{29}Al. This conclusion is based mainly upon the failure of the shell model to predict the correct spin sequence and upon the lack of extensive calculations concerning gamma ray transition strengths. However, as pointed out by de Voigt et al [17], the shell model calculations for ^{29}Al might possibly be improved by expanding the wave function configuration space described in Section 3.1.

Table 3.2 Experimental situation for the second, third, and fourth excited states in ^{29}Al as a result of the present work. The theoretical transition strengths of reference [27] were calculated using the Nilsson model.

E_i (keV)	E_f (keV)	J_i^π	J_f^π	δ[a]	τ[b]	M1 Strength ($\times 10^{-2}$ W.u.) Exp.	M1 Strength ($\times 10^{-2}$ W.u.) Ref. [27]	E2 Strength (W.u.) Exp.	E2 Strength (W.u.) Ref. [27]
1760	0	$7/2^+$	$5/2^+$	-0.24 ± 0.03	80 ± 40	6.8	36.1	6.2	8.6
		$3/2^+$	$5/2^+$	$0.22^{+0.10}_{-0.06}$		6.9	36.1	5.3	8.6
				$2.2^{+0.4}_{-0.5}$		1.2	36.1	94.5	8.6
2230	0	$3/2^+$	$5/2^+$	0.33 ± 0.20	110 ± 50	2.3	7.4	2.5	10.8
				1.9 ± 0.7		0.6	7.4	19.9	10.8
2880	1440	$3/2^+$	$1/2^+$	$0.0^{+0.13}_{-0.08}$	150 ± 70	3.0	0.01	---	1.0

[a] Mixing ratios taken from references [38] and [37]

[b] Lifetimes taken from reference [7]

4. LIFETIME, ANGULAR CORRELATION, AND LINEAR POLARIZATION MEASUREMENTS ON ^{61}Ni

4.1 Review of the ^{61}Ni Nucleus

4.1.1 Shell model calculations. The ^{56}Ni nucleus, with $1f_{7/2}$ shell closures for both neutrons and protons, has been the subject of intensive theoretical investigations using the shell model. These calculations have naturally been extended to other Nickel isotopes, the results being that these nuclei are among those most thoroughly studied in terms of the shell model.

There are three basic approaches for making shell model calculations [24]. In general, all three suffer the common deficiency that the configuration spaces used in the calculations are severely restricted by practical considerations such as computing time and memory size for the computers involved. The fundamental difference between the three procedures is the manner in which each accounts for residual interactions in the nucleus.

For the first procedure, some detailed form of the residual interaction potential is assumed. This potential has adjustable parameters such as its range, depth, etc., and these are determined usually by fitting experimentally observed energy levels. The interaction matrix elements are then calculated for states composed of the allowed configurations. One additional displeasing feature of this particular method is that the exact nature of the residual interaction is not investigated.

This is also true of the phenomenological approach of Talmi et al. [22]. Here, the interaction matrix elements themselves are treated as parameters and determined directly from fits to observed energy levels.

The third method for shell model calculations involves the determination of the effective matrix elements directly from free two-nucleon interactions. This method follows that of Kuo and Brown [41] who have used the Hamada-Johnston free nucleon potential in their calculations. To the extent that the two-body interaction dominates the residual interactions, this is probably the most pleasing approach from a theoretical point of view. However, its success depends upon a detailed knowledge of the two-body interaction and there is no physical evidence that many-body interactions may be discounted.

Shell model calculations for the Nickel isotopes using the three procedures described above have been made by various authors [2, 3, 4,15,24,30,42,54]. However, only recently have such calculations been performed for the odd-mass nuclei with the specific purpose of describing the gamma decay of their low-lying excited states. Glaudemans et al. [26] have calculated excitation energies, spins, lifetimes, mixing ratios, and branching ratios for the seven excited states in ^{61}Ni below 1200 keV . The wave functions were generated with neutrons in the 2p 3/2 , 1f 5/2 , and 2p 1/2 orbits outside an inert ^{56}Ni core. It was assumed that possible core excitations could be taken into account implicitly by the effective interaction and, for transition strengths, by the effective reduced single-particle transition matrix elements. For electric quadrapole

transitions, an effective neutron charge of $e_n = (1.70 \pm 0.08)e$ was obtained from a least squares fit to experimental data. Effective single particle matrix elements for magnetic dipole transitions were obtained through a similar fitting procedure. The $1g\ 9/2$ orbit was not included in the configuration space because, as pointed out in reference [15], this single particle orbit in ^{57}Ni lies approximately three MeV above the $2p\ 3/2$ orbit. This energy is above the energy of the $1f\ 7/2$ single-hole state in ^{57}Ni. These results served as a rough guide for ^{61}Ni, and thus it appeared pointless to include the $1g\ 9/2$ orbit when core excitations were not considered explicitly.

4.1.2 Core-coupling model calculations. The core-coupling model [59] has been applied to ^{61}Ni by Hoffmann-Pinther et al. [29]. The ground state ($J^\pi = 0^+$) and the first excited state ($J^\pi = 2^+$) of ^{60}Ni were coupled to the quasi-particle states $2p\ 3/2$, $1f\ 5/2$, and $2p\ 1/2$. Under the assumptions of the core-coupling model, the nuclear Hamiltonian can be written as

$$H = H_c + H_p + H_{int} \qquad 4.1$$

where H_c is the Hamiltonian describing the core, H_p is the Hamiltonian describing the particle which moves in the average potential generated by the core, and H_{int} represents the core-particle interaction. The basis set of wave functions used in the calculations are the eigenfunctions of $H_c + H_p$ and are written as

$$|\alpha_c J_c, \alpha_p j_p, IM\rangle \qquad 4.2$$

where α_p represents the additional quantum numbers required to describe a core state of spin, J_c, α_p and j_p play a similar role for the particle, and I represents a coupled state with spin projection, M. For a given spin, I, the matrix elements for the total Hamiltonian are written as

$$\langle J_c' j_p', IM|H|J_c, j_p, IM\rangle \qquad 4.3$$

where J_c', j_p' and J_c, j_p represent two different sets of core and particle states whose spins couple to I. The contribution to this total matrix element from the interaction Hamiltonian, H_{int}, can be written as a product of two reduced matrix elements, one of which concerns only the core while the other concerns only the particle moving outside the core. That is,

$$\langle J_c' j_p', IM|H_{int}|J_c, j_p, IM\rangle \sim$$

$$\langle J_c'\|H_{int}^c\|J_c\rangle\langle j_p'\|H_{int}^p\|j_p\rangle \qquad 4.4$$

where H_{int}^c and H_{int}^p represent the parts of the interaction Hamiltonian which deal with the core and particle, respectively.

The explicit form taken by the interaction Hamiltonian generally contains one or two parameters which describe the strength of the core-particle coupling. The reduced matrix elements $\langle J_c'\|H_{int}^c\|J_c\rangle$, are also treated as parameters since the exact nature of the core states is usually not known. During the diagonalization process for the total Hamiltonian, H, all these parameters are adjusted to give the best fit to experimentally observed energy levels. The number of

parameters is kept small by considering only the ground state and one or two excited states of the core. The single particle matrix elements, $\langle j_p' \| H^p_{int} \| j_p \rangle$, are usually calculated using harmonic oscillator wave functions or wave functions produced by some other standard technique. The eigenstates of H thus produced are next used to predict the characteristics of the electromagnetic decay of the excited states. These calculations are similar to those made using wave functions generated with any other nuclear model.

4.1.3 Experimental situation prior to this work. There appear to be some seventeen excited states in ^{61}Ni below 2200 keV excitation energy. A comprehensive summary of the experimental information on these states prior to the beginning of the present work is given in reference [60].

Eleven of these seventeen states have been observed to be populated in the β^+-decay of the $3/2^-$ ground state of ^{61}Cu [8,13,50]. Spin and parity assignments for these levels were made using measured $\log(fT_{1/2})$ values and the beta decay selection rules. Branching ratios were also determined in terms of numbers of transitions per one hundred decays of ^{61}Cu by studying the subsequent gamma decay of the excited states.

These eleven states, along with six additional levels, have also been identified through proton and deuteron inelastic scattering [16, 34,58], (d, p) stripping reactions [16,23], and (d, t) pickup reactions [23]. Spin and parity assignments have been made based upon cross section measurements and the ℓ-values of the neutrons transferred

in the stripping and pickup reactions. These assignments largely confirm those made in the beta decay studies. As shown in reference [60], lifetimes have been measured in ^{61}Ni for only the three lowest excited states.

4.2 Experimental Procedure

The experimental situation concerning ^{61}Ni prior to the beginning of this work suggested that this nucleus might lend itself to the application of the series of gamma ray spectroscopic measurements described generally in Chapter 1. This has indeed been found to be the case, and it is the purpose of this section to describe the procedures through which these measurements were made. The resulting branching ratios, spins, mixing ratios, and lifetimes have been used to calculate experimental transition strengths which hopefully will add to the systematics for this mass region while also providing a basis for comparison with theoretical calculations.

The levels in ^{61}Ni below 2200 keV were populated in two reactions, ^{58}Fe(α,nγ)^{61}Ni (Q_0 = - 3.83 MeV) and ^{60}Ni(d,pγ)^{61}Ni . The ^{58}Fe target was a 4 mg/cm^2 selfsupporting foil enriched to 87 percent ^{58}Fe . This target was bombarded with eight MeV alpha particles from the T.U.N.L. van de Graaff accelerator. The ^{60}Ni target was produced by evaporating 99.7 percent isotopically pure nickel metal onto glass slides which were first covered with a very thin film of water soluble cesium iodide. These self-supporting targets were floated off the slides and mounted on target rings. The targets were approximately 100 μg/cm^2 thick, and they were bombarded with six MeV deuterons.

The $^{60}Ni(d,p\gamma)^{61}Ni$ reaction was performed so that the added resolution of the solid state proton detector could be used in determining the branching scheme for the excited states. In order to obtain greater particle yield, the protons were detected at fifty degrees with respect to the beam direction as shown in Figure 4.1. Gamma rays in coincidence with these protons were detected at 90° to the recoil direction of the ^{61}Ni nuclei as determined by the reaction kinematics. Thus the energies of these gamma rays were free of any Doppler shifts.

The lifetime, angular correlation, and linear polarization studies were made using the $^{58}Fe(\alpha,n\gamma)^{61}Ni$ reaction. The following is a discussion of how each individual measurement was performed.

4.2.1 Lifetime measurements. Electromagnetic lifetimes for thirteen low-lying levels in ^{61}Ni were determined using the Doppler shift attenuation method (DSAM). Detailed discussions of this technique are given in references [48] and [61], and therefore only a brief outline will be presented here.

This particular method is used to measure nuclear lifetimes which fall roughly within the range 10^{-15} seconds $\leq \tau \leq 10^{-11}$ seconds. When considered with respect to this time scale, the secondary light particles from a nuclear reaction can be assumed to be emitted instantaneously (see Figure 1.1). Therefore, the residual nuclei, whose excited states ultimately decay by gamma emission, recoil through the target material with a time dependent velocity, $V(t)$. As shown in Figure 4.2, this velocity is the sum of two other velocities, $\bar{V}_{c.m.}$, the velocity of the center of mass of the residual

Figure 4.1 Diagram showing the detector arrangement for the measurements made using the $^{60}Ni(d,p\gamma)^{61}Ni$ reaction

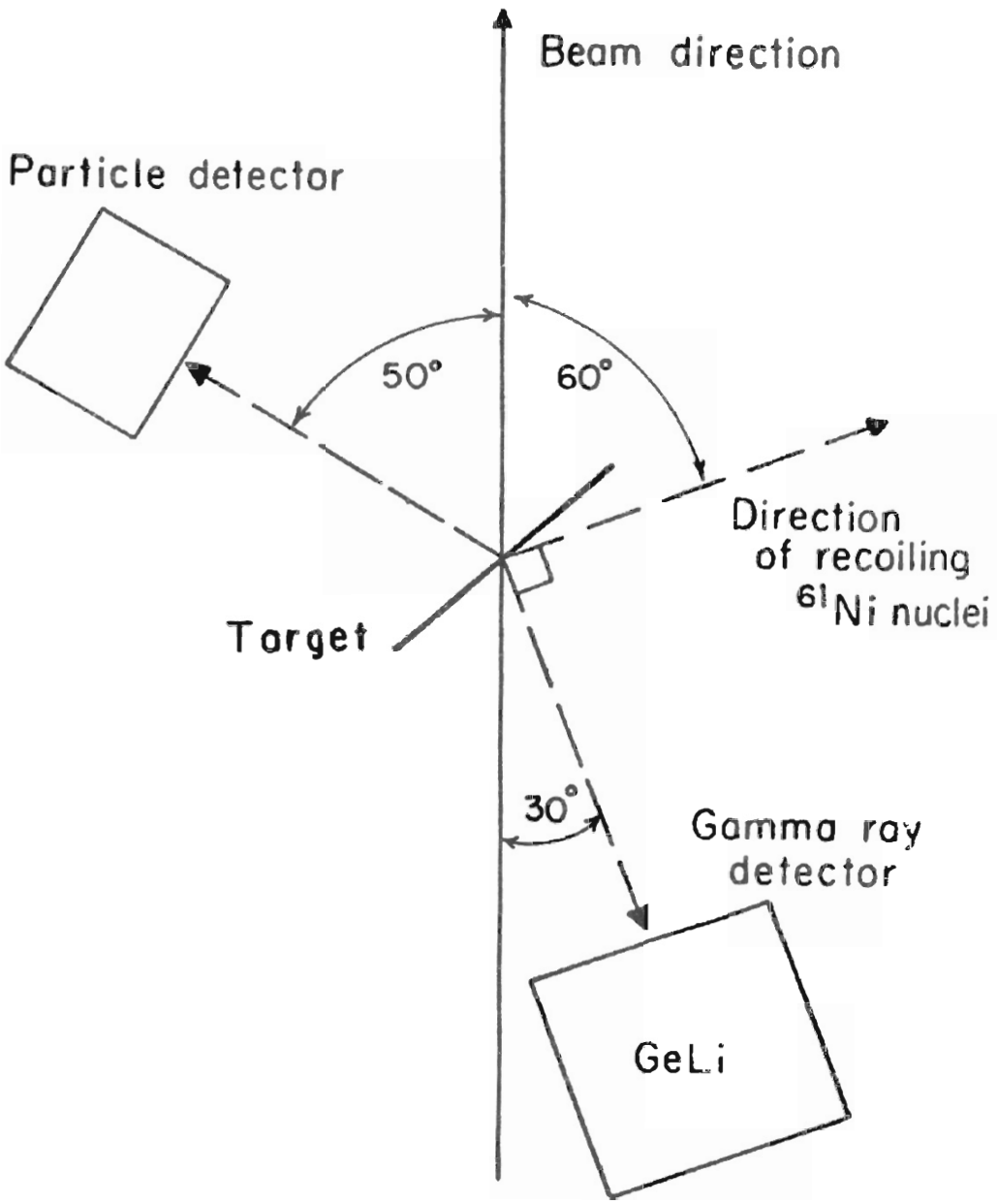
Beam direction
Particle detector
50°
60°
Direction
of recoiling
61Ni nuclei
Target
30°
Gamma ray
detector
GeLi

Figure 4.2 As measured in the laboratory reference frame, the recoil velocity of the residual nucleus is the sum of two other velocities, $\bar{V}_{c.m.}$, the velocity of the center of mass of the residual nucleus and the outgoing light particle, and, $\bar{V}_R$, the velocity in the center of mass imparted to the residual nucleus by the emission of the light particle

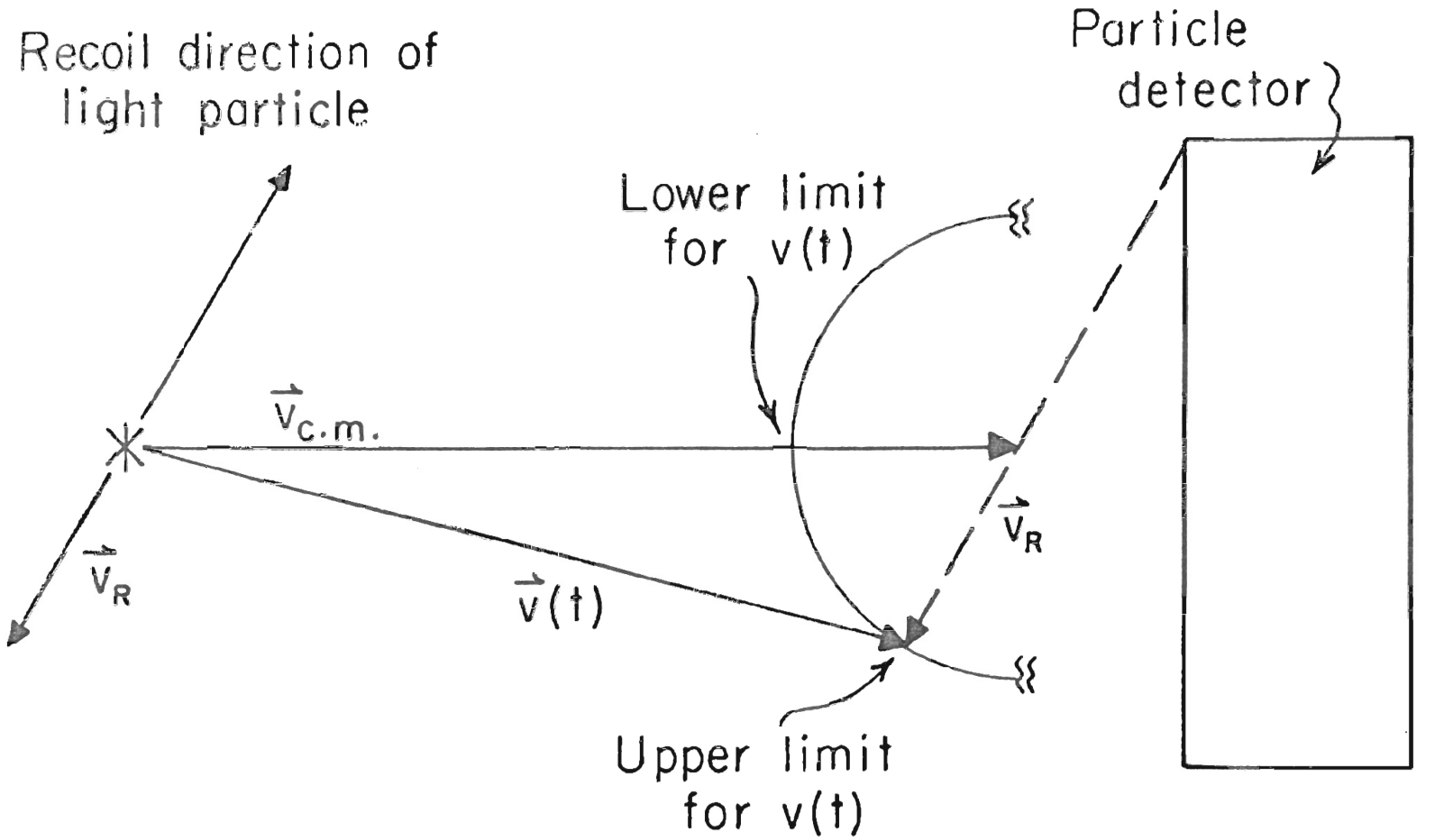
Recoil direction of light particle
Particle detector
Lower limit for v(t)
$\vec{v}_{c.m.}$
$\vec{v}_R$
$\vec{v}(t)$
$\vec{v}_R$
Upper limit for v(t)

nucleus and the secondary light particle, and $\bar{V}_R$, the velocity with respect to the center of mass imparted to the residual nucleus by the emission of the secondary, light particle. When these particles are detected at zero degrees, the recoil velocity of the residual nucleus is limited as shown in Figure 4.2. For endoergic nuclear reactions, energy conservation requires that $|\bar{V}_R|$ be less than $|\bar{V}_{c.m.}|$, and so the recoiling nuclei will have some average velocity component along the direction of the incident beam.

Next, consider an ensemble of excited nuclei whose members recoil symmetrically about the beam axis. This situation is depicted in Figure 4.3 where $\Psi(t)$ is the angle between the recoil direction and the direction of the gamma ray detector. The light particles are detected at zero degrees in the particle detector.

The angle, $\Psi(t)$, may be written as $\Psi(t) = \theta + \varphi(t)$ where θ locates the gamma detector with respect to the beam axis, and $\varphi(t)$ is the time dependent angle between the beam axis and the direction of the recoiling nucleus. The energy of a gamma ray emitted by this nucleus will be shifted according to the Doppler equation

$$E_\gamma(t) = E_{\gamma 0}\left[1 + \frac{V(t)}{c} \cos \Psi(t)\right] \qquad 4.5$$

where c is the speed of light and $E_{\gamma 0}$ is the unshifted gamma ray energy. The energy shift is

$$\Delta E_\gamma(t) = E_\gamma(t) - E_{\gamma 0}$$

$$= E_{\gamma 0} \frac{V(t)}{c} \cos \Psi(t). \qquad 4.6$$

Figure 4.3 A diagram showing the time dependent angle, $\Psi(t)$, between the direction of the gamma ray detector and the direction of a recoiling nucleus whose time dependent velocity is $\bar{V}(t)$

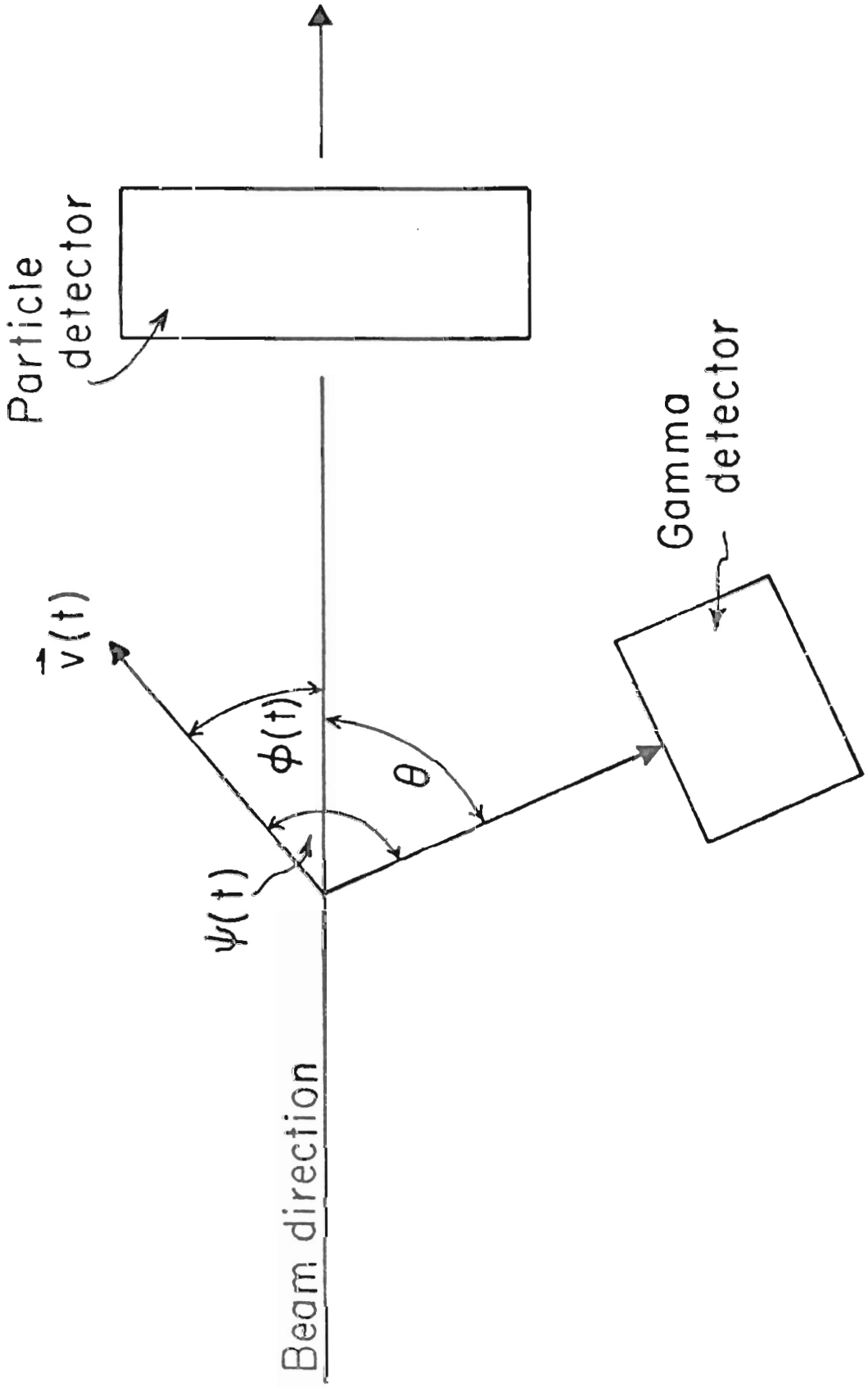
Particle
detector
Gamma
detector
$\vec{v}(t)$
$\phi(t)$
θ
$\psi(t)$
Beam direction

As discussed in reference [48], cos $\Psi(t)$ may be expanded in terms of θ and $\varphi(t)$. Equation 4.6 is then averaged over the entire ensemble of recoiling nuclei so that, at a given time, t, the average energy shift can be written as

$$\overline{\Delta E_\gamma(t)} = E_{\gamma 0} \frac{V_Z(t)}{c} \cos\theta \qquad 4.7$$

where $V_Z(t) = \overline{V(t) \cos \varphi(t)}$ and is the average recoil velocity of the ensemble along the beam axis.

In the ensemble, the number of nuclei emitting gamma radiation of a particular energy can be written as

$$N(t) = N_0 \exp(-t/\tau) \qquad 4.8$$

where N_0 is the number of nuclei at $t = 0$, and τ is the lifetime of the excited state. The number of nuclei which decay per unit time is then

$$\left|\frac{dN(t)}{dt}\right| = \frac{N_0}{\tau} \exp(-t/\tau) . \qquad 4.9$$

The average energy shift for the entire ensemble can be found by integrating the product of Equations 4.7 and 4.9 over all time. That is,

$$\Delta E_\gamma = \frac{\int_0^\infty \overline{\Delta E_\gamma(t)}\ (dN(t)/dt)dt}{\int_0^\infty (dN/dt)dt} . \qquad 4.10$$

If the residual nuclei were recoiling in vacuum, then ΔE_γ would have its largest value which is just equal to the energy shift at $t = 0$. Thus, from Equation 4.7,

$$\Delta E_\gamma^{max} = E_{\gamma 0} \frac{V_Z(t=0)}{c} \cos\theta \ . \qquad 4.11$$

In general, however, the excited nuclei slow down as they recoil through the target material so that ΔE_γ is less than its maximum value. The Doppler shift attenuation factor, $F(\tau)$, is defined as the ratio of the observed energy shift to the maximum possible shift. Equations 4.7, 4.9, 4.10, and 4.11 give

$$F(\tau) = \frac{1}{V(t=0)\tau} \int_0 V_Z(t) \exp(-t/\tau)\, dt. \qquad 4.12$$

In Equation 4.12, $V(t=0)$ is determined from the reaction Kinematics, and an approximation to the form of $V_Z(t)$ can be obtained from the stopping power theories of Blaugrund [12] and Lindhard, Scharff, and Shiøtt [43] (see reference [48] for details). These theories describe the manner in which the recoiling nuclei slow down in the target.

Therefore, for a given experimental situation, the values of $F(\tau)$ can be determined as a function of the nuclear lifetime, τ. For the $^{58}Fe(\alpha,n\gamma)^{61}Ni$ reaction, the values of $F(\tau)$ were calculated using the computer code FTAU from reference [48]. The results are shown in Figure 4.4 where the inclusion of a $\pm$ 15% error for the LSS electronic stopping power parameter was found to have a negligible effect.

The problem now remaining is that of determining the experimental values of $F(\tau)$ so that the lifetimes can be extracted by comparisons with $F(\tau)$ values calculated as described above. Referring once again to Figure 4.3, the energy of a detected gamma ray is written as

Figure 4.4 Theoretical values of the Doppler shift attenuation factor, $F(\tau)$, as a function of the lifetime, τ. The inclusion of a $\pm$ 15 percent error for the LSS stopping power parameter was found to have a negligible effect on this curve.

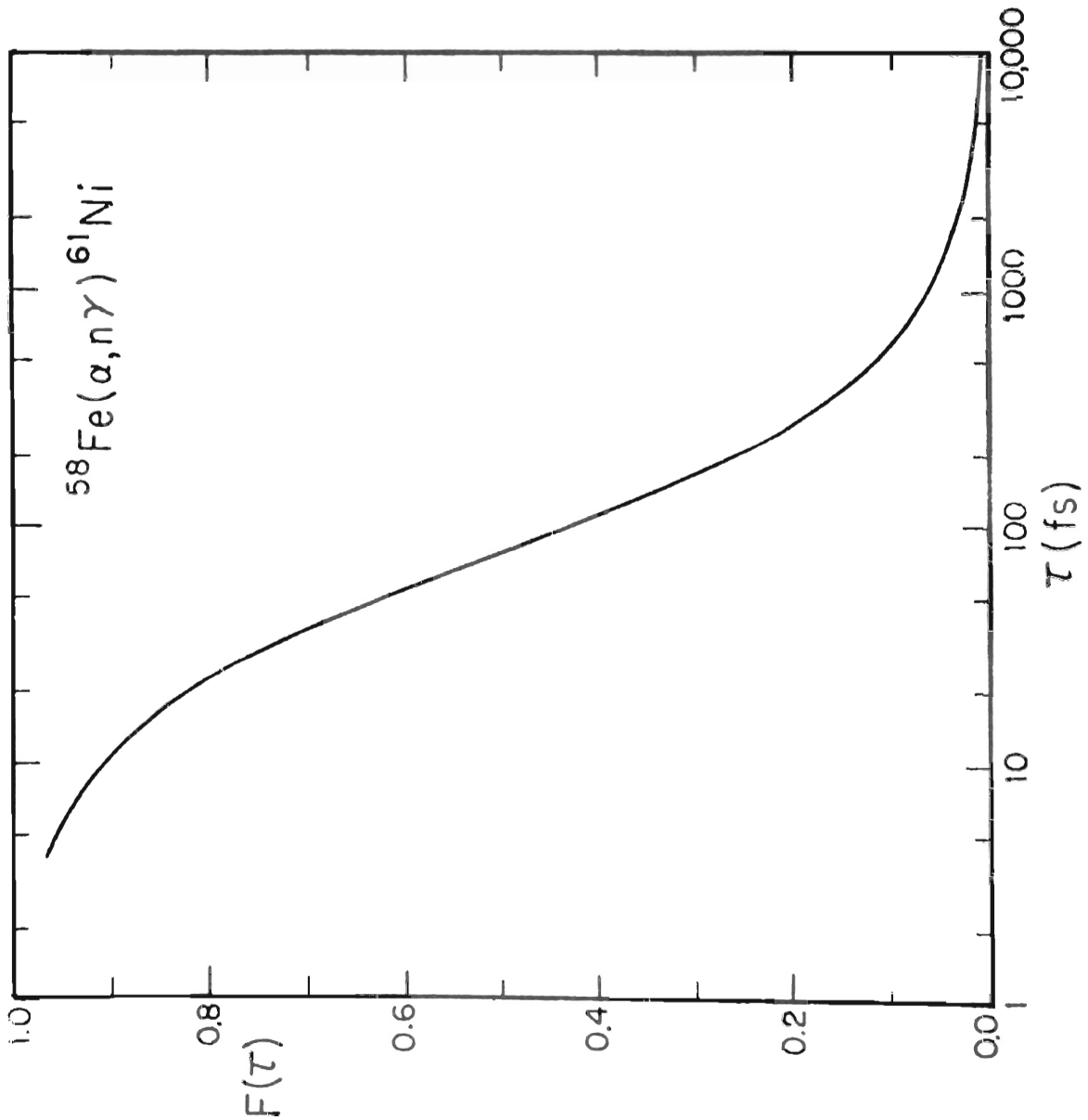
$^{58}Fe(\alpha,n\gamma)^{61}Ni$
F(τ)
τ (fs)
0.0
0.2
0.4
0.6
0.8
1.0
1
10
100
1000
10,000

$$E_\gamma(\theta) = E_{\gamma 0} + \Delta E_\gamma(\theta) \qquad 4.13$$

where $\Delta E_\gamma(\theta)$ is the observed energy shift. $\Delta E_\gamma(\theta)$ can in turn be written as

$$\Delta E_\gamma(\theta) = \Delta E_\gamma^{max}(\theta) \cdot \frac{\Delta E_\gamma(\theta)}{\Delta E_\gamma^{max}(\theta)}$$

$$= \Delta E_\gamma^{max}(\theta) \cdot F(\tau) \; . \qquad 4.14$$

Equations 4.13 and 4.14 then give

$$E_\gamma(\theta) = E_{\gamma 0} + \Delta E_\gamma^{max}(\theta = 0^\circ) F(\tau) \cos \theta \qquad 4.15$$

where

$$\Delta E_\gamma^{max}(\theta) = \Delta E_\gamma^{max}(0^\circ) \cos \theta \; .$$

Equation 4.15 takes the form

$$E_\gamma(\theta) = E_{\gamma 0} + M \cos \theta \qquad 4.16$$

with

$$M = \Delta E_\gamma^{max}(0^\circ) F(\tau) \; .$$

Therefore, the experimental procedure is to measure the energy of a gamma ray at several different forward and back angles. According to Equation 4.16 these energies can be plotted as a function of $\cos \theta$ and fitted with a straight line. The quantities $E_{\gamma 0}$ and M are determined from this fit, and the experimental value of $F(\tau)$ is determined after $\Delta E_\gamma^{max}(0^\circ)$ is obtained from the reaction kinematics.

Finally, an electromagnetic lifetime is extracted using the experimental value of $F(\tau)$ and a plot such as shown in Figure 4.4.

The lifetime measurements made in this work for the $^{58}Fe(\alpha,n\gamma)^{61}Ni$ reaction were performed using the target chamber and detector arrangement shown in Figure 4.5. Neutrons were detected at zero degrees in the NE213 liquid scintillator placed 16.5 cm from the target. The scintillator was shielded from gamma radiation by 2.5 cm of lead. Gamma rays in coincidence with the neutrons were detected at 129° , 90° , and 51° to the beam with a 50 cc germanium detector (GeLi). The detector was 6.5 cm from the target. The data taken at 90° , in addition to being used in the lifetime measurements, was also used to determine the decay scheme of the excited states. With 100 nA of beam current on target, data were accumulated at each angle for approximately seven hours.

A diagram of the electronic circuitry used for these measurements is shown in Figure 4.6. Standard pulse shape discrimination techniques were used to distinguish between neutrons and gamma rays detected in the liquid scintillator. For an event consisting of a coincidence between the liquid scintillator and the GeLi detector, five pieces of digital information were generated corresponding to

(a) the energy of the neutron (or gamma ray) detected in the scintillator,

(b) a pulse shape discrimination signal which identified this event as either a neutron (or photon),

Figure 4.5 Target chamber for the lifetime, linear polarization, and angular correlation measurements made on ^{61}Ni using the $^{58}Fe(\alpha,n\gamma)^{61}Ni$ reaction

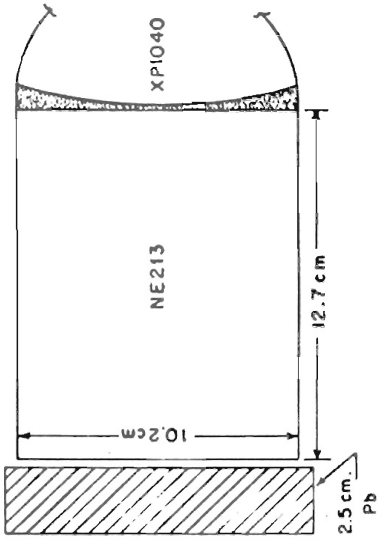
XP1040
NE213
12.7 cm
10.2cm
2.5 cm. Pb

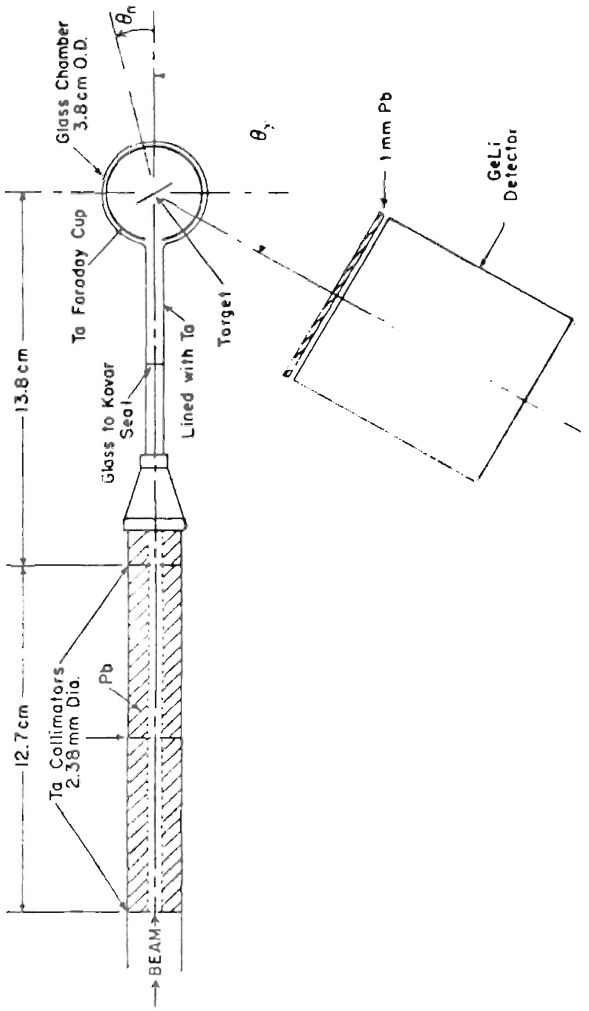
Glass Chamber 3.8cm O.D.
θ_n
θ_γ
1 mm Pb
Ge(Li) Detector
To Faraday Cup
Target
Lined with Ta
Glass to Kovar Seal
13.8 cm
12.7cm
Ta Collimators 2.38 mm Dia.
Pb
BEAM

Figure 4.6 A diagram of the electronic circuit used in the lifetime and n-γ angular correlation measurements on ^{61}Ni

AMP main amplifier

DISC fast discriminator

TIMING SCA time single channel analyzer

TAC time-to-amplitude converter

GATE GEN. gate and delay generator

BLR PILEUP baseline restorer and pileup rejector

ADC analog-to-digital converter

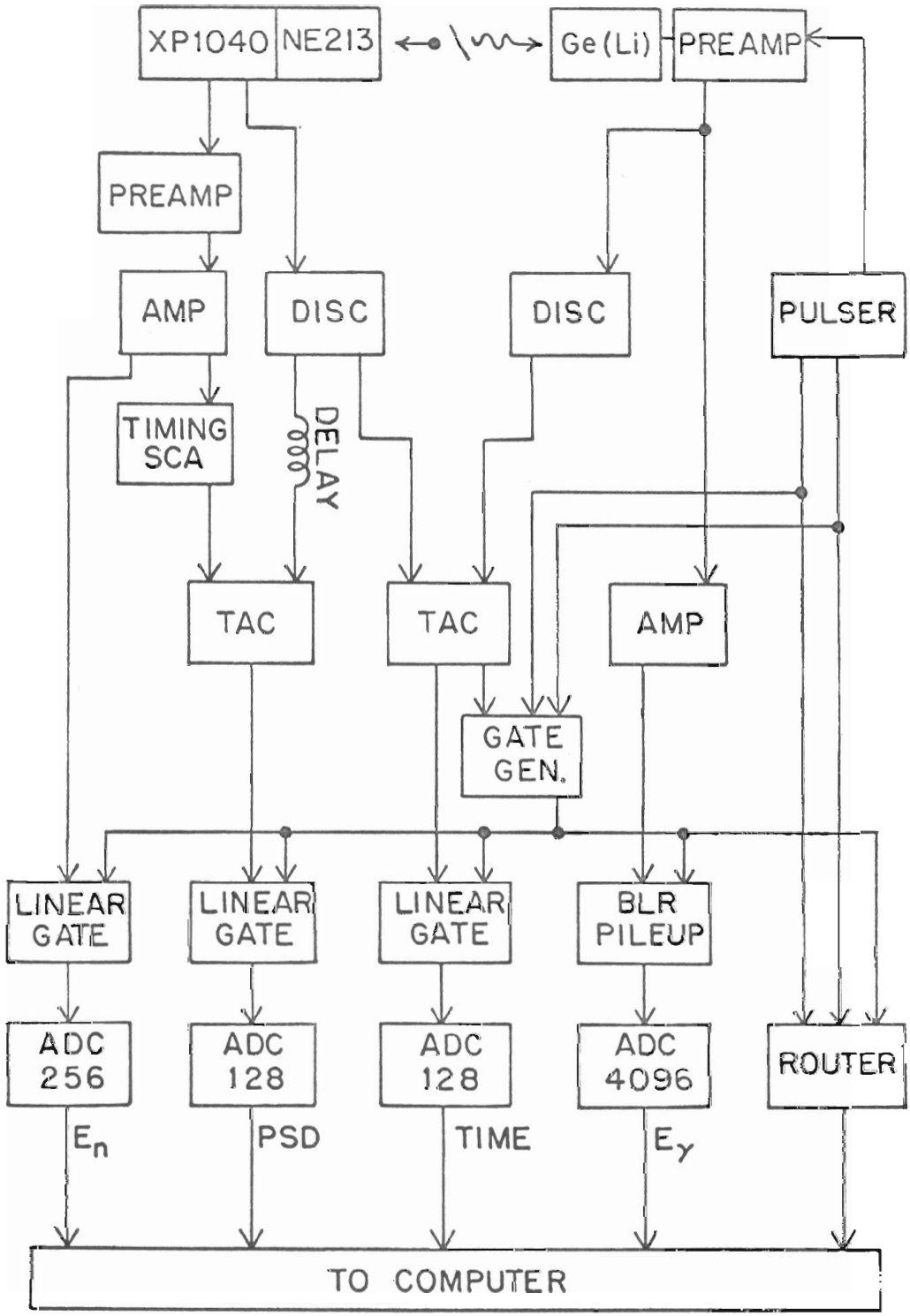
XP1040
NE213
Ge(Li)
PREAMP
PREAMP
AMP
DISC
DISC
PULSER
TIMING SCA
DELAY
TAC
TAC
AMP
GATE GEN.
LINEAR GATE
LINEAR GATE
LINEAR GATE
BLR PILEUP
ADC 256
ADC 128
ADC 128
ADC 4096
ROUTER
E_n
PSD
TIME
E_γ
TO COMPUTER

(c) the time difference for a coincidence which involved the scintillator and the GeLi detector,

(d) the energy of the gamma ray detected by the GeLi crystal, and

(e) a routing signal to distinguish between these photons and pulser signals.

With the exception of the routing information, these digital half-words were written event-by-event onto magnetic tape for later use during off-line analysis. The pulser, whose outputs were constant to with 0.2 keV , was used to provide the means for off-line gain stabilization of the gamma ray data. Pulser signals, simulating alternately high and low energy gamma events, were fed to the preamp of the GeLi detector and processed just as a genuine gamma ray energy signal. However, these signals were tagged with an appropriate routing signal so that after processing by the analog-to-digital converter (ADC), their corresponding channel numbers could be identified and stored by the computer in two separate sets of storage locations. At designated intervals, two centroids were calculated and dumped on magnetic tape along with the other data. During off-line analysis, these centroids were used to correct the gamma ray spectra for electronic gain shifts. These spectra were then used as described earlier in this section to determine electromagnetic life-times.

4.2.2 Angular correlation measurements. The gamma radiation from the low-lying levels in ^{61}Ni was studied through angular distribution measurements made with the photons detected in singles and in neutron coincidence. The coincidence measurements were made under the same experimental conditions as those for the lifetime studies. The same electronic circuit was used with the exception that the data were not gain stabilized since small gain shifts are not usually significant in correlation studies. Data were accumulated for approximately four hours at each of six back angles between 90 and 180 degrees.

The experimental conditions and procedures for the singles measurements differed from those of the coincidence measurements only in that the electronic circuitry was much simplified. This circuit consisted only of the gamma ray detector of Figure 4.6, a linear amplifier, a baseline restorer and pileup rejector, and one analog-to-digital converter. Data, stored in binary form on magnetic tape, were accumulated for approximately one hour at each of eight angles between zero and 90 degrees.

4.2.3 Linear polarization measurements. The polarimeter used for the polarization measurements on ^{61}Ni was not the five crystal, sodium iodide (NaI) polarimeter described in Chapter 2, but rather an instrument constructed from two cylindrical germanium (GeLi) crystals mounted with their axes parallel as shown in Figure 4.7. This type of polarimeter, in which both crystals serve to scatter the incident radiation, has been discussed in detail by Bass et al. [5]. When compared to the NaI instrument, the outstanding advantage of the

Figure 4.7 The symmetric, two crystal, GeLi polarimeter. The incident radiation is represented by γ , the Compton scattered radiation by γ' .

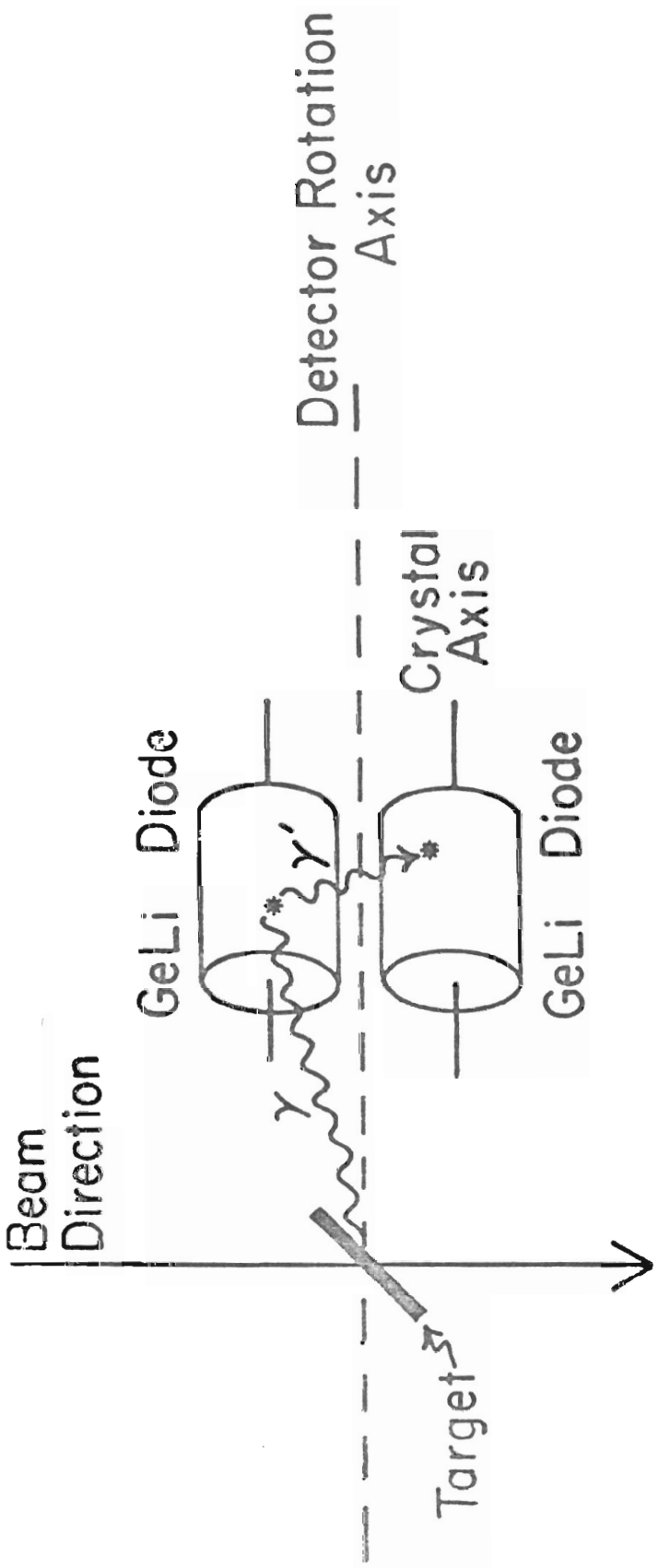
Detector Rotation Axis
Crystal Axis
GeLi Diode
GeLi Diode
Beam Direction
Target
γ
γ'

GeLi polarimeter is that its improved energy resolution allows it to be used without a particle coincidence requirement, the result being that substantially increased counting rates are obtained.

Each germanium crystal had an active volume of 30 cc, and they were mounted inside a cryostat so that, when the cryostat sat upright, the plane defined by the parallel axes of the crystals made a 45° angle with the reaction plane. Thus, by rotating the cryostat through 45° to first one side and then the other, the plane of the crystal axes could be placed either parallel or perpendicular to the reaction plane. The rotation axes of the polarimeter is the line along which the surfaces of the crystals would touch if placed in contact.

A diagram of the electronic circuitry used with the polarimeter is shown in Figure 4.8 where a coincidence between the two crystals produced four pieces of digital information to be stored by the computer. Photopeak energies for the incident gamma rays were obtained by summing the energy signals from each separate detector. A timing signal was also generated with amplitude corresponding to the time difference between events in the two crystals. The time resolution was approximately 120 nanoseconds full width half maximum (FWHM) which, with a modest counting rate of about 2000 counts per second, gave a true to chance ratio of better than 100 to one. The energy resolution of the individual detectors was 2.4 keV FWHM for a 1.33 MeV gamma ray, while the resolution for the summed events was 3.5 keV .

The polarimeter was calibrated at 90° with respect to the beam and with the front face of the cryostat approximately 13 cm from the

Figure 4.8 A diagram of the electronic circuit used with the GeLi polarimeter

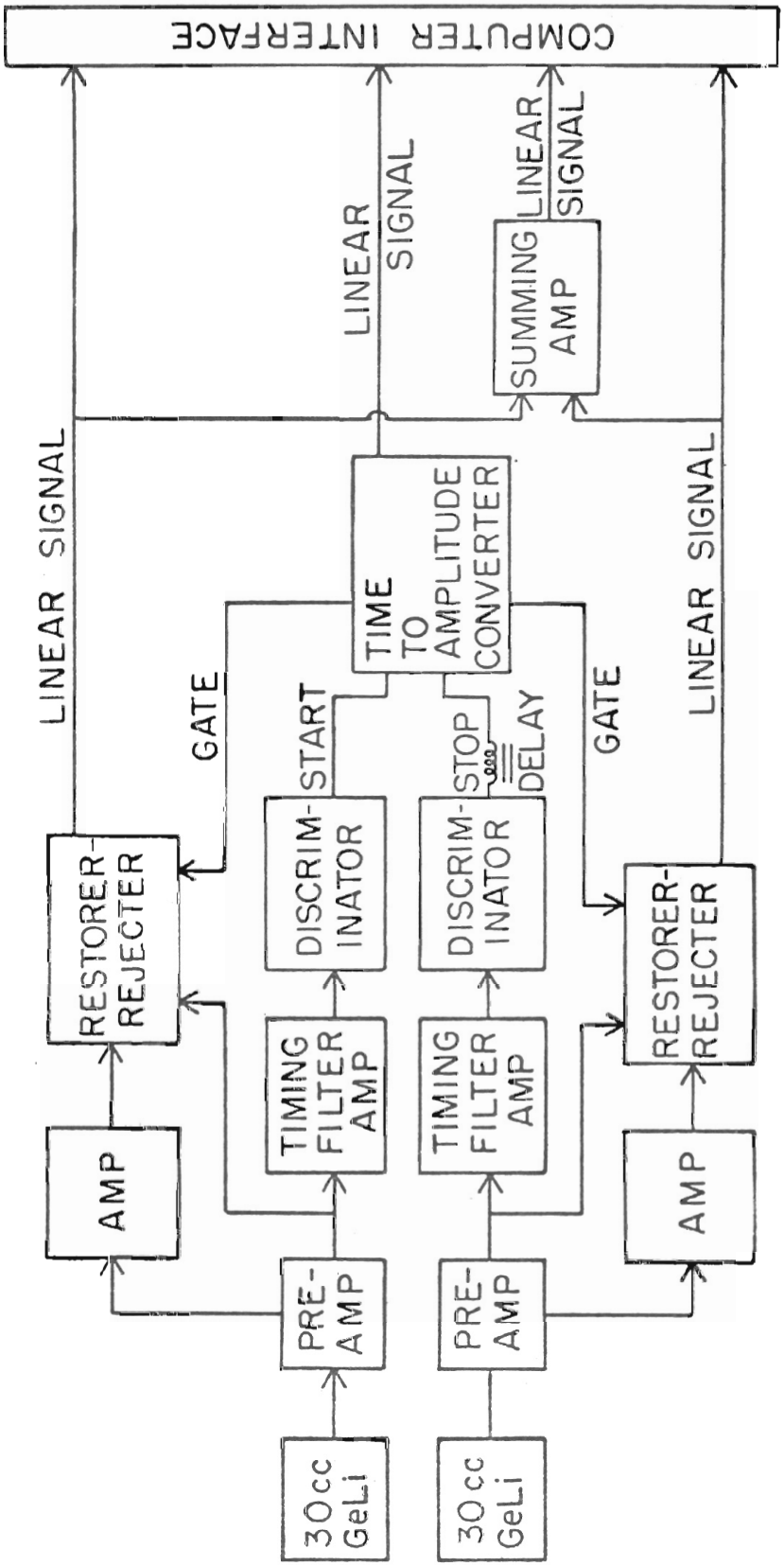
COMPUTER INTERFACE
LINEAR SIGNAL
LINEAR SIGNAL
LINEAR SIGNAL
LINEAR SIGNAL
SUMMING AMP
TIME TO AMPLITUDE CONVERTER
GATE
GATE
START
STOP
DELAY
DISCRIM-INATOR
DISCRIM-INATOR
TIMING FILTER AMP
TIMING FILTER AMP
RESTORER-REJECTER
RESTORER-REJECTER
AMP
AMP
PRE-AMP
PRE-AMP
30 cc GeLi
30 cc GeLi

target. Following the procedure described in Chapter 2 and as a function of incident gamma ray energy, the polarization sensitivity, S , was determined from angular distribution and asymmetry measurements on the radiation which resulted from the pure electric quadrupole (E2) , $2^+ \rightarrow 0^+$ transitions in ^{56}Fe , ^{24}Mg . ^{50}Ti , and ^{28}Si , and the $5/2^+ \rightarrow 3/2^+$ transitions in $^{107,109}Ag$ which were also known to be pure E2 . The asymmetry data were analyzed subject to the off-line application of 150 keV lower level thresholds to the energy signals from the separate detectors. The experimental results are shown in Figure 4.9. The smooth curve is a fit made to these data using the computer code described in Chapter 2.

Next, consider the plane angle subtended in the reaction plane and at the target by the combination of the two germanium crystals (see Figure 4.7). The size of this angle depends upon the orientation of the plane of the detectors with respect to the reaction plane. Therefore, the possibility existed that, for different orientations, angular distribution effects might change the intensity of the radiation incident upon the polarimeter. These considerations were included in the calculation of the calibration curve in Figure 4.9; however, the effects were found to be negligible. Finally, when checked with unpolarized radiation from a radioactive source, the asymmetry measured with the polarimeter was found to be zero within statistical error.

Polarization measurements for ^{61}Ni were made under experimental conditions (beam energy, target thickness, etc.) identical to those for the singles angular distribution measurements. Data were accumulated for approximately four hours in each of two positions

Figure 4.9 The calibration curve for the GeLi polarimeter showing the polarization sensitivity as a function of the energy of the incident radiation

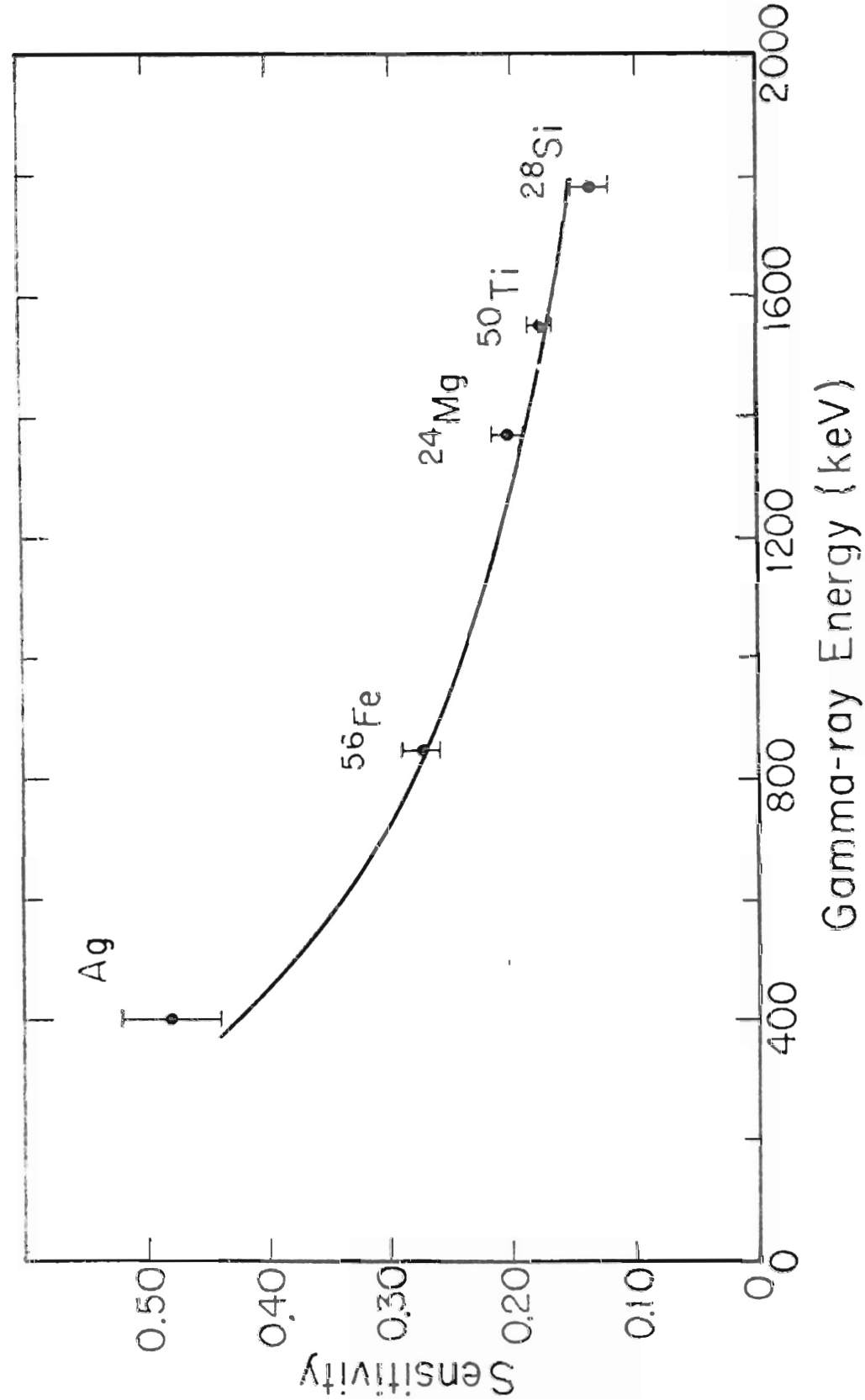
Sensitivity
0.50
0.40
0.30
0.20
0.10
0
400
800
1200
1600
2000
Gamma-ray Energy (keV)
Ag
56Fe
24Mg
50Ti
28Si

defined when the plane of the detectors was, alternately, parallel and perpendicular to the reaction plane. The measurements were then repeated, giving a total of eight hours of data for each position. Normalization was with respect to the integrated beam current.

4.3 Analysis and Results

The $^{58}Fe(\alpha,n\gamma)^{61}Ni$ reaction was initiated with an incident alpha particle energy of 8.0 MeV . The ground state Q-value for the reaction is - 3.83 MeV so that energy considerations allowed the population of excited states up to approximately 4.0 MeV . Therefore there existed the possibility that the levels below 2200 keV were fed from levels at higher energies. This feeding problem was investigated using the lifetime data.

First, the buffered tapes containing the 90° lifetime data were read back, and a time spectrum was produced in a manner similar to that described in Section 3.3. After selecting appropriate "real" and "random" windows for this spectrum, the buffered tapes were read again, and a three-dimensional, energy versus pulse-shape discrimination (E vs. PSD) display was generated which described the events detected in the liquid scintillator. For a given event, the associated energy was plotted along one horizontal axis while the corresponding PSD information was plotted along the other. The vertical axis represented the number of events found to have a particular energy and PSD parameter. The display resembled a plane surface with two raised areas. One of these areas represented the neutrons detected by the scintillator, and the other represented the

detected gamma radiation. After setting an appropriate two-dimensional window about the area corresponding to the neutrons, the 90° lifetime data were read once again in order to produce the coincident gamma ray spectrum shown in Figure 4.10. This spectrum contains some 35 gamma rays from ^{61}Ni along with four contaminant gamma rays which resulted from the ^{56}Fe(α,nγ)^{59}Ni reaction. Next, 16 of these gamma rays were selected so that the excitation energies of their parent states ranged from 656 to 2708 keV . A reasonably liberal window was chosen for each peak, and 16 separate neutron spectra were generated, one for each gamma ray. In order to increase statistics in the neutron spectra, the four remaining lifetime runs, two at 129° and two at 51° , were read back and added to the 90° data.

The detection characteristics of the NE213 liquid scintillator are such that the energy deposited by an incident neutron can range from zero to its maximum value. Therefore, no energy resolution is obtained for the neutron energies, and an energy spectrum will resemble a decreasing exponential curve. However, for some of the sixteen spectra mentioned above, the channel number for which the neutron yield approached zero could be judged approximately. When these channel numbers were plotted versus the energies of the different excited states, a reasonable calibration curve was obtained for the neutrons. This curve is shown in Figure 4.11 along with two neutron spectra which correspond to the population of the levels in ^{61}Ni at 1611 and 2708 keV . An arbitrary error of $\pm$ 10 has been set on the neutron channel numbers. The neutron energies were stored

Figure 4.11 Calibration curve for the coincident neutrons. Several neutron spectra were generated, each corresponding to the population of a different excited state in ^{61}Ni. For each spectrum, a channel number was chosen at which the neutron yield appeared to approach zero. These channel numbers, with an aribtrary error of $\pm$ 10 channels, were then plotted as a function of excitation energy. The dotted portion of the curve corresponds to excited states whose neutron energies were off scale.

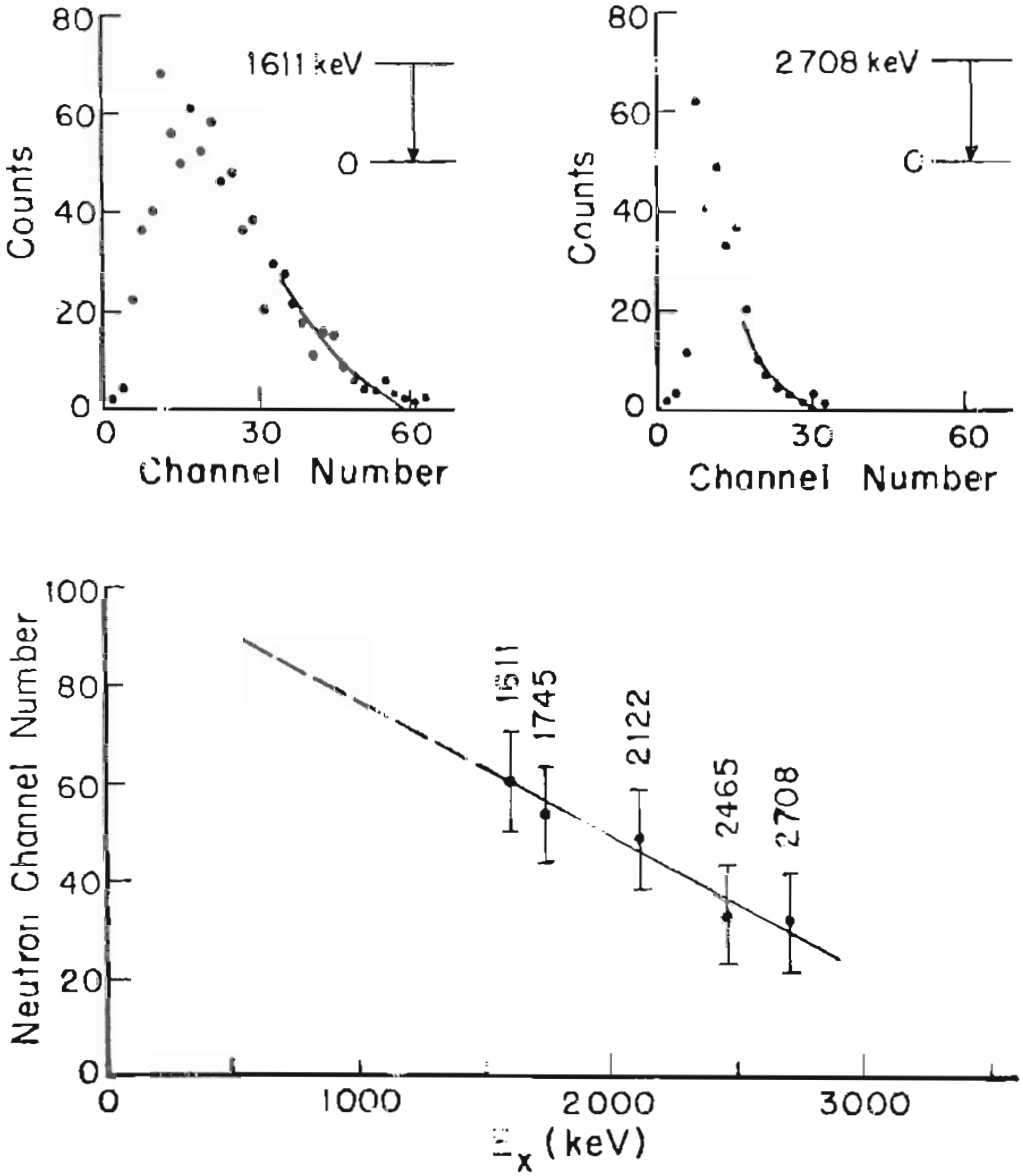
1611 keV
0
Counts
Channel Number
2708 keV
0
Counts
Channel Number
Neutron Channel Number
1511
1745
2122
2465
2708
E_x (keV)

Figure 4.12 Level diagram for the states in ^{61}Ni below 2200 keV. The J^{π} assignments for the levels at 0, 67, 283, 656, 1100, and 1997 keV are from reference [60] as are the lifetimes for the first three excited states. The remaining information has been either confirmed or obtained in the present work. For purposes of tabulation, the lifetimes are shown with symmetric errors obtained from the actual errors given in Table 4.1.

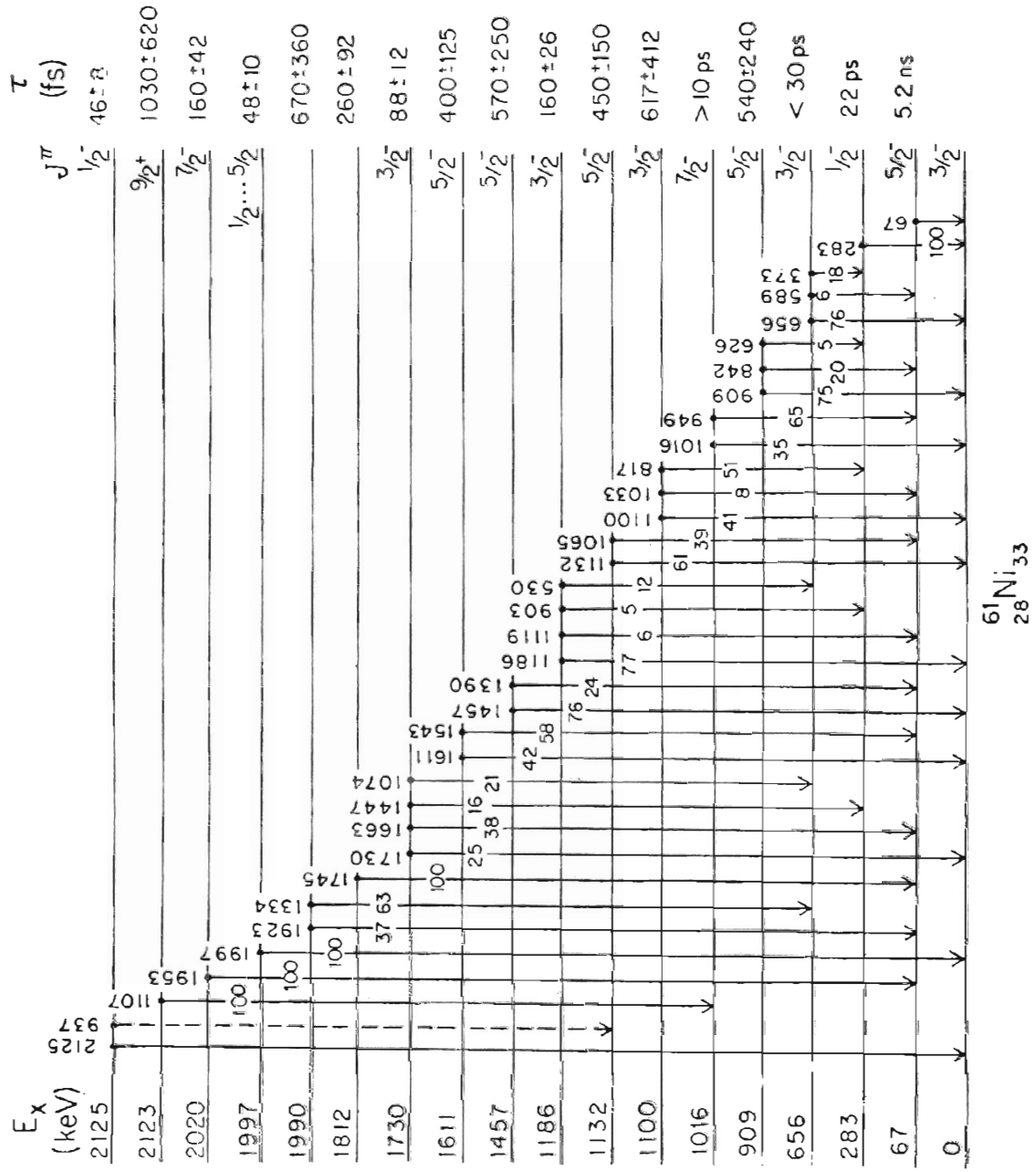
$^{61}_{28}Ni_{33}$
E_x (keV)
J^π
τ (fs)
2125
2123
2020
1997
1990
1812
1730
1611
1457
1186
1132
1100
1016
909
656
283
67
0
$1/2^-$
$9/2^+$
$7/2^-$
$1/2^- \ldots 5/2^-$
$3/2^-$
$5/2^-$
$5/2^-$
$3/2^-$
$5/2^-$
$3/2^-$
$7/2^-$
$5/2^-$
$3/2^-$
$1/2^-$
$5/2^-$
$3/2^-$
46±8
1030±620
160±42
48±10
670±360
260±92
88±12
400±125
570±250
160±26
450±150
617±412
>10 ps
540±240
< 30 ps
22 ps
5.2 ns
2125
937
1107
1953
1997
1923
1334
1745
1730
1663
1447
1074
1611
1543
1457
1390
1186
1119
903
530
1132
1065
1100
1033
817
1016
949
909
842
626
656
589
373
283
67
100
100
100
100
37
63
100
25
38
16
21
42
58
76
24
77
6
5
12
61
39
41
8
51
35
65
75
20
5
76
6
18

in 64 channels and, as shown by the dotted portion of the calibration curve, these energies were off scale for the population of levels below about 1400 keV . This unfortunate situation resulted from an oversight during data acquisition.

The 90° gamma ray data were next read back with a neutron window set so that gamma rays from only the first three excited states were observed with any strength. The width of this window was expressed as 64-X where X was some number slightly less than 64 . The value of X was gradually decreased and recorded whenever gamma rays began to appear from the next highest excited state. In this manner, neutron windows were determined which allowed the elimination of essentially all feeding between states below 1400 keV .

The results of the two procedures described above were used to eliminate any suspected level feeding during the analysis of the lifetime data. As mentioned earlier, five sets of lifetime data were taken, two at 120° , one at 90° , and two at 51° . Before each set was accumulated, an energy calibration was made using a ^{56}Co source. After data analysis, these calibration spectra were used to determine the energies of the peaks of interest in the various gamma ray spectra. These energies were then used as described in Section 4.2 to determine the experimental values of $F(\tau)$. Whenever possible, the final $F(\tau)$ value for any particular state was taken as the weighted average of the $F(\tau)$ values for the different branches of the level. The theoretical values of $F(\tau)$ were taken from Figure 4.4. The electromagnetic lifetimes (with symmetric errors) determined by comparing these values to the measured $F(\tau)$ values are shown in Figure 4.12.

Figure 4.10 Coincident gamma ray spectrum taken at 90 degrees for the lifetime measurements on ^{61}Ni . The peaks are labeled according to the energy of radiation.

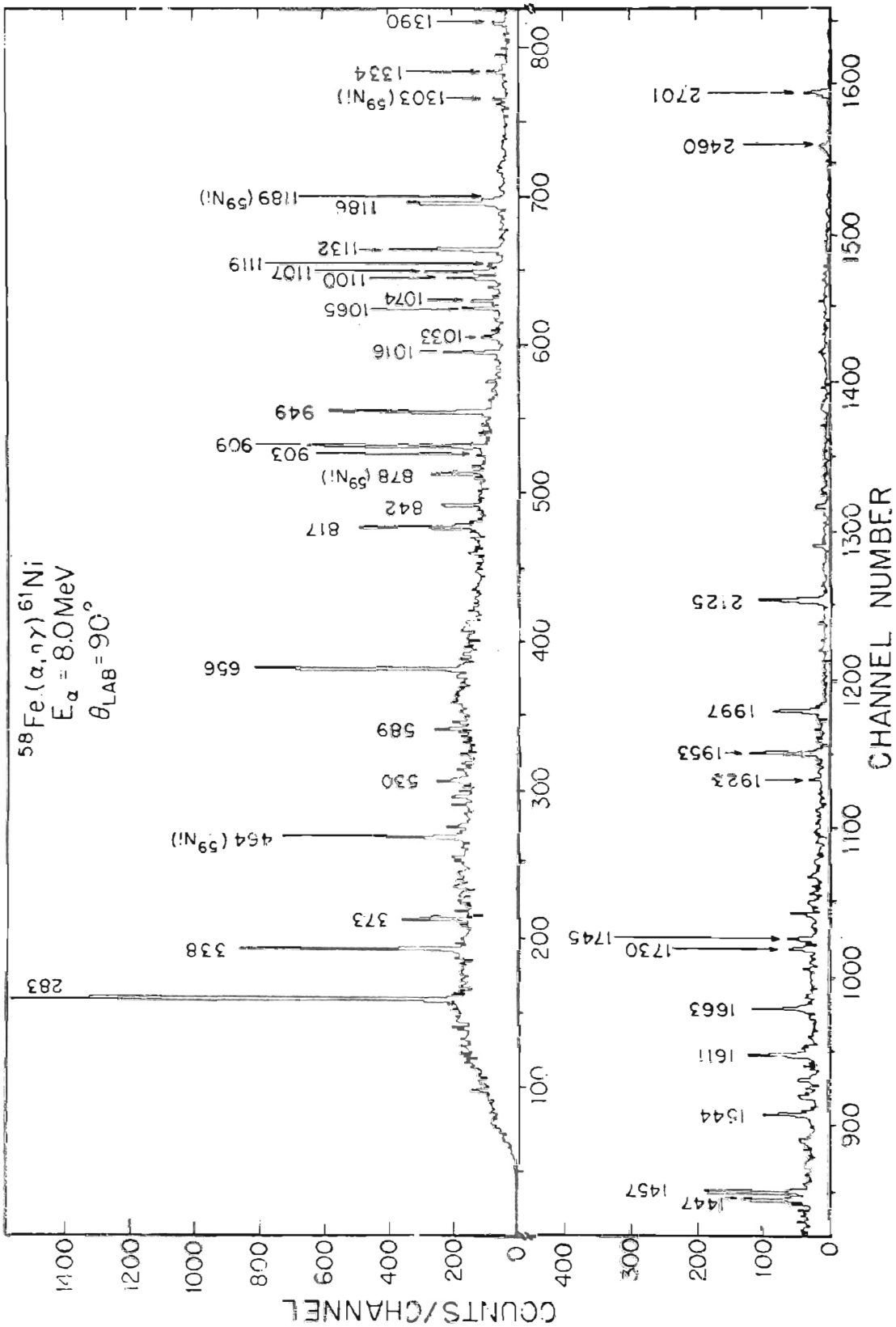
$^{58}Fe(\alpha,n\gamma)^{61}Ni$
$E_\alpha = 8.0$MeV
$\theta_{LAB} = 90°$
283
338
373
464 (^{59}Ni)
530
589
656
817
842
878 (^{59}Ni)
903
909
949
1016
1033
1065
1074
1100
1107
1119
1132
1186
1189 (^{59}Ni)
1303 (^{59}Ni)
1334
1390
1447
1457
1544
1611
1663
1730
1745
1923
1953
1997
2125
2460
2701
COUNTS/CHANNEL
CHANNEL NUMBER

Analysis of the lifetime data lead to the conclusion that only a few states above 2200 keV were more than weakly populated, and these states were generally found to have a large branch to either the first or second excited state. With the exception of the states at 2123 and 2125 keV , all other states between 909 keV (fourth excited state) and 2200 keV were found to decay entirely to one or more of the levels in the group of levels which consisted of the ground state and the first three excited states. Analysis of the (d,p) data yielded a possible branch of the level at 2125 keV to the eighth excited state at 1186 keV (see Figure 4.12). However, this branch was very weak and not seen at all in the (α,n) data. The level at 2123 keV was found to decay 100 percent to the fifth excited state at 1016 keV . The fifth excited state in turn was found to decay to both the ground state and the first excited state so that three gamma rays were involved in this two-level cascade. Analysis of the singles angular distribution data for these three gamma rays showed that the fifth excited state was directly populated over 90 percent of the time as opposed to less than 10 percent indirect population from the decay of the level at 2123 keV . The general conclusion was that feeding was not a problem for the levels of interest in ^{61}Ni .

The angular correlation data taken in $n - \gamma$ coincidence was analyzed without regard to level feeding. Six gamma ray spectra were generated, one for each of six angles between 90° and 180°. For the particular peaks of interests, the experimental angular correlations were determined from these spectra. Theoretical fits to these correlations were then made as described in Chapter 2 using the expression

$$\omega(\theta) = \sum_K A_K Q_K P_K (\cos \theta) \qquad 4.17$$

where K is even, Q_K is a finite geometry correction, and A_K is an expansion coefficient which depends upon the spins of the two states involved, the population parameters of the initial state, and the mixing ratio of the gamma radiation. With the outgoing neutrons detected at zero degrees, Equation 2.15 implies that only the $\pm 1/2$ magnetic substates are populated for levels in the residual nucleus. Therefore, the A_K coefficients of Equation 4.17 depend only upon the initial and final spins and the electromagnetic mixing ratio, δ, which, according to Equation 1.16, can range from minus infinity to plus infinity. During the fitting procedure for a particular transition, the final spin was known and several different spins were assumed for the emitting level. For each assumed spin, δ was varied over its entire range by stepping arctan δ from -90° to 90° in 19 increments of 10° each. For each step in arctan δ, a theoretical correlation was calculated and fitted to the experimental data. The goodness of the fit was measured by the quantity [9]

$$\chi^2 = \frac{1}{n} \sum_i \left[\frac{Y(\theta_i) - \omega(\theta_i)}{\Delta Y(\theta_i)}\right]^2 \qquad 4.18$$

where $Y(\theta_i)$ is the number of gamma rays detected at the angle, θ_i, $\omega(\theta_i)$ is the corresponding theoretical prediction, $\Delta Y(\theta_i)$ is the error in $Y(\theta_i)$, and n is the number of degrees of freedom which is defined as the number of data points minus the number of unknown parameters in the fit. The values of χ^2 were plotted versus arctan δ, and a 0.1 percent confidence level placed upon each plot in accordance with procedure described in reference [9]. Any spin-mixing ratio combination was ruled out if the combination produced a fit whose χ^2 value was larger than the value of χ^2 which corresponded to the confidence level. Examples of these plots will be shown later. The branching ratios for the different transitions were determined using the A_0 coefficients from the best fits to the correlation data.

The angular distribution data taken in singles were analyzed as described above with the following exception. Since the outgoing neutrons were not detected at zero degrees, the values of the population parameters could no longer be restricted to $\pm 1/2$. However, limits were set for these parameters by performing optical model calculations for different angular momentum transmission probabilities. The optical model parameters were taken from Perey and Buck [46]. For each theoretical fit to an experimental distribution, the calculation of the A_K coefficients of Equation 4.17 involved a search over this range of restricted population parameters. Thus, for a given initial spin, a best set of population parameters was determined for each of 19 values of arctan δ.

The gamma ray linear polarization data were analyzed in a manner similar to that described in Section 3.3 with the exception that 150 keV instead of 200 keV lower level thresholds were placed on the energy signals from the separate detectors. The measured polarizations extracted from this analysis were then compared to theoretical values calculated using the equations of Section 2.1 and the population parameters determined by the singles angular distribution measurements. These comparisons served to remove several spin, parity, and mixing ratio ambiguities.

The following is a level-by-level summary of the results of the spectroscopic measurements made for the gamma decay of the excited states in ^{61}Ni below 2200 keV . The earlier works to be cited during these discussions are the beta decay studies of the ground state decay of ^{61}Cu [8, 13, 50] and the (d,p) and (d,t) single particle transfer reactions investigated by Cosman et al. [16] and Fulmer et al. [23]. All this experimental information is summarized in reference [60].

4.3.1 The 67 keV, 283 keV, and 656 keV levels. These three levels are populated in the β^+-decay of ^{61}Cu ground state and in the stripping and pickup reactions referenced above. Values of $\log(fT_{1/2})$ from the beta decay studies and a Distorted Wave Born Approximation (DWBA) analysis of the J-dependence of the charged particle cross sections from the reaction data have resulted in the following J^π assignments: $5/2^-$ (67 keV) , $1/2^-$ (283 keV) , and $3/2^-$ (656 keV) . Also, as shown in reference [60], lifetimes or

lifetime limits have been determined for all three levels. In the present work, these levels were found to be strongly fed from higher excited states (see Figure 4.12). The feeding was eliminated by the application of neutron windows; however, this procedure reduced the gamma ray yield from direct population to such an extent that no lifetime or angular correlation measurements were possible. The only experimental results obtained for these levels are the branching ratios shown in Figure 4.2.

4.3.2 The 909 keV level. The J^{π} assignment of $5/2^{-}$ made for this level as a result of the beta decay studies is consistent with the $\ell = 3$ neutron transfer observed in the (d,p) measurements. In the present work, branching ratios of 75 ± 5, 20 ± 3, and 5 ± 2 percent were determined for the decay of this level to the ground state and the first and second excited states, respectively.

For the ground state branch of this level ($E_{\gamma} = 909$ keV), the results of the lifetime measurements are shown on the right side of Figure 4.13. The Doppler shift between the 129° and 51° centroids of the resulting gamma ray corresponded to a total energy shift of 0.8 keV. The gamma ray energy was plotted as a function of angle, and the experimental value of $F(\tau)$ was determined, as described in Section 4.21, from a straight line fit to these data. Finally, using the curve from Figure 4.4, a lifetime of $450 \begin{smallmatrix} + 330 \\ - 150 \end{smallmatrix}$ fs was obtained.

The measured, $n - \gamma$ angular correlation for the 909 keV gamma ray is shown at the top left of Figure 4.13 where the solid curve represents a theoretical fit to these data assuming a spin of 5/2

Figure 4.13 Experimental results from the angular correlation and lifetime measurements made in neutron coincidence for the level at 909 keV . The theoretical fit to the measured distribution is for $J = 5/2$.

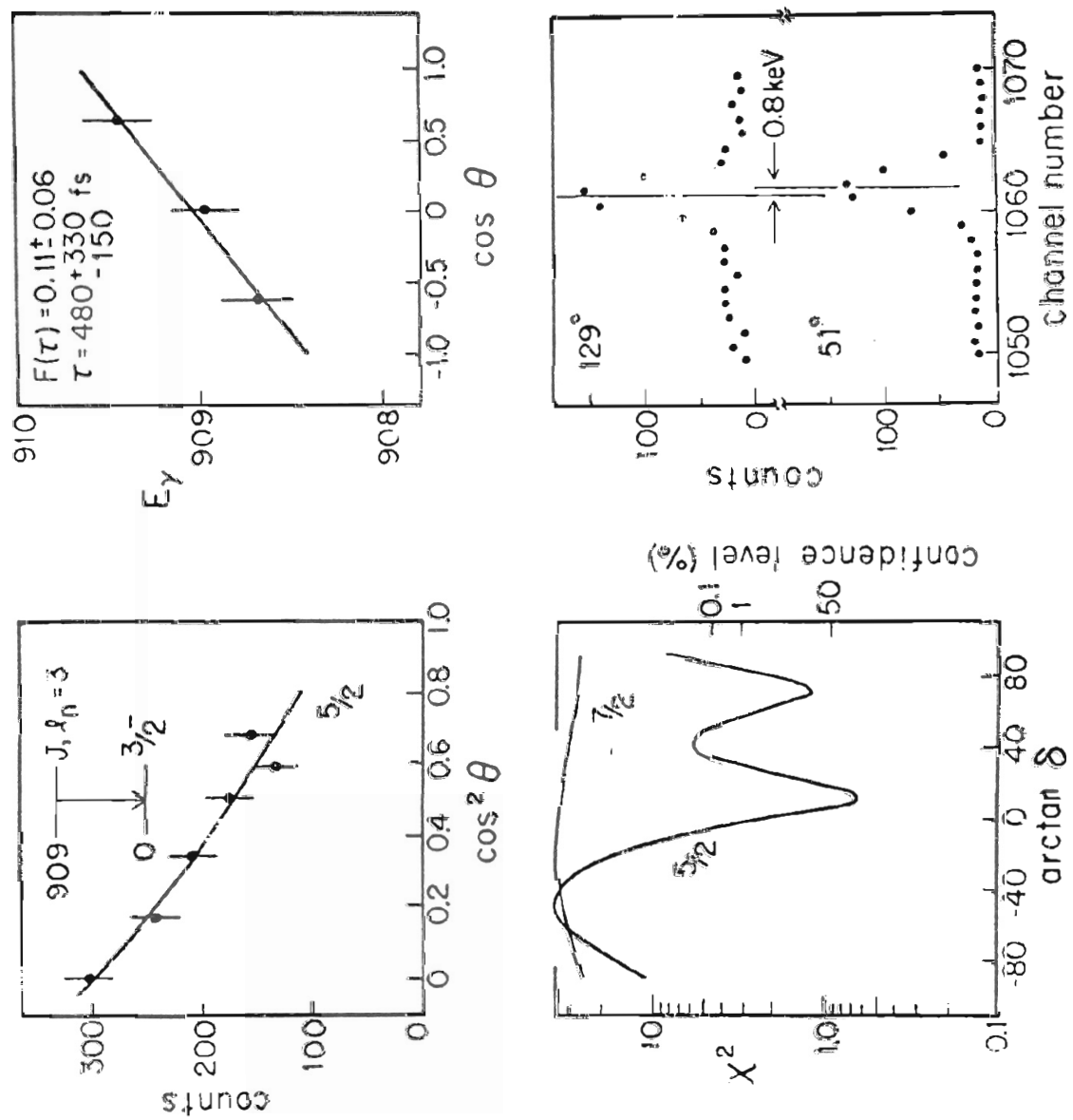
counts
909
J, ℓ_n = 3
0
3/2⁻
5/2
cos² θ
E_γ
F(τ) = 0.11 ± 0.06
τ = 480 +330 −150 fs
cos θ
129°
51°
0.8keV
Channel number
χ^2
7/2
5/2
arctan δ
confidence level (%)

for the emitting level. As stated earlier, the results of stripping reaction measurements using a ^{60}Ni target have determined that this level is populated with $\ell = 3$ neutron transfer. Therefore, since the ground state spin of ^{60}Ni is zero, these measurements limit the spin of the 909 keV level to $J = \ell \pm 1/2$ (i.e., 7/2 or 5/2). Attempts to fit the gamma ray angular correlation using these two spins produced the results shown in the χ^2 plots of Figure 4.13. The 7/2 assignment is clearly eliminated, and two possible ranges of the mixing ratio are selected for the 5/2 fit.

The results of the singles angular distribution and linear polarization measurements are shown in Figure 4.14a. The measured polairzation of -0.15 ± 0.04 gives only one mixing ratio range consistent with both the singles and $n - \gamma$ correlation measurements. Thus, these three measurements when considered together, give $\delta = 0.20 \begin{smallmatrix} + 0.16 \\ - 0.03 \end{smallmatrix}$. The theoretical polarizations in Figure 4.14a were calculated assuming no parity change (i.e., assuming an M1E2 transition), and, as can be seen, the experimental results confirm the negative parity assignment for the 909 keV level.

In Figure 4.14b are shown the results of the singles measurements for the $909 \rightarrow 67$ keV transition. The measured polarization is 0.01 ± 0.11, and the mixing ratio is restricted to $-1.19 \leq \delta \leq -0.36$. The endpoints of this range are subtended by the intersection of the curve representing the calculated polarization with the boundaries of the cross-hatched area representing the allowed values of the measured polarization.

Figure 4.14 Results of the linear polarization and angular distribution measurements made in singles for the level at 909 keV

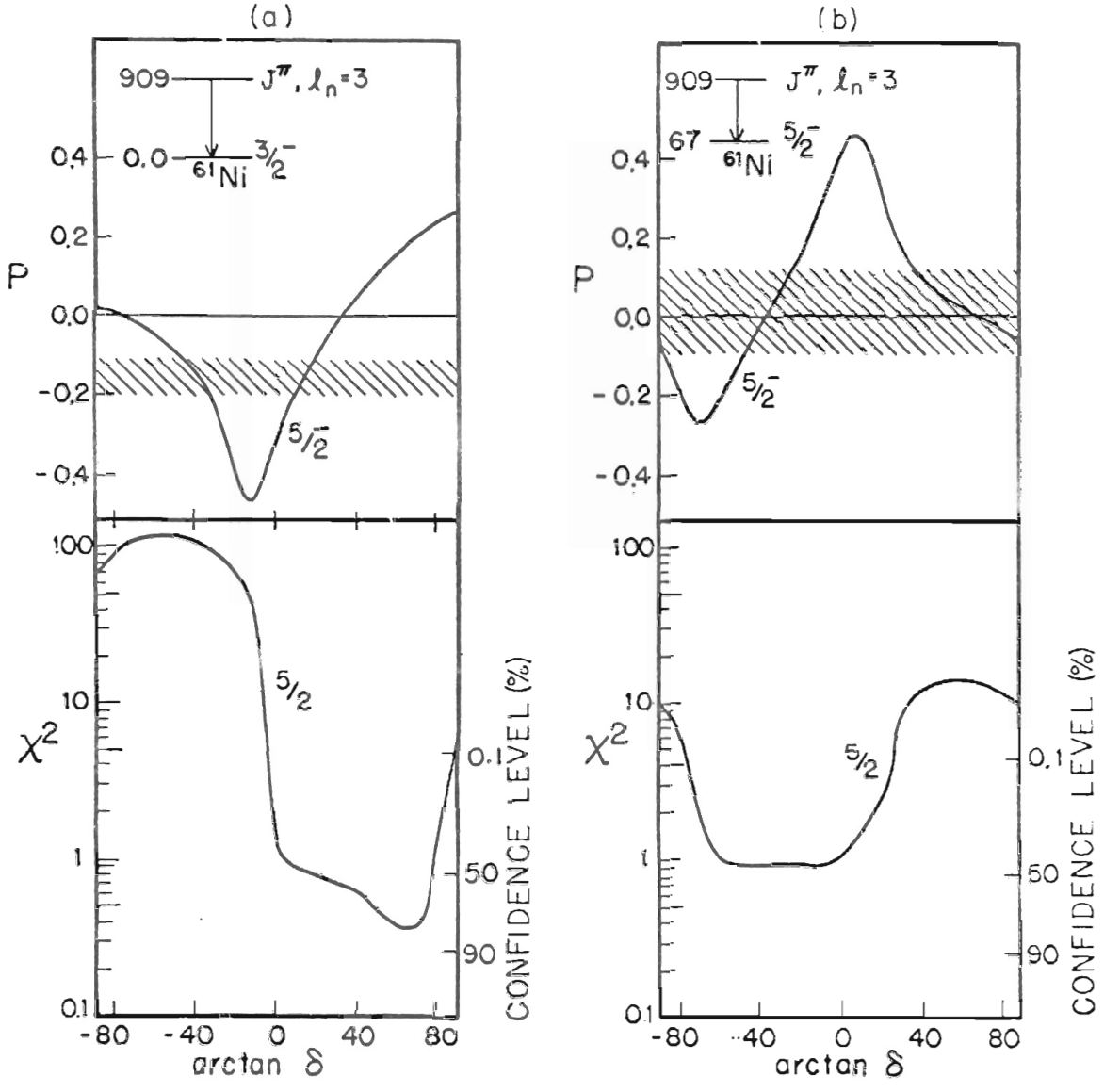
(a)
909
J^π, ℓ_n=3
0.0
^{61}Ni
3/2⁻
5/2⁻
P
0.4
0.2
0.0
-0.2
-0.4
100
10
1
0.1
χ^2
5/2
0.1
50
90
CONFIDENCE LEVEL (%)
-80
-40
0
40
80
arctan δ
(b)
909
J^π, ℓ_n=3
67
^{61}Ni
5/2⁻
5/2⁻
P
0.4
0.2
0.0
-0.2
-0.4
100
10
1
0.1
χ^2
5/2
0.1
50
90
CONFIDENCE LEVEL (%)
-80
-40
0
40
80
arctan δ

4.3.3 The 1016 keV level. The spin and parity of this level were unknown at the time the present work was undertaken. DWBA analyses of the (d,p) and (d,t) data were inconclusive, and no ℓ-values were determined for the transferred neutrons. Reference [60] shows the level to be populated in the β^+-decay of ^{61}Cu ; however, as nearly as can be determined, this suggestion is based solely upon the work of Beraud et al. [8] who are careful to point out that their observation of the gamma decay of this level is rather tenuous. These authors identified what they thought might possible be the ground state decay of the level. The results of the present work have shown this ground state transition to be a 35 ± 3 percent branch. The 1016 keV level also has a 65 ± 5 percent branch to the first excited state at 67 keV . This stronger branch has not been reported in any of the various beta decay studies which suggests that the 1016 keV level is not populated in the β^+-decay of ^{61}Cu . As for the results of the lifetime measurements, the centroids obtained for both branches of this level were found to be unshifted, the result being that only a lower limit of $\tau > 10$ ps could be set for the lifetime. An upper limit was determined by examining the time spectra which corresponded to n - γ coincidences for the $909 \rightarrow 0$, $1016 \rightarrow 67$, and $1100 \rightarrow 0$ keV transitions. Essentially no shifts were observed between the centroids of these three spectra, all of which had a dispersion of approximately two nanoseconds per channel. Therefore, since the 909 and 1100 keV levels were found to have lifetimes on the order of 500 fs , a conservative upper limit of $\tau < 10$ ns was taken for the lifetime of the level at 1016 keV .

The results of the singles measurements for the 1016 → 67 keV transitions are shown in Figure 4.15a . χ^2 plots are shown only for those spin assignments which give solutions below the 0.1 percent confidence level. If the emitting level is assumed to have negative parity, the 9/2 assignment is not consistent with the observed, 35 percent ground state branch since such an assignment would require M3E4 radiation. For positive parity, the radiation emitted in the ground state decay would be E3M4 . With this radiation assumed to be pure E3 , a transition strength of 248 W.u. was calculated using the upper limit of 10 ns for the lifetime. Such an E3 enhancement is clearly unreasonable, and therefore, the 9/2 assignment will not be considered further.

The above arugments result in a 7/2 spin assignment for the 1016 keV level. The level also has negative parity as shown in Figure 4.15a by the results of the linear polarization measurements for the 1016 → 67 keV transition. The measured polarization is -0.22 ± 0.05 , and this value selects a mixing ratio which agrees with the value, $\delta = -2.5^{+0.4}_{-0.5}$, taken from the angular distribution measurements. The large E2 strength implied by this mixing ratio is consistent with other observations in this mass region (e.g., see reference [31]).

The results of the angular distribution measurements for the ground state decay of this level are shown in Figure 4.15b. There appear to be three possible values for the mixing ratio. However, when used with the 10 ns upper limit for the lifetime of this level, the values $\delta = \pm \infty$, were found to require an M3 enhancement of 10^6 W.u.

Figure 4.15 Results of the linear polarization and angular distribution measurements made in singles for the level at 1016 keV

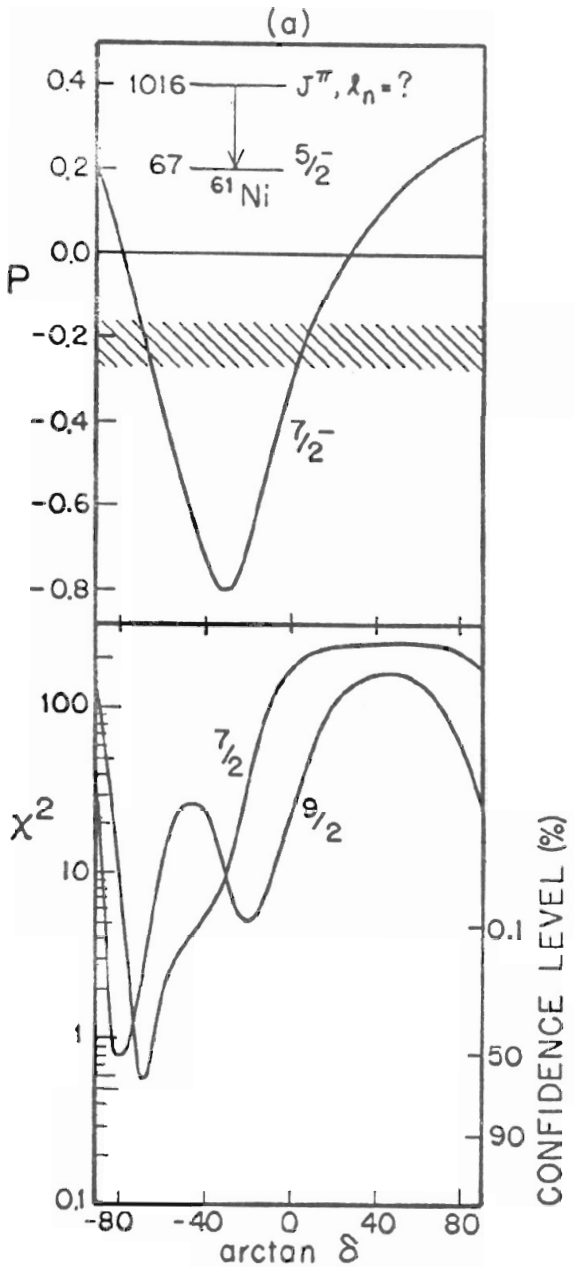
(a)
1016
$J^\pi, \ell_n = ?$
67
$5/2^-$
^{61}Ni
P
$7/2^-$
χ^2
$7/2$
$9/2$
arctan δ
CONFIDENCE LEVEL (%)

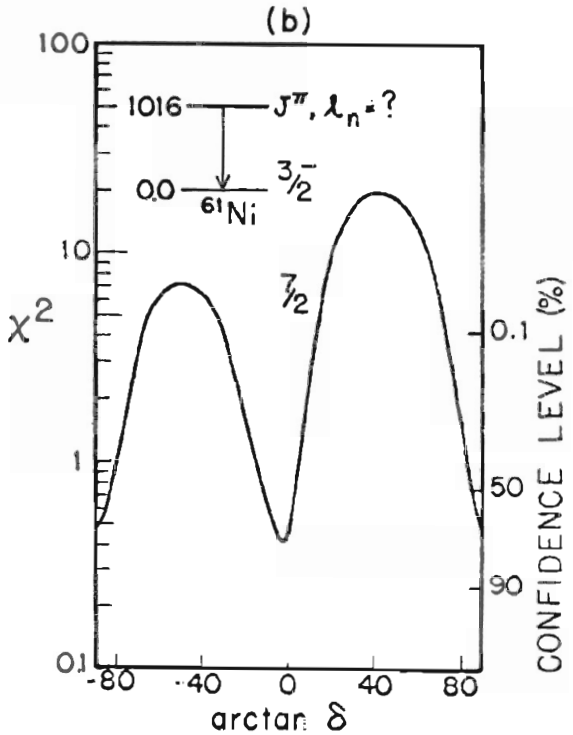
(b)
1016
$J^\pi, \ell_n = ?$
0.0
$3/2^-$
^{61}Ni
χ^2
$7/2$
arctan δ
CONFIDENCE LEVEL (%)

Such an enhancement is obviously unreasonable, thus eliminating the possibility of pure M3 radiation and leaving $\delta = -0.03 \begin{smallmatrix} + 0.12 \\ - 0.22 \end{smallmatrix}$ in Figure 4 15b. The measured polarization for this transition is 45 ± 10 percent which is consistent with a value of 60 percent calculated for $\delta = 0.0$ using Equation 2.34.

4.3.4 The 1100 keV level. This level has been assigned a J^{π} value of $3/2^{-}$ as a result of the beta decay studies and the $\ell = 1$ neutron transfer observed in the (d,p) and (d,t) work. In the present work, the level has been found to have a lifetime of $360 \begin{smallmatrix} + 670 \\ - 155 \end{smallmatrix}$ fs with branches of 41 ± 4, 8 ± 2, and 51 ± 5 percent to the ground state and the first and second excited states, respectively.

The results of the singles measurements for the 1100 → 0 keV transition are shown in Figure 4.16 where the measured polarization is -0.02 ± 0.23. As can be seen, these measurements do not distinguish between the spin assignments of 1/2 and 3/2, and essentially no limits can be placed upon the allowed values of the mixing ratio. Additionally, assuming the 3/2 assignment to be correct, these measurements do not determine the parity of the level.

Results similar to these were also obtained for the 1100 → 283 keV transition so that, with the exception of the lifetime and branching ratios, no information can be given for the gamma decay of this level.

Figure 4.16 Results of the linear polarization and angular distribution measurements made in singles for the level at 1100 keV

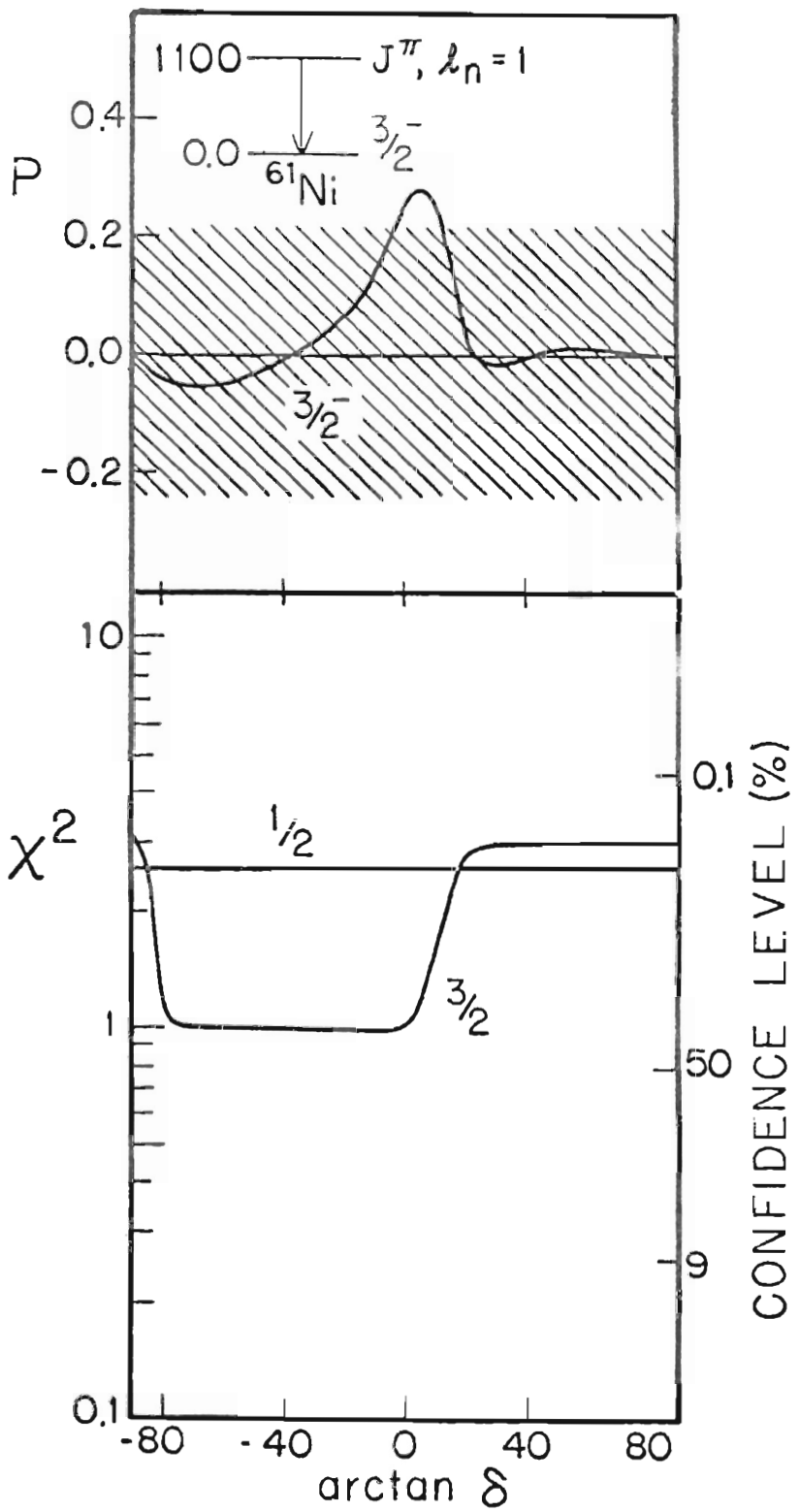
1100
J^π, $\ell_n = 1$
0.0
^{61}Ni
$3/2^-$
P
0.4
0.2
0.0
-0.2
$3/2^-$
10
1
0.1
χ^2
$1/2$
$3/2$
0.1
50
9
CONFIDENCE LEVEL (%)
-80
-40
0
40
80
arctan δ

4.3.5 The 1132 keV level. A mean lifetime of $400 \begin{smallmatrix} + 200 \\ - 100 \end{smallmatrix}$ fs has been measured for this level which has also been found to have branches of 61 ± 6 and 39 ± 5 percent to the ground state and first excited state, respectively. The J^{π} assignment of $5/2^{-}$ from the beta decay studies is consistent with the $\ell = 3$ neutron transfer observed in the stipping and pickup reactions.

As can be seen in Figure 4.17a, this spin assignment is confirmed by the results of the $\gamma - \gamma$ correlation measurements for the 1132 → 0 keV transition. The results of the singles measurements for this branch are shown in Figure 4.17b. The measured polarization of $- 0.03 \pm 0.05$ is consistent with the negative parity assigned to this level, and the range of the mixing ratio is restricted to $0.36 \leq \delta \leq 0.70$.

The result of the singles measurements for the 1132 → 67 keV transition are shown in Figure 4.18. The allowed ranges of the mixing ratio are $-\infty \leq \delta \leq -0.84$ and $2.14 \leq \delta \leq \infty$. Both ranges give substantial E2 transition strengths.

4.3.6 The 1186 keV level. This level has previously been assigned a J^{π} value of $3/2^{-}$ as a result of the beta decay studies and the $\ell = 1$ neutron transfer observed in the (d,p) and (d,t) reactions. The results of the present work indicate that this level has branches of 77 ± 8, 6 ± 2, 5 ± 2, and 12 ± 3 percent to the levels at 0, 67, 283, and 656 keV, respectively.

Unfortunately, the strongest of these branches, the 1186 → 0 keV transition, was contaminated by the ground state decay of the

Figure 4.17 The level at 1132 keV

(a) n - γ angular correlation results

(b) Results of the linear polarization and angular distribution measurements made in singles

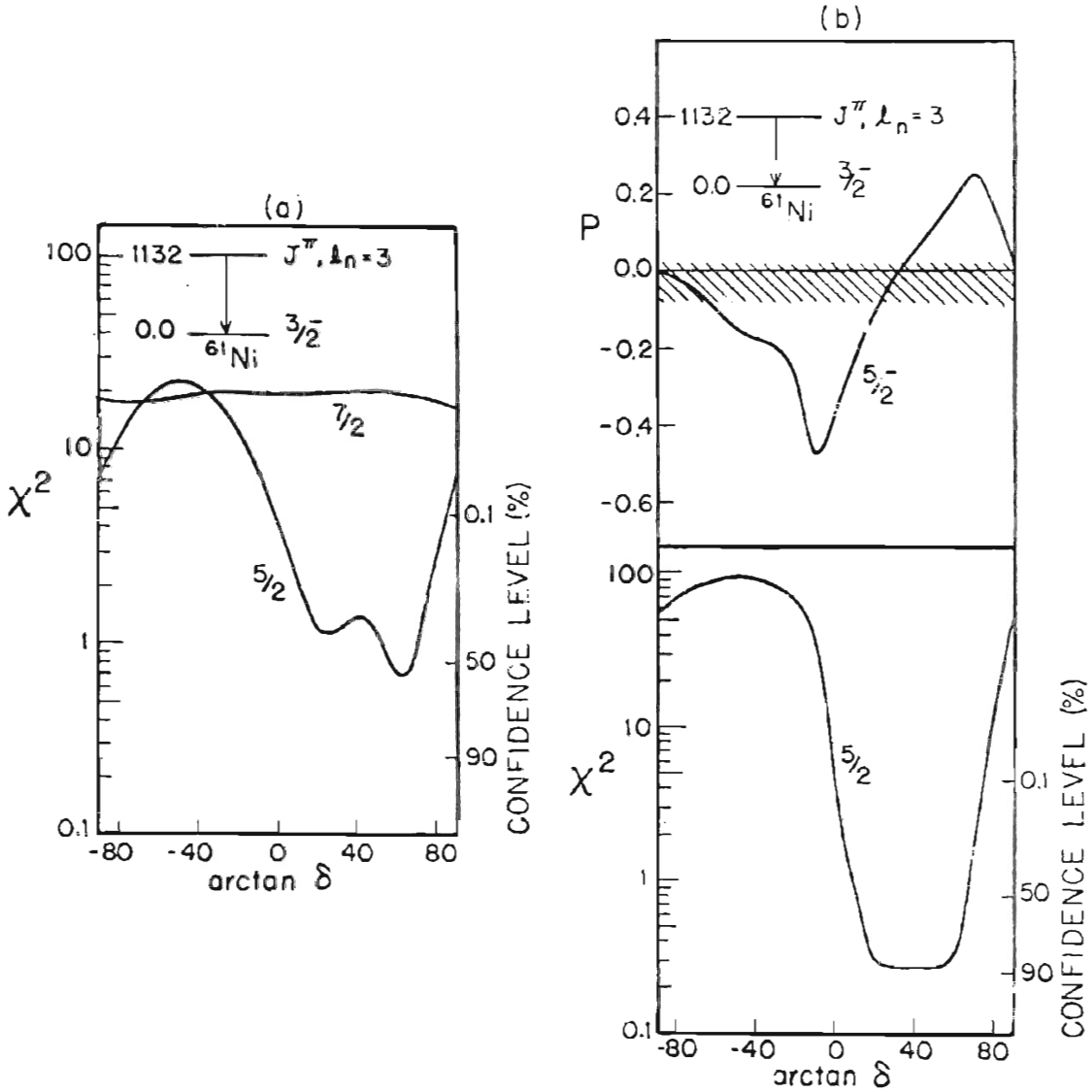
(a)
1132
$J^\pi, \ell_n = 3$
0.0
^{61}Ni
$3/2^-$
$7/2$
$5/2$
χ^2
CONFIDENCE LEVEL (%)
arctan δ
(b)
1132
$J^\pi, \ell_n = 3$
0.0
^{61}Ni
$3/2^-$
P
$5/2^-$
$5/2$
χ^2
CONFIDENCE LEVEL (%)
arctan δ

Figure 4.18 Results of the linear polarization and angular distribution measurements made in singles for the level at 1132 keV

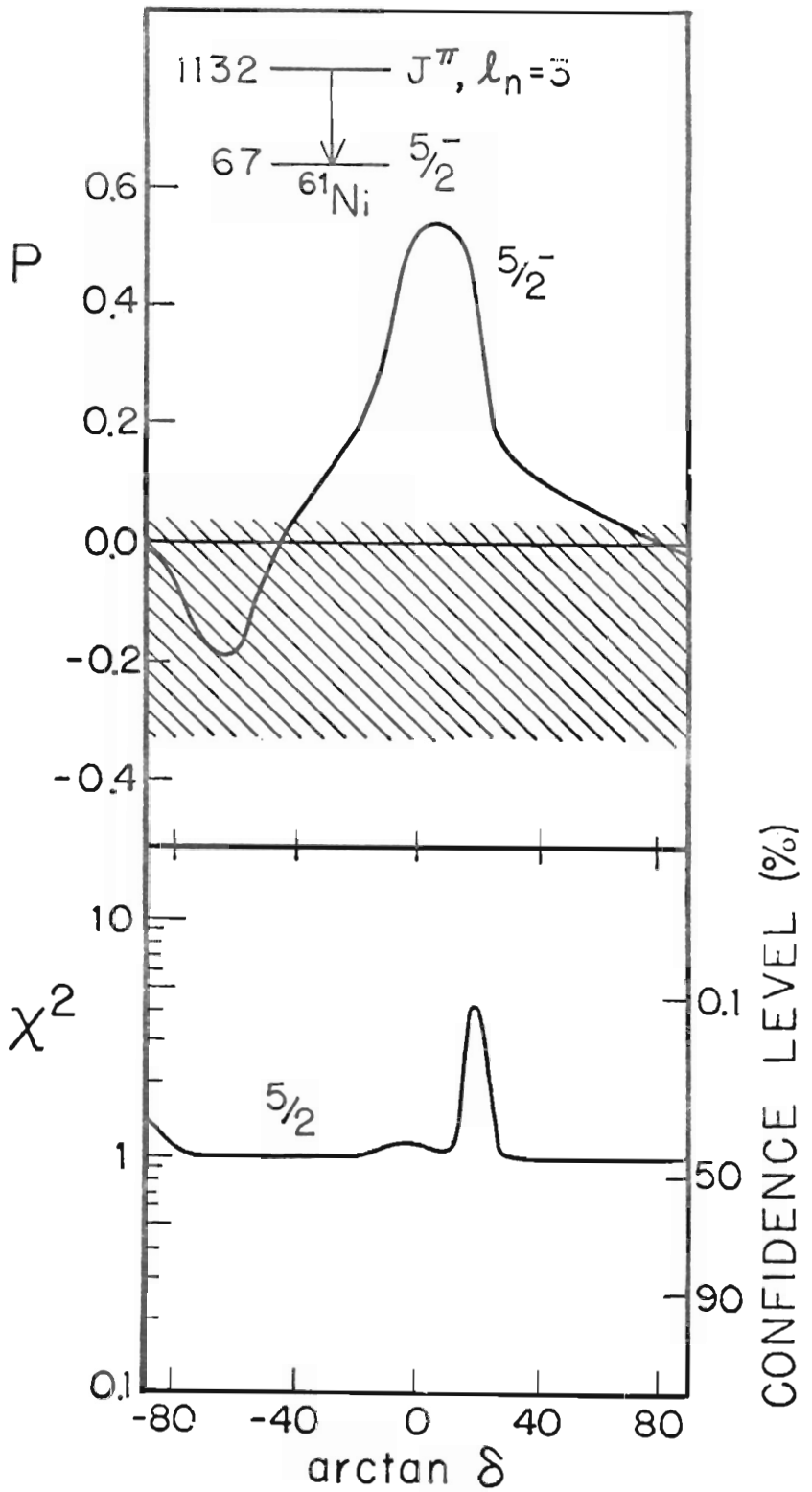
1132
$J^\pi, \ell_n = 3$
67
^{61}Ni
$5/2^-$
P
0.6
0.4
0.2
0.0
-0.2
-0.4
$5/2^-$
10
1
0.1
χ^2
$5/2$
0.1
50
90
CONFIDENCE LEVEL (%)
-80
-40
0
40
80
arctan δ

forth excited state in ^{59}Ni (E_γ = 1184 keV). This level was populated in the $^{56}Fe(\alpha,n\gamma)^{59}Ni$ reaction. As a result, singles measurements were not made for the 1186 → 0 keV transition. Neither were such measurements made for any of the other branches.

However, for the coincidence measurements, the contaminant gamma was eliminated by setting a proper neutron window. The ground state Q-values for the (α,n) reactions on ^{56}Fe and ^{58}Fe are - 3.09 and - 3.83 MeV , respectively. Therefore, neutrons leading to the population of the 1184 keV level in ^{59}Ni have about 1.3 MeV less energy than the neutrons which populate the 1186 keV level in ^{61}Ni . The contaminant radiation from ^{59}Ni was eliminated by setting a neutron window which excluded gamma rays from levels of about 2.4 MeV excitation energy in ^{61}Ni . In this manner, a lifetime of 160 $\pm$ 26 fs was determined for the level at 1186 keV .

The results of the $n - \gamma$ angular correlation measurements are shown in Figure 4.19 . The 1/2 spin assignment is eliminated, and though the range in rather wide, the mixing ratio can be limited to $-\infty \leq \delta \leq 0.27$.

4.3.7 The 1457 keV level. This level has not been reported populated in the β^+-decay of ^{61}Cu , and neither has a neutron ℓ-value been assigned from a DWBA analysis of the proton angular distribution obtained in the (d,p) work of reference [16]. However, $\ell = 3$ neutron transfer has been reported in both the (d,t) study of reference [23] and the $(^3He,\alpha)$ work of reference [52]. These results have favored a 7/2 spin assignment based upon the J-dependence

Figure 4.19 Results of the n - γ angular correlation measurements for the level at 1186 keV

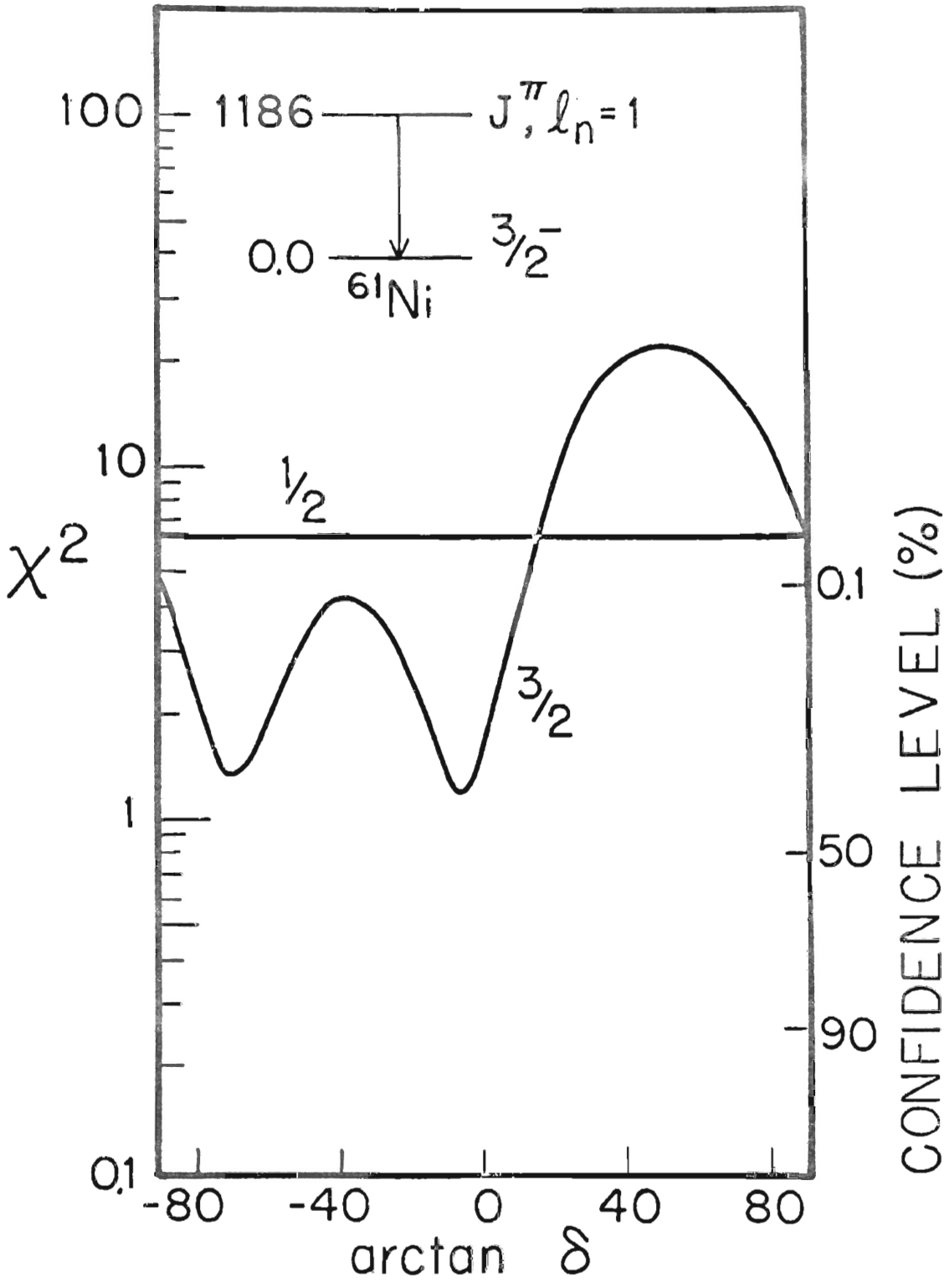
100
10
1
0.1
1186
$J^{\pi}, \ell_n = 1$
0.0
$3/2^-$
^{61}Ni
χ^2
1/2
3/2
0.1
50
90
CONFIDENCE LEVEL (%)
-80
-40
0
40
80
arctan δ

exhibited by the triton and alpha particle angular distributions. Analysis from the present work has resulted in a mean lifetime of $480 \begin{smallmatrix} + 340 \\ - 160 \end{smallmatrix}$ fs and branches of 76 ± 8 and 24 ± 4 percent for the gamma decay of this level to the ground state and first excited state, respectively.

The angular distribution measured in singles for the ground state transition is shown in Figure 4.20a. The solid curves represent theoretical fits to the data for $J = 7/2$ with $\delta = 0.0$ and $J = 5/2$ with $\delta = -0.72 \begin{smallmatrix} + 0.20 \\ - 0.29 \end{smallmatrix}$. For the $5/2$ fit, the mixing ratio was taken from the results of the $\alpha - \gamma$ correlation measurements. These results are shown in Figure 4.20c where, for the $5/2$ assignment, they can be seen to be consistent with the results of the singles measurements shown in Figure 4.20b. With $P = -0.12 \pm 0.22$, the polarization measurements confirm the negative parity assignment for this level.

No theoretical calculations are shown in Figure 4.20b for the polarization of the E2M3 radiation required by a $7/2$ spin assignment for the emitting level. However, the correlation measurements alone limit the mixing ratio to either 0.14 ± 0.04 or $5.7 \begin{smallmatrix} + 5.7 \\ - 2.0 \end{smallmatrix}$. For $J^{\pi} = 7/2^{-}$, the ground state decay of this level would normally be expected to decay by the emission of pure E2 radiation. Therefore, for $\delta = 0.14 \pm 0.04$, there arose the question of whether or not there was some unexplained error which caused the mixing ratio to be nonzero. The most probable source of such an error was the fact that the calculation of an error for δ did not include errors for the population parameters used in the fit.

Figure 4.20 The level at 1457 keV

(a) Angular distribution measured in singles. The theoretical fit is for $J = 5/2$.

(b) Results of the linear polarization and angular distribution measurements made in singles

(c) n - γ angular correlation results

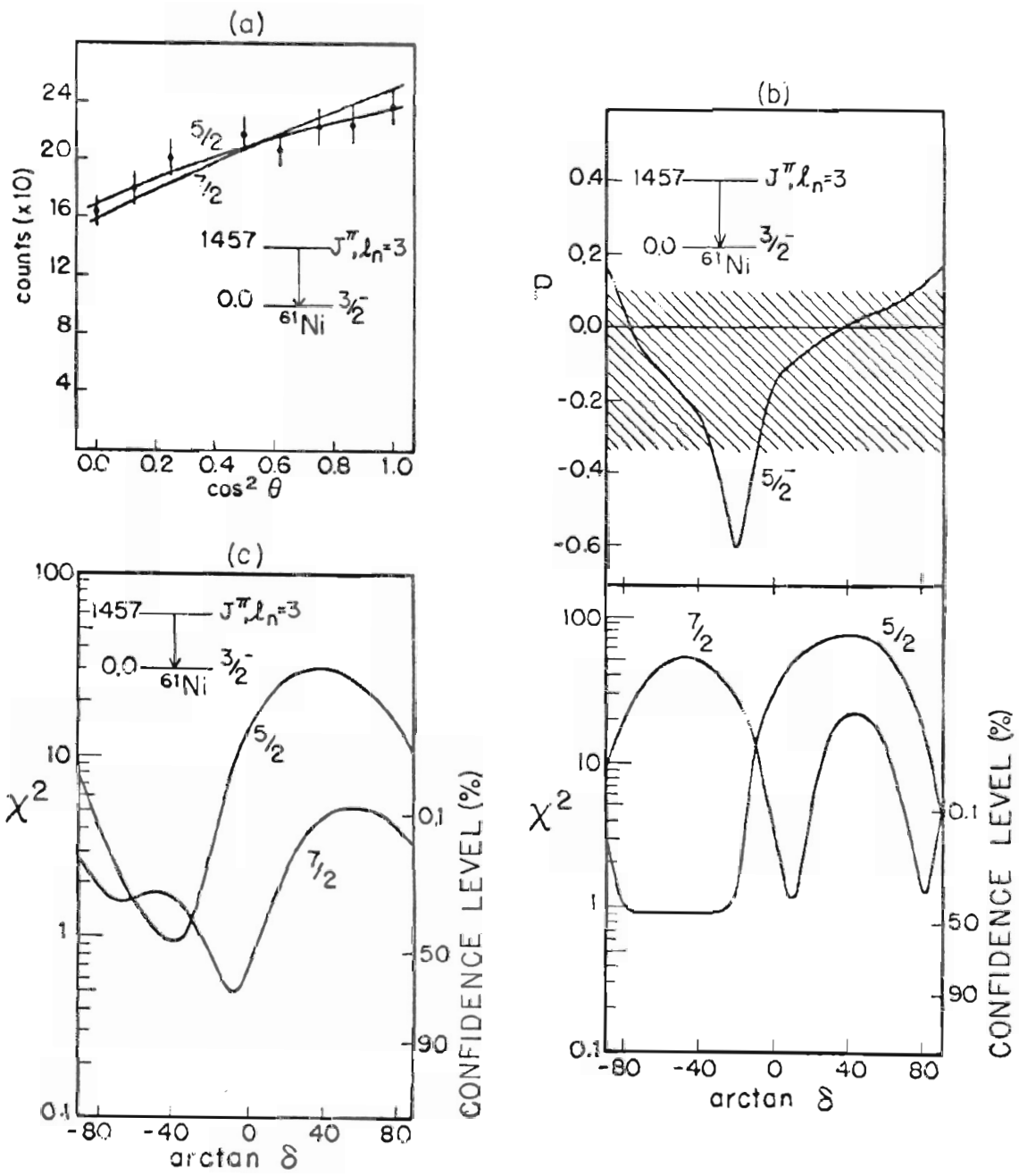
(a)
counts (x10)
cos² θ
5/2
7/2
1457
J^π, ℓ_n=3
0.0
61Ni
3/2⁻
(b)
D
5/2⁻
(c)
χ²
CONFIDENCE LEVEL (%)
arctan δ

This problem was investigated in the following manner. As described earlier, the fitting procedure used for the singles correlation measurements involved limiting the allowed population parameters to ranges determined by adding $\pm$ 20 percent to the values calculated with transmission probabilities obtained from optical model calculations. The theoretical fit to the angular distribution presently being considered gave a χ^2 value of 0.99 with population parameters $P(1/2) = 0.43$, $P(3/2) = 0.41$, and $P(5/2) = 0.16$. These results are in agreement with a recently developed procedure for analyzing angular distributions by assuming a gaussian distribution for the population parameters [53]. The optical model calculations implied $P(7/2) < 10$ percent, and, as a result, population of this substate was not considered during the fitting procedure.

This same angular distribution was next analyzed with no restrictions on the population parameters. The results were χ^2 = 0.90 for $\delta = 0.10 \pm 0.09$ and $P(1/2) = 0.60$, $P(3/2) = 0.06$, and $P(5/2) = 0.34$. These results can be interpreted as implying that an unphysical set of population parameters is required to give a mixing ratio most nearly equal to zero. Thus it appears that the original fit with restricted substate population is valid. From these results, an M3 transition strength of 2.6×10^5 W.u. was calculated using the smallest allowed mixing ratio ($\delta = 0.10$) and the largest possible lifetime ($\tau = 820$ fs). Such an enhancement is obviously unreasonable, and, on this basis, the 7/2 assignment can be eliminated.

Finally, the results of the coincidence and singles measurements are shown in Figures 4.21a and 4.21b, respectively, for the 1457 → 67 keV transition. Only a 5/2 spin assignment was considered, and, as can be seen, the mixing ratio is limited to $-2.75 \leq \delta \leq 0.36$.

4.3.8 The 1611 keV level. Prior to the beginning of this work a tentative spin assignment of 5/2 had been made for this level solely as a result of the beta decay studies. No neutron ℓ- values were obtained from the (d,p) and (d,t) measurements. The results of the present work show that this level has branches of 42 ± 6 and 58 ± 9 percent to the levels at zero and 67 keV, respectively. The mean lifetime was found to be $365\ ^{+160}_{-\ 90}$ fs.

As shown in Figure 4.22a, the 1/2 and 3/2 spin assignments are eliminated by the singles angular distribution measurements. These measurements also restrict the mixing ratio to $0.18 \leq \delta \leq 2.75$ for the 5/2 assignment. This range for δ is in agreement with the results of the polarization measurements for which the measured polarization is 0.05 ± 0.20.

The results of the singles measurements for the 1611 → 67 keV transition are shown in Figure 4.22b. The polarization measurements, with $P = 0.49 \pm 0.19$, definitely confirm a J^{π} value of $5/2^-$ for the emitting level. The mixing ratio is restricted to $-0.18 \leq \delta \leq 0.18$.

4.3.9 The 1730 keV level. The $\ell = 1$ neutron transfer which characterized this level in the (d,p) and (d,t) studies is consistent with the reported population of the level in the β^+-decay

Figure 4.21 The level at 1457 keV

(a) n - γ angular correlation results

(b) Results of the linear polarization and angular distribution measurements made in singles

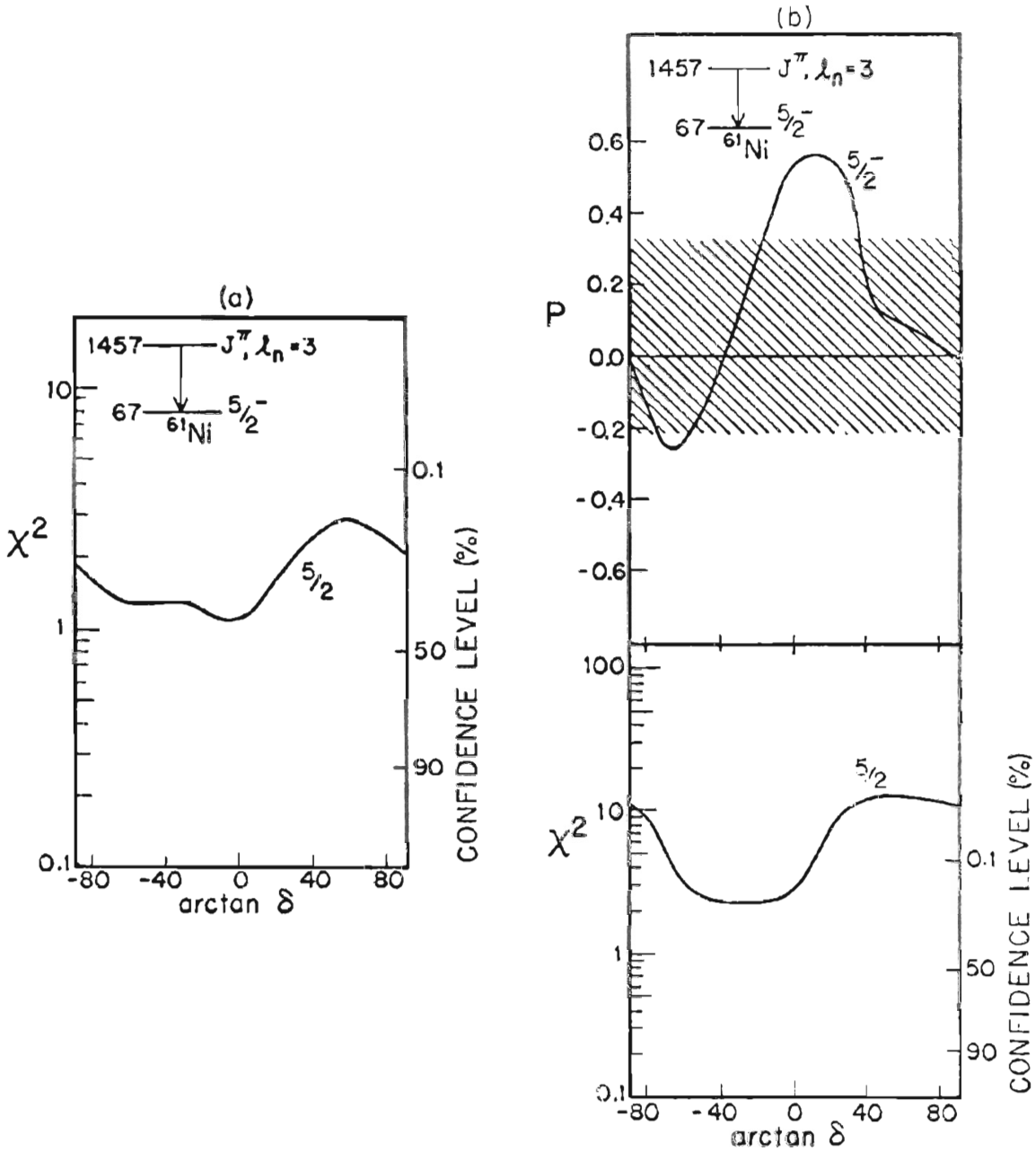
(a)
1457
$J^\pi, \ell_n = 3$
67
^{61}Ni
$5/2^-$
χ^2
$5/2^-$
arctan δ
CONFIDENCE LEVEL (%)
(b)
P
$5/2^-$
χ^2
$5/2^-$
arctan δ
CONFIDENCE LEVEL (%)

Figure 4.22 Results of the linear polarization and angular distribution measurements made in singles for the level at 1611 keV

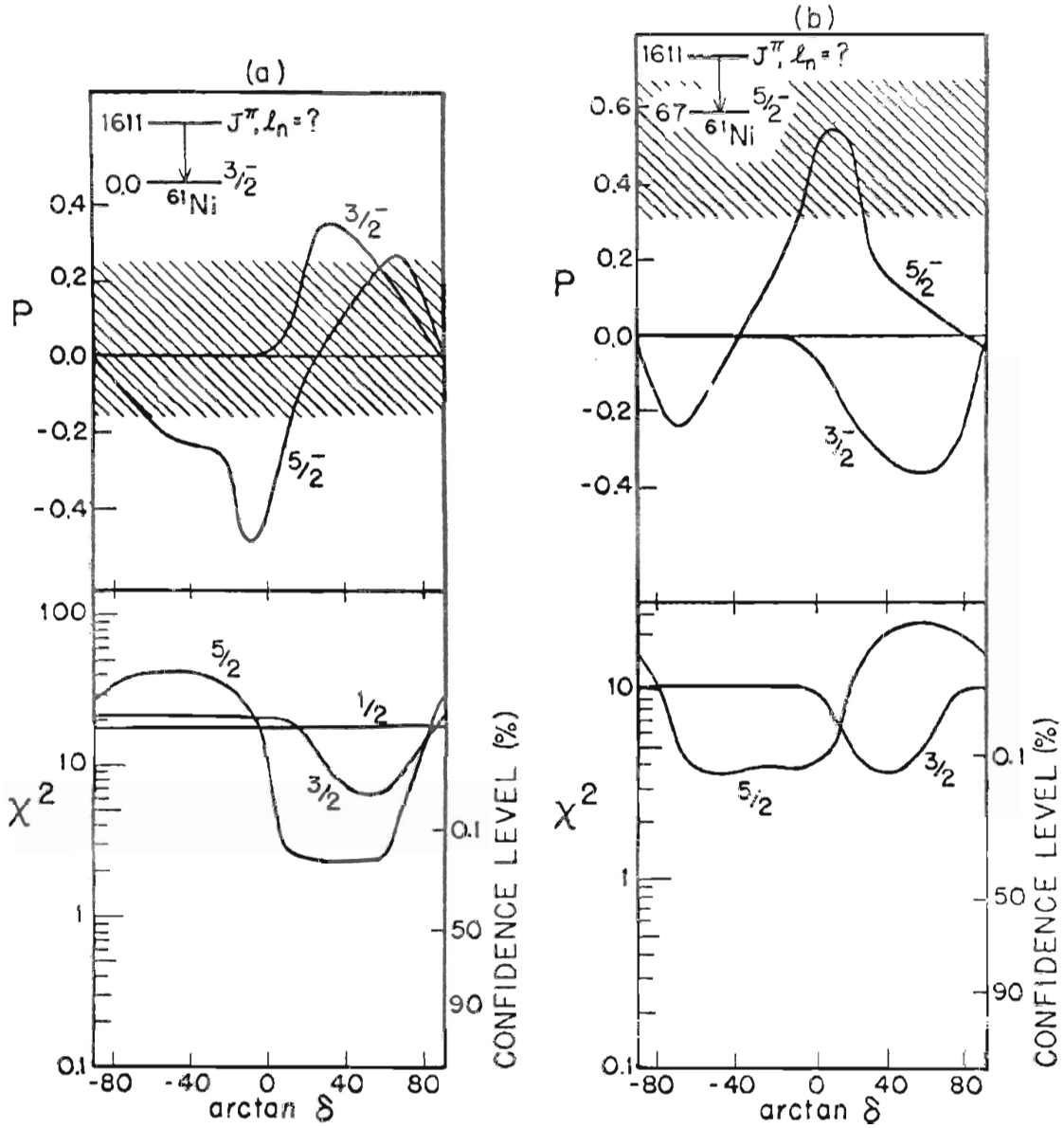
(a)
1611
$J^\pi, \ell_n = ?$
0.0
$3/2^-$
^{61}Ni
P
$3/2^-$
$5/2^-$
χ^2
$5/2$
$1/2$
$3/2$
CONFIDENCE LEVEL (%)
arctan δ
(b)
1611
$J^\pi, \ell_n = ?$
67
$5/2^-$
^{61}Ni
P
$5/2^-$
$3/2^-$
χ^2
$5/2$
$3/2$
CONFIDENCE LEVEL (%)
arctan δ

of ^{61}Cu . However, these measurements have not been able to distinguish between the J^{π} assignments of $1/2^-$ and $3/2^-$.

As a result of the coincidence measurements made in the present work, this level has been found to have a mean lifetime of 88 ± 12 fs and four branches of 25 ± 5 , 38 ± 6 , 16 ± 5 , and 21 ± 5 percent to the levels at 0 , 67 , 283 , and 656 keV , respectively. These branches participated in the decay of this level with approximately equal strength, and the resulting $n - \gamma$ correlation for the radiation from any particular branch was very weak. These correlations were used only to determine the branching ratios. No attempt was made to extract mixing ratio information.

For reasons similar to those just stated, the singles measurements for this level also provided to be of little use. The one exception was the polarization measurement made for the gamma ray resulting from the 1730 → 656 keV transition (E_γ = 1074 keV). For most forward angles, Doppler energy shifts resulted in the contamination of this transition by the gamma ray from the 1132 → 67 keV transition (E_γ = 1065 keV). However, at 90° the two gamma rays were separated reasonably well, and the contaminant radiation was removed by fitting the two peaks with a double gaussian. The resulting polarization for the 1074 keV gamma ray was 0.63 ± 0.32 which is consistent only with a $3/2$ spin assignment for this level.

4.3.10 The 1812, 1990, and 1997 keV level. These three levels were weakly populated in the present study, and all attempts to make J^{π} assignments and extract mixing ratios proved futile. This is

unfortunate because neither have spin assignments been made in any of the previously referenced beta decay and charged particle reaction studies.

Lifetimes measured for these levels in this work are given as follows: $230 \,^{+\,120}_{-\,65}$ fs (E_x = 1812 keV), $500 \,^{+\,530}_{-\,190}$ fs (E_x = 1990 keV), and 48 ± 10 fs (E_x = 1997 keV). The 1812 keV level was found to decay 100 percent to the first excited state, and the 1997 keV level decayed 100 percent to the ground state. Branches of 37 ± 12 and 63 ± 16 percent were determined for the decay of the 1990 keV level to the levels at 67 and 656 keV, respectively.

4.3.11 The 2020 keV level. The only information available for this level prior to the beginning of the present work was an $\ell = 3$ assignment for the neutron transfer observed in the (d,t) work. This level has since been found to have a lifetime of $155 \,^{+\,50}_{-\,33}$ fs with a 100 percent branch to the first excited state.

The results of the singles measurements for three possible spin assignments are shown in Figure 4.23. As can be seen, the measured polarization of -0.65 ± 0.27 is consistent with only a J^{π} assignment of $7/2^-$. The corresponding mixing ratio from the angular distribution measurements is $\delta = 0.03 \pm 0.16$.

4.3.12 The 2123 and 2125 keV levels. As reported in the (d,p) work of reference [16], the angular distribution for protons leading to the population of levels near 2130 keV could be described by a combination of DWBA fits, one characterized by $\ell = 1$ neutron transfer and the other with $\ell = 4$ transfer. This result was correctly

Figure 4.23 Results of the linear polarization and angular distribution measurements made in singles for the level at 2020 keV

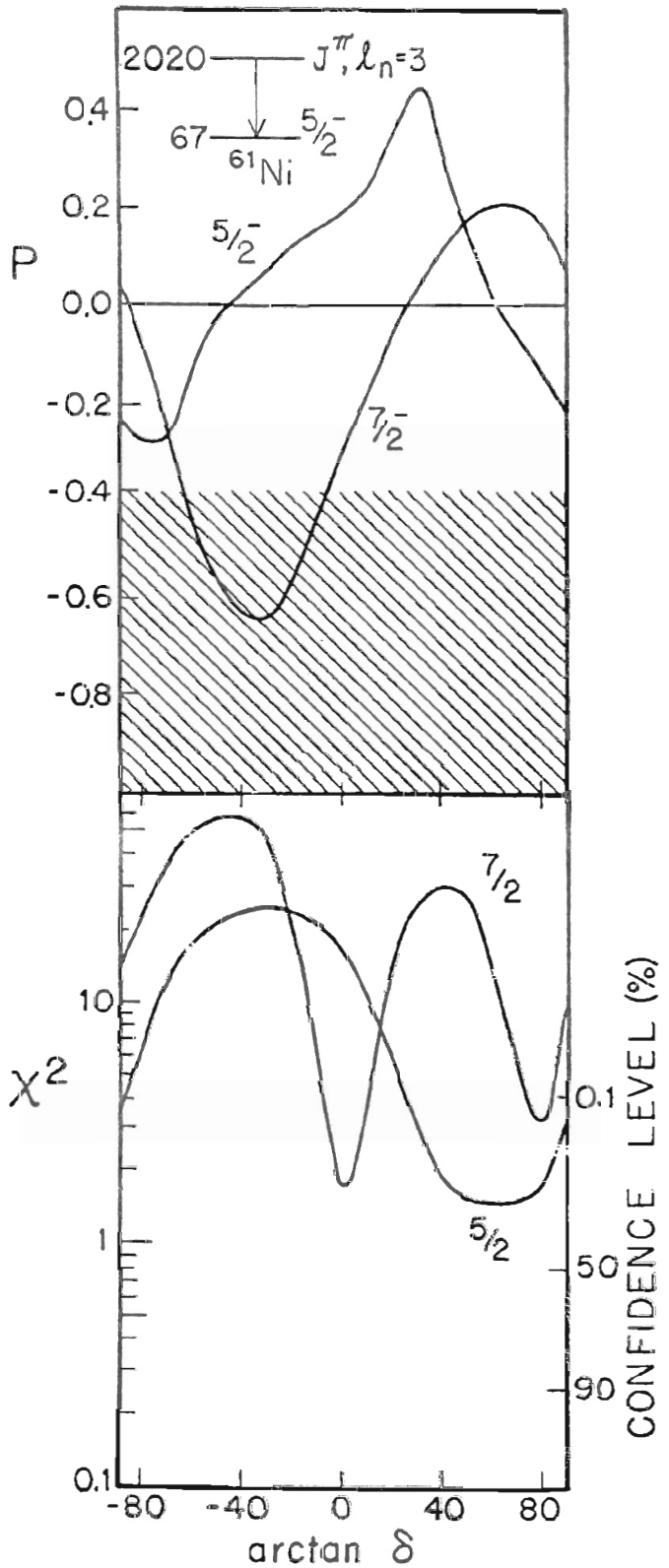
2020
$J^\pi, \ell_n=3$
67
$5/2^-$
^{61}Ni
$5/2^-$
$7/2^-$
P
0.4
0.2
0.0
-0.2
-0.4
-0.6
-0.8
$7/2$
$5/2$
χ^2
10
1
0.1
0.1
50
90
CONFIDENCE LEVEL (%)
-80
-40
0
40
80
arctan δ

interpreted as signifying the existence of an unresolved doublet at this excitation energy. The results of the present work confirm this interpretation with the resolution of this doublet with members separated by approximately two keV . With an excitation energy of 2125 keV , the upper member of the doublet has been observed in the β^+-decay of ^{61}Cu and is therefore the level populated by the $\ell = 1$ neutron transfer. This level has been found to have a mean lifetime of 46 ± 8 fs with branches of greater than 95 percent and less than five percent to the levels at zero and 1186 keV , respectively. The five percent branch is a tentative assignment based on (d,p) measurements made in this work (see Section 4.2). Finally, an isotropic angular distribution was obtained for the gamma radiation resulting from the ground state decay of this level. This result is consistent with the 1/2 spin assignment made in the beta decay work.

There now remains the lower member of the doublet. The assertion that this level is populated by $\ell = 4$ neutron transfer is supported by the observed, 100 percent decay of the level to the $7/2^-$ state at 1016 keV . The level has been found to have a mean lifetime of $585 \begin{smallmatrix} + 1065 \\ - 175 \end{smallmatrix}$ fs , and its positive parity make it the lowest such level found in ^{61}Ni .

The results of the singles, angular distribution measurements are shown in Figure 4.24 where, in accordance with the $\ell = 4$ neutron transfer only the spins, 7/2 and 9/2 , have been considered. Both these assignments result in E1M2 radiation since the emitting level has positive parity. The smallest allowed mixing ratio for $J = 7/2$ is $\delta \approx 0.4$ ($\arctan \delta \approx 20°$) . This value was used with the maximum

Figure 4.24 Results of the linear polarization and angular distribution measurements made in singles for the level at 2123 keV

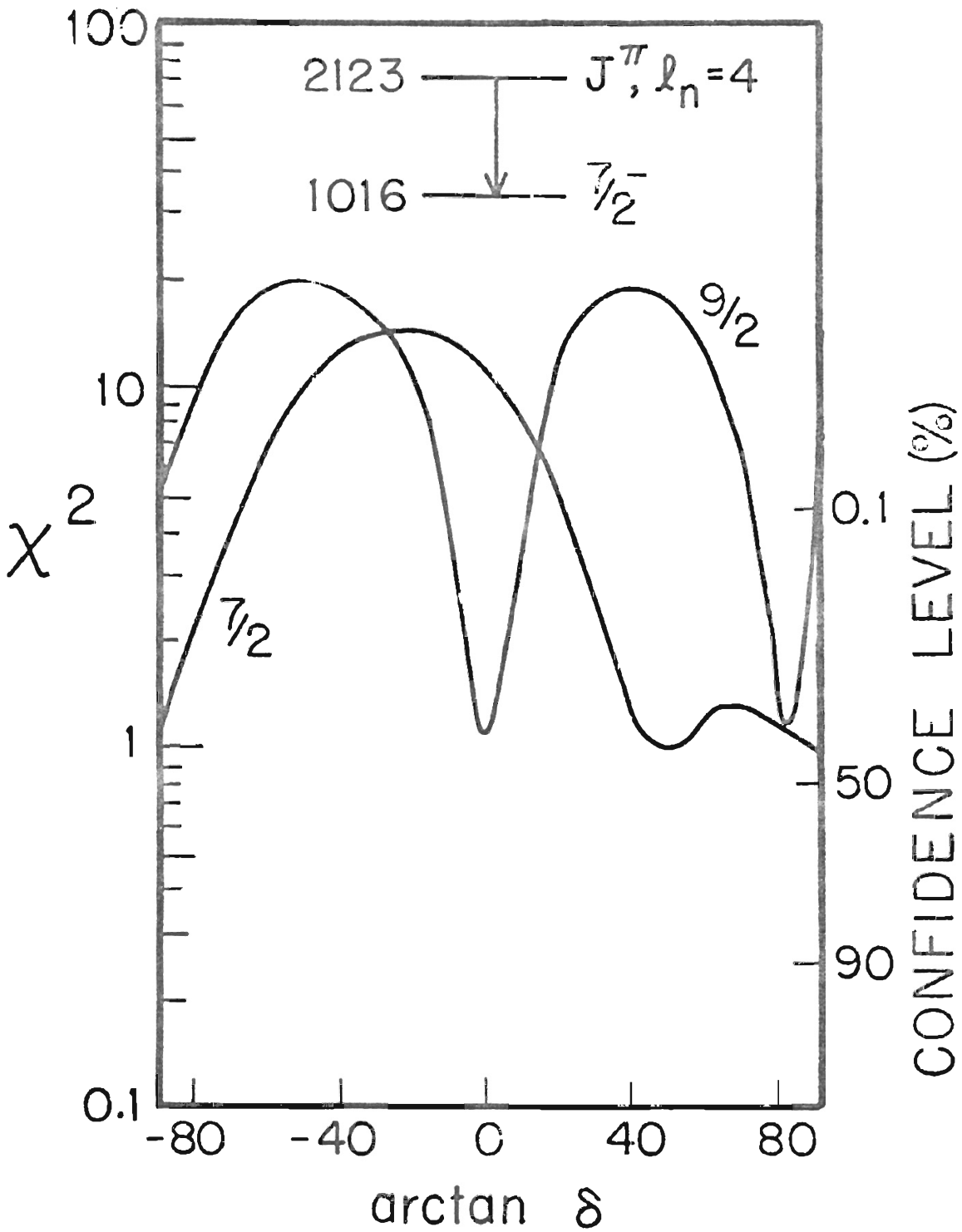
100
10
1
0.1
χ^2
2123
$J^\pi, \ell_n=4$
1016
$7/2^-$
9/2
7/2
-80
-40
0
40
80
arctan δ
0.1
50
90
CONFIDENCE LEVEL (%)

possible lifetime (1650 fs) to calculate a lower limit of 145 W.u. for the M2 transition strength. This enhancement contradicts the discussion of reference [1] in which M2 strengths in the $1f_{7/2}$ shell are reported to be generally retarded by a factor of 10 to 100 . On this basis then, the 7/2 assignment can be ruled out. This same argument can also be used to eliminate the larger of the two allowed mixing ratios for the 9/2 assignment, thus leaving $\delta = -0.03 \pm 0.28$.

The linear polarization of the 1107 keV gamma ray resulting from this transition was not determined for the following reason. As described in Section 4.2, the resolution of the polarimeter was reduced from 2.4 keV (FWHM , 1.33 MeV) for the individual crystals to 3.5 keV for the summed energy signals. This degraded resolution prevented the reliable separation of the gamma rays from the $1100 \rightarrow 0$, $2123 \rightarrow 1016$, and $1186 \rightarrow 67$ keV transitions.

4.4 Summary

The results of the above discussions are summarized in Table 4.1 where, for a range of the mixing ratio including $\pm \infty$, the corresponding transition strengths have been calculated with δ taken as the finite limit of the range. For a finite range of δ , the mixing ratio was chosen as the midpoint of the range. The theoretical transition strengths have been determined in the present work using the lifetimes, branching ratios, and mixing ratios predicted by the shell model calculations of Glaudemans *et al.* [26]. For the first seven excited states, these values are shown in Figure 4.25 along with

Table 4.1 Experimental situation for the states in ^{61}Ni below 200 keV. The theoretical transition strengths of reference [60] were calculated using the shell model. The J^{π} assignments for the levels at 0, 67, 283, 656, 1100, and 1997 keV are from reference [26] as are the levetimes for the first three excited states. The remaining information has been either confirmed or obtained in the present work.

E_i (keV)	E_f	J_i^{π}	J_f^{π}	τ (fs)	B.R. (%)	δ	M1 Strength ($\times 10^{-2}$ W.u.) Exp.	M1 Strength Ref [26]	E2 Strength (W.u.) Exp.	E2 Strength Ref [26]
67	0	$5/2^{-}$[a]	$3/2^{-}$	5.2 ns[a]	100					
283	0	$1/2^{-}$[a]	$3/2^{-}$	22ps[a]	100					
656	0	$3/2^{-}$[a]	$3/2^{-}$	< 30ps[a]	76±					
	67		$5/2^{-}$		8±					
	283		$1/2^{-}$		16±					
909	0	$5/2^{-}$	$3/2^{-}$	450^{+330}_{-150}	75 ± 5	0.20 ± 0.68	6.8	0.08	5.9	9.0
	67		$5/2^{-}$		20 ± 3	$-1.19 \leq \delta \leq -0.36$	1.5[b]	0.9	22.0[b]	0.7
	283		$1/2^{-}$		5 ± 2					
1016	0	$7/2^{-}$	$3/2^{-}$	> 10ps	35 ± 3	$-0.03^{+0.12}_{-0.22}$		8.2	< 1.8	40.0
	67		$5/2^{-}$		65 ± 5	-2.5 ± 0.5	< 0.03		< 4.2	
1100	0	$1/2^{-}$,$3/2^{-}$	$3/2^{-}$	360^{+670}_{-155}	41 ± 4					
	67		$5/2^{-}$		8 ± 2					
	283		$1/2^{-}$		51 ± 5					

Table 4.1 (Continued)

E_i (keV)	E_f (keV)	J_i^π	J_f^π	τ (fs)	B.R. (%)	δ	M1 Strength ($\times 10^{-2}$ W.u.) Exp.	M1 Strength ($\times 10^{-2}$ W.u.) Ref [26]	E2 Strength (W.u.) Exp.	E2 Strength (W.u.) Ref [26]
1132	0	$5/2^-$	$3/2^-$	400^{+200}_{-100}	61 ± 6	$0.36 \leq \delta \leq 0.70$	2.6[b]	0.2	10.0[b]	0.14
	67		$5/2^-$		39 ± 5	$-\infty \leq \delta \leq -0.84$	< 1.3[c]	0.07	>12.0[c]	2.1
						$2.14 \leq \delta \leq \infty$	< 0.5[c]	0.07	>33.0[c]	2.1
1186	0	$3/2^-$	$3/2^-$	160 ± 26	77 ± 8	$-\infty \leq \delta \leq 0.27$	< 9.2[c]			
	67		$5/2^-$		6 ± 2					
	283		$1/2^-$		5 ± 2					
	656		$3/2^-$		12 ± 3					
1457	0	$5/2^-$	$3/2^-$	480^{+340}_{-160}	76 ± 8	$-0.72^{+0.23}_{-0.29}$	1.1		4.7	
	67		$5/2^-$		24 ± 4	$-2.75 \leq \delta \leq -0.36$	17.0[b]		3.9	
1611	0	$5/2^-$	$3/2^-$	365^{+160}_{-90}	42 ± 6	$0.18 \leq \delta \leq 2.75$	0.3[b]		4.1[b]	
	67		$5/2^-$		58 ± 9	$-0.18 \leq \delta \leq 0.18$	1.4[b]			
1730	0	$3/2^-$	$3/2^-$	88 ± 12	25 ± 5					
	67		$5/2^-$		38 ± 6					
	283		$1/2^-$		16 ± 5					

Table 4.1 (Continued)

E_i (keV)	E_f	J_i^π	J_i^π	τ (fs)	B.R. (%)	δ	M1 Strength ($\times 10^{-2}$ W.u.) Exp. Ref [26]	E2 Strength (W.u.) Exp. Ref [26]
1730	656	$3/2^-$	$3/2^-$	88 ± 12	21 ± 5			
1812	67	?	$5/2^-$	230^{+120}_{-65}	100			
1990	67	?	$3/2^-$	500^{+530}_{-190}	37 ± 12			
	656		$3/2^-$		63 ± 16			
1997	0	$1/2^{[a]}$ or $5/2^{[a]}$	$3/2^-$	48 ± 10	100			
2020	67	$7/2^-$	$5/2^-$	155^{+50}_{-33}	100	0.03 ± 0.16	2.7	0.01
2125	0	$1/2^-$	$3/2^-$	45 ± 8	> 95			
					< 5			
							E1 Strength	M2 Strength
2123	1016	$9/2^+$	$7/2^-$	585^{+1065}_{-175}	100	-0.03 ± 0.28	0.08	2.7

[a] From reference [60]

[b] Calculated using the mid-range value of δ

[c] Calculated using the finite limit of the range of δ

Figure 4.25 A comparison of experimental results and theoretical predictions for the first seven excited states of ^{61}Ni. Shell model calculations have been performed by Glaudemans *et al.* while Hoffmann-Pinther *et al.* used the core-coupling model. With the exception of the lifetimes for the first three excited states (see reference [60]), all the experimental information is from the present work.

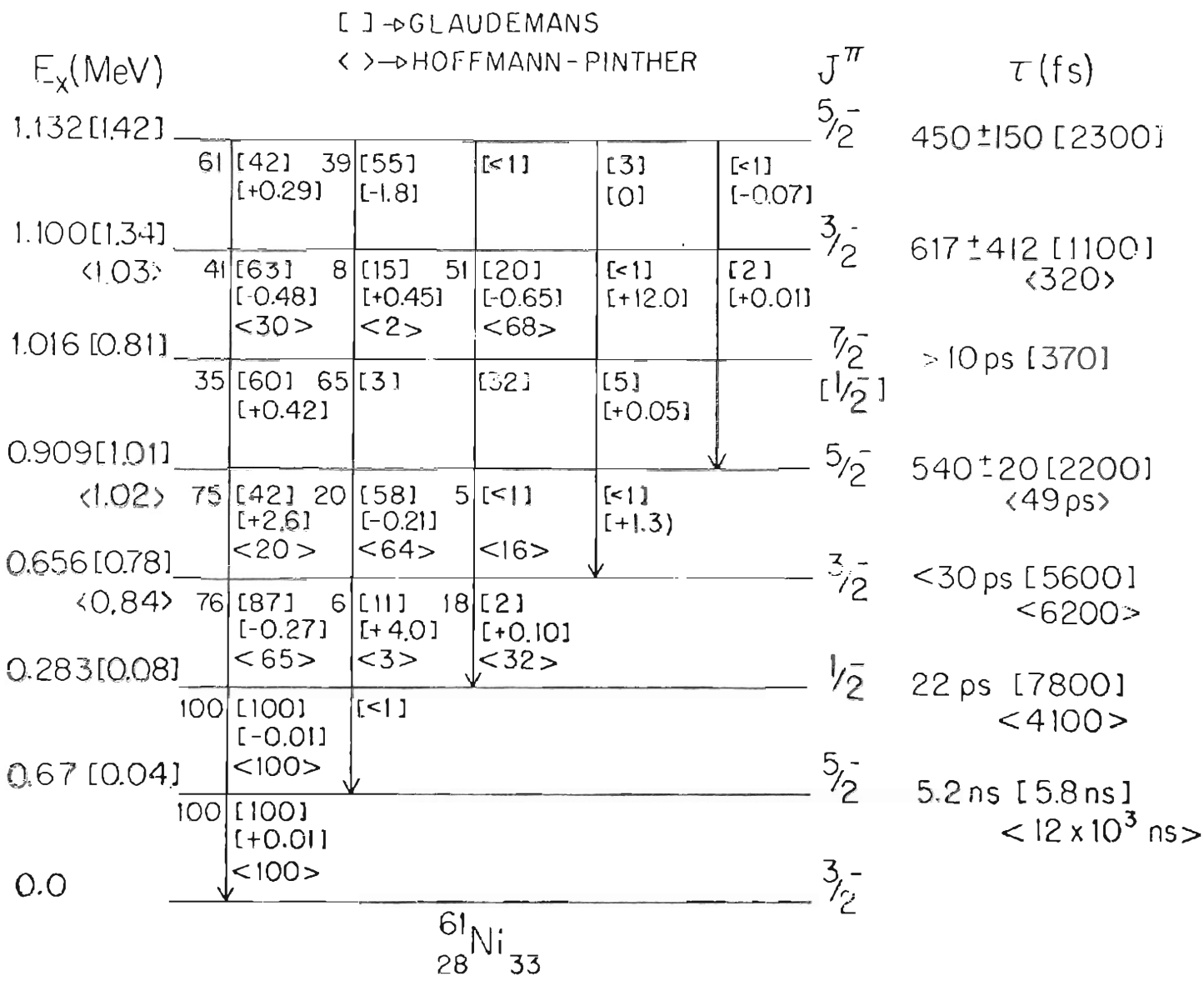
[ ] → GLAUDEMANS
< > → HOFFMANN - PINTHER
E_x(MeV)
J^π
τ (fs)
1.132 [1.42]
5/2⁻
450 ± 150 [2300]
61
[42] 39
[+0.29]
[55]
[-1.8]
[<1]
[3]
[0]
[<1]
[-0.07]
1.100 [1.34]
3/2⁻
617 ± 412 [1100]
<320>
<1.03>
41
[63] 8
[-0.48]
<30>
[15] 51
[+0.45]
<2>
[20]
[-0.65]
<68>
[<1]
[+12.0]
[2]
[+0.01]
1.016 [0.81]
7/2⁻
> 10 ps [370]
35
[60] 65
[+0.42]
[3]
[32]
[5]
[+0.05]
[1/2⁻]
0.909 [1.01]
5/2⁻
540 ± 20 [2200]
<49 ps>
<1.02>
75
[42] 20
[+2.6]
<20>
[58] 5
[-0.21]
<64>
[<1]
<16>
[<1]
[+1.3]
0.656 [0.78]
3/2⁻
<30 ps [5600]
<6200>
<0.84>
76
[87] 6
[-0.27]
<65>
[11] 18
[+4.0]
<3>
[2]
[+0.10]
<32>
0.283 [0.08]
1/2⁻
22 ps [7800]
<4100>
100
[100]
[-0.01]
<100>
[<1]
0.67 [0.04]
5/2⁻
5.2 ns [5.8 ns]
< 12 x 10³ ns>
100
[100]
[+0.01]
<100>
0.0
3/2⁻
61 28 Ni 33

the experimental results and the predictions of the core-coupling model calculations of Hoffmann-Pinther et al. [29].

As described in Section 4.11, the shell model calculations of Glaudemann's et al. were performed with the five neutrons outside the 1f 7/2 shell closure allowed to take on all possible configurations in the 2p 3/2 , 1f 5/2 , and 2p 3/2 orbits. Explicit excitation of the ^{56}Ni core was not considered. Calculations for electric, quadrupole radiation were made with five reduced single-particle matrix elements corresponding to the transitions p 3/2 → p 3/2 , f 5/2 → f 5/2 , p 1/2 → p 1/2 , p 3/2 → f 5/2 , and p 3/2 → p 1/2 . These matrix elements were determined from a least squares fit to 33 observed E2 transition strengths using an effective neutron charge of (1.70 ± 0.08)e.

For the magnetic dipole transitions, the reduced single-particle matrix elements were obtained by a least squares fit to some 30 M1 strengths observed in this mass region. An effective value of + 0.58 was used in the calculations for the matrix element representing the p 3/2 → f 5/2 transition. This transition is normally considered to be ℓ-forbidden for M1 radiation.

Referring to Table 4.1 and Figure 4.25, the agreement between experiment and the shell model predictions does not appear to be good. The most obvious disagreement concerns the spin assignment for the level at 1016 keV. This discrepancy renders futile any further comparisons for the gamma decay of this level. Perhaps a larger compilation of experimental information for this mass region would aid in the least squares fitting procedure used with the shell model calculations; however, as pointed out by Glaudemanns et al., better

agreement will most likely be obtained when core excitation can be considered explicitly in the theoretical calculations.

The agreement with experimental observation does not appear to be improved substantially by the results of the core-coupling model calculations of Hoffmann-Pinther et al. As pointed out in Section 4.2, core excitation was considered by coupling the first 2^+ state in ^{60}Ni to the single particle states 2p 3/2 , 1f 5/2 , and 2p 1/2 . Therefore, the calculations for the decay of the low-lying excited states were performed using only pure M1 and E2 operators, the results being as shown in Figure 2.25. As with the shell model calculations, the most obvious discrepancy concerns the fifth excited state, whose existence the core-coupling model fails to predict. Hoffmann-Pinther et al. have recently performed these same calculations using effective M1 and E2 operators; however, the results of these calculations are not available at this time.

The experimental M1 and E2 strengths determined in this work for ^{61}Ni agree very well with previous observations in this mass region [1]. The one M2 strength determined for the decay of the level at 2123 keV (2.7 W.u.) appears to be enhanced by about 20, compared with earlier tabulations.

It is hoped that the results presented here will help to improve the knowledge of the systematics for this mass region since only information of this type can provide a foundation for a general study of the medium mass nuclei.

5. LIST OF REFERENCES

1. Arns, R. G. 1971. Ohio State University Report VDG-008, p. 51, Columbus, Ohio.

2. Arvieu, R., O. Bohigas, and C. Quesne. 1970. Nucl. Phys. A143, 577.

3. Auerbach, N. 1967. Phys. Rev. 163, 1203.

4. Barman, B. Roy, Ram Raj, and M. L. Rustgi. 1970. Phys. Rev. C1, 207.

5. Bass, R., J. Brinkmann, C. von Charzewski, and H. Hanle. 1972. Nucl. Instr. and Meth. 104, 33.

6. Bearse, R. C., D. H. Youngblood, and J. L. Yntema. 1968. Phys. Rev. 167, 1043.

7. Beck, F. A., T. Byrski, G. Costa, and P. Engelstein. 1974. Nucl. Phys. A218, 213.

8. Beraud, R., I. Berkes, J. Daniere, Michele Levy, G. Marest, and R. Rougny. 1967. Nucl. Phys. A99, 577.

9. Bevington, P. R. 1969. Data Reduction and Error Analysis for the Physical Sciences. McGraw-Hill Book Co., Inc., New York, New York.

10. Biedenharn, L. C. and M. E. Rose. 1953. Rev. Mod. Phys. 25, 729.

11. Blatt, J. M. and V. F. Weisskopf. 1952. Theoretical Nuclear Physics. John Wiley and Sons, Inc., New York, New York, p. 796.

12. Blaugrund, A. E. 1966. Nucl. Phys. 88, 501.

13. Bolotin, H. H. and H. J. Fischbeck. 1967. Phys. Rev. 158, 1069.

14. Cohen, B. L. 1971. Concepts of Nuclear Physics. McGraw-Hill Book Co., Inc., New York, New York.

15. Cohen, S., R. D. Lawson, M. H. Macfarlane, S. P. Pandya, and Michitoshi Soga. 1967. Phys. Rev. 160, 903.

16. Cosman, E. R., D. N. Schramm, H. A. Enge, A. Sperduto, and C. H. Paris. 1967. Phys. Rev. 163, 1134.

17. de Voigt, M. J. A., P. W. M. Glaudemans, J. de Boer, and B. H. Wildenthal. 1972. Nucl. Phys. A186, 365.

18. Devons, S. and L. J. B. Goldfarb. 1957. Handbuch der Physik. Springer Verlay, Berlin, Germany, 42, 362.

19. Endt, P. M. and C. van der Leun. 1974. Atomic Data and Nuclear Data Tables 13, 67.

20. Evans, R. D. 1955. The Atomic Nucleus. McGraw-Hill Book Co., Inc., New York, New York, p. 672.

21. Fagg, L. W. and S. S. Hanna. 1959. Rev. Mod. Phys. 31, 711.

22. Federman, P. and I. Talmi. 1965. Phys. Letts. 19, 490.

23. Fulmer, R. H. and W. W. Daehnick. 1965. Phys. Rev. 139, B579.

24. Gambhir, Y. K. and Ram Raj. 1967. Phys. Rev. 161, 1125.

25. Glaudemans, P. W. M., P. J. Brussaard, and B. H. Wildenthal. 1967. Nucl. Phys. A102, 593.

26. Glaudemans, P. W. M., M. J. A. de Voigt, and E. F. M. Steffens. 1972. Nucl. Phys. A198, 609.

27. Hilko, R. 1974. Unpublished Ph.D. dissertation. Duke University, Department of Physics, Durham, N. C.

28. Hirko, R. G., R. A. Lindgren, A. J. Howard, J. G. Pronko, M. W. Sachs, and D. A. Bromley. 1971. Part Nucl. 1, 372.

29. Hoffman-Pinther, P. and J. L. Adams. 1974. Private communication.

30. Hsu, L. S. 1967. Nucl. Phys. A96, 624.

31. Hutton, J. D., N. R. Roberson, G. R. Gould, and D. R. Tilley. 1973. Nucl. Phys. A206, 403.

32. Jackson, J. D. 1967. Classical Electrodynamics. John Wiley and Sons, Inc., New York, New York, p. 550.

33. Jaffe, A. A., F. de S. Barros, P. D. Forsyth, J. Muto, I. J. Taylor and S. Ramavataran. 1960. Phys. Soc. Proc. (London, England) 76, 914.

34. Jolly, R. K., E. K. Lin, and B. L. Cohen. 1962. Phys. Rev. 128, 2292.

35. Jones, A. D. W. 1969. Phys. Rev. 180, 997.

36. Jones, A. D. W., J. A. Becker, and R. E. McDonald. 1971. Phys. Rev. C3, 724.

37. Kean, D. C., K. W. Carter, C. J. Piluso, and R. H. Spear. 1969. Nucl. Phys. A132, 241.

38. Kean, D. C., K. W. Carter, and R. H. Spear. 1969. Nucl. Phys. A123, 430.

39. Klein, O. and Y. Nishina. 1929. Z. Physik 52, 853.

40. Krane, K. S. 1972. Nucl. Instr. and Meth. 98, 205.

41. Kuo, T. T. S. and G. E. Brown. 1968. Nucl. Phys. A114, 241.

42. Lawson, R. D., M. H. Macfarlane, and T. T. S. Kuo. 1966. Phys. Letters 22, 168.

43. Lindhard, J., M. Scharff, and H. E. Schiott. 1963. Kgl. Danske Videnskab. Selskab, Mat.-Fys. Medd. 33, No. 14.

44. Litherland, A. E. and A. J. Ferguson. 1961. Can. J. Phys. 39, 788.

45. Nelson, R. O. and D. G. Rickel. 1974. Private communication.

46. Perey, F. and B. Buck. 1962. Nucl. Phys. 32, 353.

47. Poletti, A. R. and E. K. Warburton. 1965. Phys. Rev. 137, B595.

48. Ragan, C. E., III. 1970. Unpublished Ph.D dissertation. Duke University, Department of Physics, Durham, N. C.

49. Rickel, D. G., N. R. Roberson, R. O. Nelson, D. R. Tilley, and J. R. Williams. 1974. Measurement of Mean Lifetimes, γ-Ray Angular Distributions, and Linear Polarizations for Low-Lying Levels of 50V. (To be published)

50. Ritter, J. C. and R. E. Larson. 1967. Nucl. Phys. A127, 399.

51. Rose, H. J. and D. M. Brink. 1967. Rev. Mod. Phys. 39, 306.

52. Rundquist, D. E., M. K. Brussel, and A. I. Yavin. 1968. Phys. Rev. 168, 1296.

53. Sawa, Z. P. 1971. The Structure of 1f 7/2 Nuclei. (R. A. Ricci, Editor). Editrice Compositori, Bologna, Italy, p. 287.

54. Singh, R. P., R. Raj, M. L. Rustgi, and H. W. Kung. 1970. Phys. Rev. C2, 1715.

55. Taras, P. 1971. Can. J. Phys. 49, 328.

56. Taras, P. and J. Matas. 1968. Nucl. Instr. and Meth. 61, 317.

57. Taras, P. and J. Matas. 1969. Can. J. Phys. 47, 1605.

58. Tee, R. G. and A. Aspinall. 1967. Nucl. Phys. A98, 417.

59. Thankappan, Y. K. and William W. True. 1965. Phys. Rev. 137 4B, 793.

60. Vervier, J. 1968. Nuclear Data Sheets for A = 61. Nuclear Data B2-5-81.

61. Warburton, E. K. 1967. Nuclear Research with Low Energy Accelerators. (J. B. Marion and D. M. van Patter, Editors). Academic Press, New York, New York, p. 43.

62. Winn, W. G. and D. G. Sarantites. 1968. Nucl. Instr. and Meth. 66, 61.